



Title      The Development of an assistive chair for  
              elderly with sit to stand problems

Name     Hang Lu

This is a digitised version of a dissertation submitted to the University of Bedfordshire.

It is available to view only.

This item is subject to copyright.

**The Development of an Assistive Chair for Elderly  
with Sit to Stand Problems**

Hang Lu

Ph.D

2016

UNIVERSITY OF BEDFORDSHIRE

The Development of an Assistive Chair for Elderly with Sit to Stand Problems

by

Hang Lu

A thesis submitted to the University of Bedfordshire in partial fulfilment of the requirements  
for the degree of Doctor of Philosophy

June 2016

# **ABSTRACT**

## **I**

Standing up from a seated position, known as sit-to-stand (STS) movement, is one of the most frequently performed activities of daily living (ADLs). However, the aging generation are often encountered with STS issues owing to their declined motor functions and sensory capacity for postural control. The motivated is rooted from the contemporary market available STS assistive devices that are lack of genuine interaction with elderly users. Prior to the software implementation, the robot chair platform with integrated sensing footmat is developed with STS biomechanical concerns for the elderly.

The work has its main emphasis on recognising the personalised behavioural patterns from the elderly users' STS movements, namely the STS intentions and personalised STS feature prediction. The former is known as intention recognition while the latter is defined as assistance prediction, both achieved by innovative machine learning techniques. The proposed intention recognition performs well in multiple subjects scenarios with different postures involved thanks to its competence of handling these uncertainties. To the provision of providing the assistance needed by the elderly user, a time series prediction model is presented, aiming to configure the personalised ground reaction force (GRF) curve over time which suggests successful movement. This enables the computation of deficits between the predicted oncoming GRF curve and the personalised one. A multiple steps ahead prediction into the future is also implemented so that the completion time of actuation in reality is taken into account.


## DECLARATION II

I declare that this thesis is my own unaided work. It is being submitted for the degree of Doctor of Philosophy at the University of Bedfordshire.

It has not been submitted before for any degree or examination in any other University.

Name of candidate: Hang Lu

Signature:

A handwritten signature in black ink, appearing to read 'Hang Lu', with a stylized flourish at the end.

Data: 15 June 2016

## ACKNOWLEDGMENTS III

I would like to express my gratefulness and deepest respect to my director of studies, Prof. Dayou Li, for his continuous encouragement, invaluable guidance and support. This thesis will not be completed without his guidance and mentorship.

As a pioneer in the field of machine learning, I can imagine he had a PhD life 10 times tougher than mine, accompanied with higher living pressure and less research resources. In terms of PhD supervisory work, he always does jobs 110% of what other student could ever expect from a supervisor. Especially during the thesis write up period he put an extraordinary amount of time to help me check the reasoning behind each method and how things should be connected to illustrate a problem. I am also grateful that whenever I felt sluggish, he has never been hesitant to get me back on track and show me why we shouldn't do certain things during our PhD study. Getting the mind-set right is the foremost thing when chasing a degree at this level.

I still remembered on the first day of the induction week, Prof. Li gathered all of us fellow students in his office. He guided us to the world of research by introducing the general procedure of analytical thinking in a simple manner. Starting with problems to be solved, efforts have been made by related studies. They might have managed to solve part of the problem, with some imperfections. Or they might introduced other problems when solving the problems. As a new researcher in this field, to what extend can you improve their techniques, mitigate the problems or generate new methods to compete against the bench marking ones... Such memory is fresh as if I had just experienced last night. This formed my own critical thinking of how should I conduct my research and tackle the problems.

Special thanks go to my mum, who has actually spent a great amount of time to stay with me in the UK after her retirement. This offered me a great luxury that most of the other students conquering the degree don't have. She also strived to provide me a healthy lifestyle, both physically and mentally, throughout the entire period of PhD study, free of suffering from as much nostalgia as other overseas students.

My father has also played an important role when it comes to the financial support. Besides, as a PhD supervisor on his own, he has set me a great example of the attitude of being a responsible researcher. He has been very concerned about my progress from time to time. I always feel like I have a strong person that holding my back.

In my research institute, the former head of department prof. Edmond Parsha has supported some miscellaneous parts components to help me built the prototype sensing footmat. academic work is checked. It is also worth mentioning that Peter Norrington, a scientific editor, has proof-read the Section 5.3-5.5 of this thesis. He has not only checked the errors in grammar, style, punctuation, formatting and spelling, but also suggested the possible corrections. This set a standard of how a competent thesis should be albeit the work was only 7 pages in length.

My thanks are also due to Beisheng Liu, Wei Li, Christopher Hanne, who gave me genuine advices in terms of programming. Although by no means these could help me directly tackle with actual problems, all the tips and suggestions they gave me have help me in a long run.

Besides, I will not forget anonymous staff in the University of Bedfordshire whoever were willing to spare 5 minutes giving me tips on soldering and safety briefings, or helping me with formatting before publishing papers. Neither will I forget a couple of good security staff who helped me open up the gate of our research block at midnight.

Although the work is sometimes confined by time and budget constraints, I believe a potential PhD candidate should have the ability to find alternations using the mere accessible resources. There are also moments in my PhD life I felt like I can never get it done and I cannot carry on a lifestyle like this. But I suffered it, and then learnt how to live in time and concentrate on the research problem itself. All of these, in my subjective opinions, are gains I have acquired during my 4-year study, let along with uncountable skills.

For me, the submission of thesis is more like a millstone rather than a stop of my research life. There will be tougher problems that challenge me, where I could apply the same amount of concentration, endeavour, creativity and passion to conquer them.

In the end, I would like to express my special thanks to Beijing Shizhi Hongyuan Technology LTD, which has endeavoured to support the first three years of my PhD study. Moreover, they have arranged at least two manufacturers in Beijing, one specialised in mechanical manufacturing and the other in PCB board industry. They both turned my design into actual prototypes without sacrificing any functionalities and performances in any fashions.



## LIST OF CONTENT IV

ABSTRACT I.....	II
DECLARATION II.....	III
ACKNOWLEDGMENTS III.....	IV
LIST OF CONTENT IV.....	VII
LIST OF FIGURES V.....	IX
LIST OF TABLES VI.....	XIII
LIST OF ABBREVIATIONS AND ACRONYMS.....	XIV
CHAPTER 1 INTRODUCTION.....	1
1.1 Background and Motivations.....	1
1.2 Problem definition.....	1
1.3 Aim and Objectives.....	2
1.4 Thesis Structure/ Overview.....	4
CHAPTER 2 LITERATURE REVIEW.....	6
2.1 Introduction.....	6
2.2 Sit-to-stand issue.....	8
2.2.1 Sit-to-stand problems and health implication.....	8
2.2.2 Biomechanics study on sit-to-stand mechanisms.....	10
2.2.3 Commercial available assistive devices.....	17
2.2.4 Experimental assistive devices.....	22
2.3 Sensing techniques for human-robot interactions.....	28
2.3.1 Introduction of HRI.....	29
2.3.2 A variety of on-chair sensory implementations.....	29
2.3.3 Critical analysis.....	36
2.4 Machine learning technologies for intention recognition.....	39
2.4.1 ANN and time series prediction.....	39
2.4.2 Fuzzy logic system.....	42
2.4.3 Adaptive neuro-fuzzy logic system.....	43
2.5 Summary.....	46
CHAPTER 3 THE DEVELOPMENT OF ROBOT CHAIR ASSEMBLY WITH INTEGRATED SENSING FOOTMAT.....	47
3.1 Design of chair mechanics.....	47
3.1.1 Biomechanical concerns.....	47
3.1.2 2D sketch and 3D CAD sketch.....	49
3.2 Design of sensing footmat.....	54
3.2.1 The sensing footmat.....	54
3.2.2 Data acquisition and software implementation.....	58
3.2.3 Data processing.....	61
3.3 Actuation.....	64
3.4 Summary.....	65
CHAPTER 4 INTENTION RECOGNITION.....	67
4.1 Background Knowledge.....	68
4.2 Feasible Features for Intention Recognition.....	71

4.2.1	Data analysis on GRF curves.....	72
4.2.2	Centre of Pressure.....	75
4.3	Fuzzy Inference System Based Classification.....	81
4.3.1	Point-wise classification.....	82
4.3.2	Accumulation change-based classification.....	87
4.3.3	Max-difference based classification.....	90
4.3.4	Discussion.....	93
4.4	Summary.....	100
CHAPTER 5	SELF-ADAPTIVE FUZZY CLASSIFIER.....	102
5.1	The need for self-adaptive classification.....	102
5.2	Self-adaptive fuzzy classification for handling 1st biomechanical feature.....	107
5.2.1	Manual adaptation and discussion.....	107
5.2.2	Self-adaptive neural fuzzy classification.....	110
5.2.3	Training and testing results.....	115
5.3	Self-adaptive fuzzy classification for handling 2nd biomechanical feature.....	119
5.3.1	Architecture of self-adaptive ANFIS classification.....	120
5.3.2	Training and testing results.....	121
5.4	Discussion.....	124
5.5	Summary.....	126
CHAPTER 6	NEURAL NETWORK BASED ASSISTANCE PREDICTION.....	128
6.1	Background Knowledge on time series prediction.....	128
6.2	Feed forward neural network and its regimes.....	129
6.3	FFNN based GRF Prediction.....	131
6.3.1	FFNN Structure.....	131
6.3.2	FFNN training.....	135
6.3.3	Prediction results and discussion.....	142
6.4	MSAP network.....	147
6.4.1	Structure and training.....	147
6.4.2	Discussion.....	152
6.5	Summary.....	158
CHAPTER 7	CONCLUSIONS AND FUTHER WORK.....	159
7.1	Research summary.....	159
7.2	Thesis contributions and publications.....	161
7.3	Limitations.....	163
7.3.1	The limited capacity of the sensory data.....	163
7.3.2	The quickness of actuation.....	164
7.4	Future extension.....	164
7.4.1	3D Biomechanical model based chair design.....	164
7.4.2	Enhancing classifications with multiple sensing channels.....	165
7.4.3	Adaptive control with gain scheduling control scheme.....	165
7.4.4	More accurate GRF prediction with deep learning.....	166
7.4.5	Embedded system implementation.....	167
PUBLICATIONS	.....	错误!未定义书签。
REFERENCES	.....	168

## LIST OF FIGURES V

Figure 2.1 A simple biomechanical model of STS movement and in sagittal plane where the hip, knee and ankle ( $\theta H, \theta K$ and $\theta A$ ), were configured as the angle between adjacent body segments (Lord et al, 2002). .....	11
Figure 2.2 Distinctive events in STS through normalised GRF to the percentage of body weight (Etnyre & Thomas, 2007) .....	12
Figure 2.3 The Antepulsion and Retropulsion postures appearing in the initiation of STS transfer (Médéric et al, 2004).....	16
Figure 2.4 Variations of standing frames: (a) ReTurn7600 (SystemRoMedic, 2012); (b) Standing frame (Praschberger, n.d.); (c) Three-wheeler; (d) Four-wheeler (Rica, n.d.) .....	17
Figure 2.5 Commercial available Electric lift chairs: (a) Restwell Seattle Intalift (Motionhaus, n.d.); (b) La-Z-Boy AVENGERluxury lift chair in operation (La-Z-Boy, 2010); (c)Pride C-30 in operation (U.S Medical Supplies, 2012).....	19
Figure 2.6 The pneumatic chair seat lift (Stuffseniorsneed, n.d.).....	21
Figure 2.7 The EJAD Standing frame inspired by the assistive motion provided by care givers when aiding STS transfers (Salah et al, 2013) .....	23
Figure 2.8 The EJAD Standing frame inspired by the assistive motion provided by care givers when aiding STS transfers (Salah et al, 2013) .....	24
Figure 2.9 The lifting chair prototype with hip-up motion (Bae & Moon, 2010 & 2011) .....	24
Figure 2.10 The Ejector chair developed by (Munro et al, 1998) with the user seated and preparing to perform assisted STS movement .....	25
Figure 2.11 The standing up robot equipped with integrated sensor networks (Kamnik & Bajd, 2004).....	26
Figure 2.12 Wearable ankle robot proposed by Jamwal et al (2014) (a) Robot in use after construction. (b) 3-D solid model of the final concept. (c) Positions of force sensors and linear potentiometers. ....	28
Figure 2.13 BPMS mats placed on chair (Tan et al, 2001) .....	31
Figure 2.14 (a): Placement of the 7 Force Sensitive Resistors (b): 4 vibrotactile at the back of the seat (Zheng & Morrell, 2010) .....	33
Figure 2.15 A hybrid sensing system incorporating vision sensor as well as EMG sensor (Taslim Reza, 2014) .....	36
Figure 2.16 ANFIS-PID control system configuration developed by (Hussain et al, 2014) .....	44
Figure 3.1 Initial position of quad-pivot structure (a) principle 2D sketch (b) side view of the chair mechanism (c) 3D view of the chair mechanism .....	50
Figure 3.2 End position of quad-pivot mechanism (a) principle 2D sketch (b) side view of the chair mechanism (c) 3D view of the chair mechanism .....	51
Figure 3.3 The placement of seatpan (graphics generated by CREO Parametric 2.0) ....	51
Figure 3.4 Technical drawing of the main frame .....	53
Figure 3.5 The final assembly of the robot chair mechanics .....	54
Figure 3.6 The schematic circuit design of the sensing footmat.....	55

Figure 3.7 Preliminary experiments on prototyping footmat with evenly distributed FSRs to test out the geometric layout and optimal number of cells .....	55
Figure 3.8 Construction sketch of sensing footmat (sketch generated by Office Visio 2007) .....	56
Figure 3.9 The sensing footmat that forms a robust structure to ensure robust force transition onto FSR cells .....	58
Figure 3.10 (a) Arduino Mega 2560 (b) Schematic diagram of CD4051B multiplexer ..	59
Figure 3.11 (a) Construction of FSR-400 sensing cell (b) Simplified voltage divider with FSR cell tied to measuring resistor ( $R=10K\Omega$ ) (c) Resistance-force characteristics of FSR-400 (Interlink electronics, 2006) .....	59
Figure 3.12 On-time serial output displayed on Matlab .....	61
Figure 3.13 Limited space for the actuator .....	64
Figure 4.1 Distinctive events in STS through normalised GRF to the percentage of body weight (Etnyre and Thomas, 2007) .....	69
Figure 4.2 Normalised GRF respecting to body weight from Successful STS movements .....	73
Figure 4.3 Normalised GRF in three cases over first 1.1 seconds .....	74
Figure 4.4 Procedure of computing COP from the sensing footmat .....	76
Figure 4.5 Magnitude of change in COP from three previously selected movements ....	77
Figure 4.6 Plot of Longitudinal shift of COP in three cases .....	77
Figure 4.7 Plot of Lateral shift of COP in three cases .....	78
Figure 4.8 Lateral shift of COP in all Unintended movements .....	79
Figure 4.9 Lateral shift of COP in all Successful STS movements .....	79
Figure 4.10 Lateral shift of COP in all Unsuccessful STS movements .....	80
Figure 4.11 Distribution of LS of COP in Unintended (100 points) and Intended (200 points) movements over the early stages .....	83
Figure 4.12 Fuzzy sets of A, B and C regarding to LS .....	83
Figure 4.13 Criteria used when determining the truth degree of Rule 1, 2 and 3 .....	84
Figure 4.14 Rules fired by Example 4.1 .....	86
Figure 4.15 Distribution of accumulated LS of the respecting Unintended and Intended movements .....	88
Figure 4.16 Fuzzy sets of A and B respecting to the accumulated LS .....	88
Figure 4.17 Rules fired by Example 4.2 .....	90
Figure 4.18 Distribution of MDLS of the respecting Unintended and Intended movements .....	91
Figure 4.19 Fuzzy sets of A and B respecting to the MDLS .....	92
Figure 4.20 Rules fired by Example 4.3 .....	93
Figure 4.21 Confusion matrix of point-wise classification with Two-fold input data .....	97
Figure 4.22 Confusion matrix of point-wise classification with pure test data .....	97
Figure 4.23 Confusion matrix of ACLS classification with 2-fold test data .....	97
Figure 4.24 Confusion matrix of ACLS classification with pure test data .....	98
Figure 4.25 Confusion matrix of MDLS classification with 2-fold test data .....	98
Figure 4.26 Confusion matrix of MDLS classification with pure test data .....	98
Figure 5.1 Confusion matrix of the original ACLS classification applied on Subject B's	

test data .....	103
Figure 5.2 Confusion matrix of the original MDLS classification with test data only applied on Subject B's test data .....	103
Figure 5.3 Distribution of ACLS of the respecting Unintended and Intended movements performed by Subject B .....	107
Figure 5.4 Input fuzzy sets of A and B of ACLS classifier for Subject B .....	108
Figure 5.5 Distribution of MDLS of the respecting Unintended and Intended movements performed by Subject B.....	109
Figure 5.6 Fuzzy sets of A and B respecting to the MDLS classifier for Subject B.....	109
Figure 5.7 Confusion Matrix of ACLS applied on Subject B after manual adjustment	110
Figure 5.8 Confusion matrix of MDLS applied on Subject B after manual adjustment	110
Figure 5.9 The distance between (a) the widest points of subject A's trainer: 116.95mm, (b) the narrowest points of Subject A's trainer: 79.85mm.....	111
Figure 5.10 The distance between (a) the widest points of subject B's flat: 83.05mm, (b) the narrowest points of subject B's flat: 81.45mm .....	111
Figure 5.11 3D mesh plot of activated FSRs with height being cell-wise GRF values generated by Subject A (a) and Subject B (b), respectively.....	112
Figure 5.12 Architecture of hybrid neural fuzzy system for ACLS and MDLS classification handling the variations in shoe width .....	114
Figure 5.13 The convergence of training error of ACLS self-adaptive classifier.....	116
Figure 5.14 Test results with the raw defuzzification outputs generated by ACLS self-adaptive classifier.....	116
Figure 5.15 Confusion Matrix of the self-adaptive ACLS classifier tested by two subjects along with their 1 <sup>st</sup> biomechanical feature (60 sets of pure test data).....	117
Figure 5.16 Confusion matrix of self-adaptive MDLS classifier tested by two subjects along with their 1 <sup>st</sup> biomechanical feature (60 sets of pure test data).....	117
Figure 5.17 Rules fired by Example 5.1 in the self-adaptive ACLS classifier .....	118
Figure 5.18 Architecture of hybrid neural fuzzy system for ACLS and MDLS classification handling the variations in stance width.....	120
Figure 5.19 The convergence of training error (MSE) of the ACLS self-adaptive classifier on 2 <sup>nd</sup> biomechanical adaptation .....	122
Figure 5.20 Confusion Matrix of self-adaptive ACLS classifier tested by two subjects along with their 2nd biomechanical feature (60 sets of pure test data) .....	123
Figure 5.21 Confusion matrix of self-adaptive MDLS classifier tested by two subjects along with their 2nd biomechanical feature (60 sets of pure test data) .....	123
Figure 6.1 Schematic structure of FFNN for time series prediction.....	130
Figure 6.2 Structure outline of FFNN used to handle time series GRF data .....	131
Figure 6.3 Prediction and deviations against the captured actual GRF curve .....	133
(a) $d = 1$ , $N = 5$ , (b) $d = 1$ , $N = 10$ , (c) $d = 1$ , $N = 20$ , (d) $d = 1$ , $N = 50$ .....	133
Figure 6.4 Prediction and deviations against the captured actual GRF curve .....	134
(a) $d = 2$ , $N = 5$ , (b) $d = 2$ , $N = 10$ , (c) $d = 2$ , $N = 20$ , (d) $d = 2$ , $N = 50$ .....	134
Figure 6.5 Prediction and deviations against the captured actual GRF curve .....	134
(a) $d = 3$ , $N = 5$ , (b) $d = 3$ , $N = 10$ , (c) $d = 3$ , $N = 20$ , (d) $d = 3$ , $N = 50$ .....	134
Figure 6.6 FFNN ( $d = 3$ , $N = 20$ ) training performance validation with early stopping	140

Figure 6.7 FFNN ( $d = 3$ , $N = 20$ ) training performance with Bayesian regularisation .	141
Figure 6.8 GRF prediction results to 3-fold test data achieved by the optimised FFNN after BR generalisation .....	143
Figure 6.9 Autocorrelation of prediction errors when $d = 3$ , $N = 20$ .....	144
Figure 6.10 Autocorrelation of prediction errors when $d = 1$ , $N = 20$ .....	145
Figure 6.11 Autocorrelation of prediction errors when $d = 2$ , $N = 20$ .....	145
Figure 6.12 The regression correlation between 3-fold test data and prediction results with FFNN generalised by BR.....	146
Figure 6.13 Plot of selected Unsuccessful GRF curves to examine the critical point which indicates the instance of falling back to seatpan.....	148
Figure 6.14 Regression of Extension of actuator respecting to time steps required.....	150
Figure 6.15 The schematic structure of MSAP using multi previously trained FFNNs (Option 1 is conducted without regulation process) .....	151
Figure 6.16 The schematic structure of MSAP with available GRF sequence within the period of PH taken for the regulation process (Option 2).....	152
Figure 6.17 The MSAP response on 5-fold training data .....	154
Figure 6.18 The MSAP response on 5-fold test data ( $MSE = 0.0019$ ) .....	154
Figure 6.19 Autocorrelation of prediction errors of 5-fold test data.....	155
Figure 6.20 Regression of MSA prediction on 5-fold test data .....	156
Figure 6.21 The MSAP response on one set of Unsuccessful STS movement .....	157
Figure 6.22 The MSAP response on another set of Unsuccessful STS movement .....	157

## LIST OF TABLES VI

Table 2.1 Vertical GRF generated by able-bodied young subjects in corresponding STS events .....	12
Table 3.1 Average event times (Etnyre and Thomas, 2007) .....	60
Table 4.1 Complete point-wise classification of all sample points for Example 4.1 .....	86
Table 4.2 LS of COP captured from No. 3 of Intended STS movements.....	91
Table 4.3 Results of point-wise classification with 2-fold data.....	95
Table 4.4 Results of point-wise classification with pure test data.....	95
Table 4.5 Results of ACLS classification with 2-fold data.....	95
Table 4.6 Results of ACLS classification with pure test data.....	96
Table 4.7 Results of MDLS classification with 2-fold data .....	96
Table 4.8 Results of MDLS classification with pure test data.....	96
Table 5.1 The biomechanical features of Subject A and B .....	102
Table 5.2 The recorded sitting postures of both subjects when performing STS movements .....	102
Table 5.3 The extracted stance width of each subject under different sitting postures .....	106
Table 5.4 Training results investigating the shape of MFs for both classifiers .....	115
Table 5.5 Training results investigating the shape of MFs for both classifiers .....	121
Table 5.6 Test results generated by ACLS and MDLS classifiers .....	124
Table 6.1 Training results of ES and BR (compared in conjunction with) respect to various initialisations of FFNN .....	142
Table 6.2 Actuator characteristics (experimentally obtained) .....	147

# LIST OF ABBREVIATIONS AND ACRONYMS

Note certain names of manufacturers and projects are not included in this list.

## Chapter 1

ADL	active daily livings
COP	centre of pressure
STS	sit-to-stand
GRF	ground reaction force
FIS	fuzzy inference system

## Chapter 2

ADL	active daily livings
ANFIS	adaptive neuro-fuzzy inference systems
ANN	artificial neural network
BR	Bayesian regularisation
BVH	bilateral vestibular hypofunction
CBM	condition based maintenance
COG	centre of gravity
COP	centre of pressure
CGM	continuous glucose monitoring
DOF	degree-of-freedom
EMG	electromyogram
ERNN	extended recurrent neural network
ES	early stopping
FES	functional electric simulation
GRF	ground reaction force
HAT	head arm torso (upper body)
HDL	high-density lipoprotein cholesterol
HRI	human-robot interaction
IADL	instructional active daily living



IMUs	inertial measured sensors
METS	metabolic equivalents
MEMS	micro electro mechanical systems
PID	proportional integral derivative
PMA	pneumatic muscle actuators
RMS	rooted mean squared
SCI	spline cord injury
STS	sit-to-stand

### Chapter 3

BW	body weight
CAD	computer aided design
COP	centre of pressure
CNC	computer numerically controlled
CREO	design software developed by PTC
DAQ	data acquisition
FSR	force sensitive resistor
IDE	integrated development environment
PH	popliteal height
Dev	resistance-related zero order deviation
$F_{cell}$	single cell force readout
$F_{Load}$	the BW of the subject and the upper mechanism (including the seatpan)
$K_c$	equivalent gravity centre with respect to the rotation point
$K_s$	safety factor
$T_s$	sampling period
$T_{event}$	duration of the shortest STS event
$T_{multi}$	delay of data propagation via multiplexer CD4051
$\eta$	mechanical efficiency
$\omega$	resistance-related coefficient (calibration required)

$i$	resistance-related coefficient (calibration required)
$V_{out}$	single cell voltage output
$R_M$	resistance of the measuring resistor

#### Chapter 4

ACLS	accumulated lateral shift of COP
ANN	artificial neural network
BW	body weight
COG	centre of gravity
COP	centre of pressure
FIS	fuzzy inference system
GRF	ground reaction force
HRI	human robot interaction
FMR	false matching rate
IDE	integrated development environment
LS	lateral shift of COP
MDLS	max-difference of lateral shift of COP
MF	Membership Functions
RHS	right hand side
RT	responding time
STS	supporting subjects
TMR	true matching rate
VD	variety of sample data
$w_i$	weight of the $i$ th rule
$Z_i$	output yielded by the $i$ th rule
$Z_f$	the final output generated from all the fired rules

#### Chapter 5

LAT	magnitude of lateral shift in COP
FSR	force sensitive resistor

MFs	membership function
LSE-BP	least squared error-back propagation
HAT	head arm torso (upper body)
Chapter 6	
C	coefficient of logistic function
ES	early stopping
BR	Bayesian regularisation
BP	backpropagation
DOF	degree of freedom
FFNN	feed forward neural network
LM	Levenberg-Marquardt algorithm
MSE	mean squared error
MSA	multiple steps ahead
MSAP	multiple steps ahead prediction
MSW	mean squared weights
N	number of neurons in hidden layer
NAR	nonlinear autoregressive
$N_{\text{output}}$	number of neurons in output layer
RNN	recurrent neural network
$t_j$	target value of prediction point
$y_j$	output of output layer
$w_{ij}$	weight between neuron $i$ and $j$
$y_i$	output of (previous) hidden layer
$\alpha$	learning constant
$\mu$	Levenberg-Marquard's damping factor
$E_{va}(k)$	MSE of the validation at $k$ th epoch
$SS_{tot}$	total sum of squared error
$SS_{res}$	residual of squared error

$y_t$	predicted value at time $t$
$t_t$	target value at time $t$
$T_{act}$	minimum time required by the actuator
$T_{step}$	time span of each time step, 0.1 seconds

## Chapter 7

ACLS	accumulated lateral shift of COP
ANN	artificial neural network
HRI	human-robot interaction
MDLS	max-difference of lateral shift of COP
MSAP	multiple steps ahead prediction
MSE	mean squared error

# **CHAPTER 1 INTRODUCTION**

## **1.1 Background and Motivations**

As people aging, physiological changes occur including reduced muscle strength and mass, musculoskeletal weakness in addition to reduced sensory capacity. Besides, their social space contracts and they tend to spend more time indoors and mainly seated in a chair. However, known as sit-to-stand (STS) movement, standing up from a seated position is one of the most common active daily livings (ADL). The performance on STS movement is crucial for independent living as is regarded as a prerequisite for other transferring activities.

However, the aging generation are more likely to be confronted with difficulties in STS movement. These difficulties may cause substantial decreasing of the elderly mobility, leading to inactive participation in social activities (sedentary lifestyle) and increasing the risk of chronic diseases that may cause premature death. Therefore, assisting the elderly to overcome these difficulties has significance for their independent living.

Thanks to the rising public awareness, various genres of STS assistive devices become market available over the decades. Nevertheless, these devices, often act like elevators with push buttons, move the lifting parts back and forth to itself end points without virtual interaction with the user. It may seem like a one-fit-all solution from the first glimpse. However, without professional clinical analysis and advice, the subject will never know the exact amount of assistance he/ she needs. The performance is far from satisfactory in the sense of encouraging the elderly to use their own motor functions.

All of these inspire the development of a robot chair that is able to aid the elderly users' STS transfers according to the elderly users' own STS performance.

## **1.2 Problem definition**

For the proposed robot chair to be able to recognise the elderly users' intention and provide

personalised assistance, the human-robot interaction (HRI) is confronted with the following difficulties:

- How a chair robot could properly assign the expected mapping according to various STS movements performed by the elderly users. Due to safety reasons the system needs to correctly recognise the STS intentions in early stages, otherwise false actuations could happen when the user does not hold an intention of standing up. The discovery on the feasible features is the key to the success of this fuzzy inference system (FIS). Owing to the limited sensing capabilities, uncertainties need to be handled so as to maximise the accuracy of the recognition.
- How to deal with biomechanical and postural differences among multiple subjects. The trail-and-error methods used in the conventional FIS based classifier can be time-consuming and poor performing. It is worth investigating if the developed fuzzy based classification performs well when users of different biomechanical features are at present. If not, adaptation can be made to cope with such uncertainties.
- How to optimise the structure of the network as well as the training methods adopted to make sure they are suitable for the prediction model. The predictor should be assessed in a way whether it is able to figure out the deficit between actual ground reaction force (GRF) curve and the personalised one indicating successful STS transfer through on-coming GRF prediction. Prediction into the future needs to be carried out as the in reality there will be delays for the actuator to complete the desired motion.

### 1.3 Aim and Objectives

This study aims to develop a robot chair for the elderly with STS problems. The chair should be capable of 1). Recognising the users' STS intention, 2). Predicting the GRF values generated by users and 3). Offering personalised assistance to aid users' STS transfers.

Specific objectives of this study are:

- **To conduct a comprehensive review of existing researches in STS problems experienced by the elderly people and the contemporary solutions:** 1). The biomechanical will also be investigated to give an in-depth understanding of why the aged

group often suffer from STS issues. 2). The commercial available STS assistive devices, followed by the critical analysis of the latency problems. 3). The state-of-art chair based sensing techniques and the feasibilities of applying to the robot chair. 4). The artificial intelligent methods that enable the interaction between chair robot and its elderly users.

- **To develop an actuated chair and a sensing footmat:** The chair structure should fully comply with the biomechanical concerns of STS problems for the aged group. The actuation of the lifting mechanism should provide the STS-suffered elderly comfort assistance while the use of user's own motor function is still encouraging. The complexity of the sensing footmat should fulfil the demand of capturing GRF value as well as pressure matrix. For further exploitation, the change in centre of pressure should also be obtained via data processing.
- **To develop a FIS based classifier that is able to recognise the chair users' STS intention in early stages.** Using the extracted key features, the FIS classification will rule out the random movements where the elderly user does not intend to stand up from seated positions. Experiments will be conducted to determine the fuzzy sets and membership functions. Which feature(s) performs the best in terms of handling the uncertainties will be verified.
- **To further extend the early stage intention recognition to a multi-users scenario:** Figuring out the extractable features to be used as manifestations of the uncertainties brought by multiple users and different sitting behaviours. Examine the performance of Experiments will be carried out for the purpose of figuring out the significance of the extracted features that best coping with the uncertainties.
- **To develop a neural network based predictor that is capable of predicting the oncoming GRF values for the STS movement:** The personalised GRF curve referring to successful STS movements will be obtained through effective training process. In order to realise the "assistance-as-needed" according to the elderly users' motor functions, deficit between the actual GRF curve and the personalised one will be computed. Depending on the quickness of the actuation, the ability of prediction a couple of time steps ahead will be investigated.

## 1.4 Thesis Structure/ Overview

The rest of the thesis will be organised into 6 chapters:

Chapter 2 gives a literature review on the sit-to-stand (STS) difficulties suffered by the elderly as well as the health implications of sedentary lifestyle, followed by the state-of-the-art of commercial available assistive devices. Afterwards, a critical analysis was presented with examples demonstrated by a series of related studies on chair based sensing techniques.

Chapter 3 describes the design and manufacture of the chair structure with biomechanical concerns. The development of the sensing footmat is also demonstrated, followed by the data processing to turn the raw data into the important feature, GRF values.

Based on such platform of the robot chair, Chapter 4 focuses on the establishing a FIS based classifier for intention recognition method. Such FIS is implemented as three classifiers, using STS feature (the shift of centre of pressure) in different variations, namely, point-wise lateral shift of centre of pressure (COP), accumulated lateral shift of COP (ACLS) and max-difference lateral shift of COP. The fuzzy sets of each classifier is designed based on the distribution of extracted from STS movements. The performance of the classifiers is later evaluated from several aspects.

In Chapter 5, the proposed classifier is equipped with self-adaptation abilities to handle the uncertainties of different users and sitting postures. It is discovered that the manually defined FIS classifiers have rather low performance when applied on multiple-user STS scenarios. The substantial difference in biomechanical features and sitting habits can be the disturbances that lead to inaccurate classification. Therefore a self-adaptive fuzzy-neural hybrid method is developed that is capable of handle these uncertainties through effective training process.

Afterwards, a neural network based predictor is elaborated in Chapter 6. This prediction contributes to the construction of personalised GRF curve indicating capable STS movement. Besides, it enables the possibility of predicting GRF values into the future, which facilitates



more actuation time. Finally, conclusions and further work are outlined in Chapter 7.

## **CHAPTER 2 LITERATURE REVIEW**

### **2.1 Introduction**

Part of the literature review (mainly Sections 2.2.2 and 2.2.4) is largely based on the journal paper published on with more content added. Also it is worth noting some terminologies in the literature review are adapted to this thesis purely for categorisation and demonstration purposes. For example, terms originally used by the authors, including “sit to stand”, “rising from seated position” and “rising to standing” are unified as sit-to-stand (STS), when appearing in the context of this chapter.

According to the charity AgeUK, the number of people over the age of 65 in the UK is currently 11.4 million and is expected to rise by 40.77% to over 16 million in the next 17 years (Various, 2016). Demographically there are more people over the age of 60 than there are under the age of 18 with nearly 1 in 5 people expecting to see their 100th birthday.

Functional declines, long-term persisting loss of functions, are often faced by the elderly after hospitalisations, equivalent to the date of discharge from one or more diseases (Kaplan et al, 1993; Murray et al, 1993).

To assess whether the elderly individual meets the requirements of independent living, active daily livings (ADLs) are proposed, including eating (feeding), transferring (locomotive activities), bathing, clothing and using the toilet (continence). Although these items may vary between the studies, it is widely used to assess the level of care criteria the elderly require.

The public awareness in regard to restoring the ADL functions (rehabilitation interventions) should be arisen because the loss of function is largely irreversible among the elderly. In a study employing over 1,250 adults age 70 or older hospitalised for acute illness, it was found that 32% had experienced functional declines to perform one or more ADLs by the time of discharge (Sager et al, 1996). In Boyd et al’s work, for the subjects at 3 months after discharge, almost

one ADL is lost compared against the assessment prior to discharge (Boyd et al, 2008). Without rehabilitation interventions of longer duration provided for those discharged with new or additional ADL disability, 41.3% died, 28.6% were alive but had not recovered to baseline function by 12 months after discharge, in contrast with those discharged without ADL disability, only 17.8% mortality and 15.2% baseline functional disabled were seen after 12 months of observation (Boyd et al, 2008).

ADL should be differentiated to instructional ADL (IADL) proposed by Lawton and Brody (Lawton and Brody, 1969) because the former is essential for fundamental functioning and considered within the scope of the thesis. The STS movement is regarded as the prerequisite for most of ADLs and IADLs. For instance, the elderly who were hospitalised with one or more lost functions in ADLs, would directly cause greater number of dependencies on IADLs (Boyd et al, 2008).

Over the past decade there have been a lot of practitioners attempting to apply robotics to physically assist the elderly in their daily life. However, the elderly people were found to be holding different attitudes despite having different physical conditions. In regard to the assessment of ADLs the elderly can be divided into the 4 primary categories as described by Lawton and Brody (1969), i). The completely independent elderly person, ii). The elderly person who is able to clothe, feed, wash, take medicine and meet appointments albeit with some reminders required, iii). The elderly whom require physical assistance in these matters and iv). Those who actively refuse assistance.

The literature review on these aspects firstly covered the importance of STS to the elderly, the sedentary lifestyle that the elderly are currently living. The two main biomechanical reasons that cause STS problems are also reviewed in Section 2.2.2. Towards the efforts have been made to tackle with STS problems, the market available assistive devices and recent experimental prototypes are reviewed in Section 2.2.3 and 2.2.4, respectively.

## **2.2 Sit-to-stand issue**

### **2.2.1 Sit-to-stand problems and health implication**

As people age, physiological changes occur including reduced muscle strength and mass, musculoskeletal weakness in addition to reduced sensory capacity. This will lead to a contracted social space in which the elderly tend to spend more time indoor and in a favourite spot. This spot from studies is often a chair from where they have maximum view of the television, neighbourhood and so on (Forlizzi et al, 2005). However, the aging population often encounter problems during unaided STS transferring process due to adverse physiological conditions like insufficient lower limbs capability and balance impairments due to the decline of neural mechanisms for postural control or asymmetric body-weight distribution between paretic and ipsilesional limbs (Engardt et al, 1995; Lord et al, 2002).

When compared with the capabilities of STS transfers performed by able-bodied young people, the lacking of strength, speed, balance, sensory as well as psychological status for the older adults are all contribution factors to the performance and duration of STS movements (Hughes et al, 1996; Lord et al, 2002). The inability to rise from a seated position not only increase the chance of failing, it also contributes to institutionalisation and hinders a number of ADLs. The psychological factors are also worth pointing out because it plays an important role as the elderly commonly go through the STS movements with the presence of pain, anxiety and depression (Lord et al, 2002).

General physiological changes when people age can be summarised as the considerable reduction in muscle strength and sensory capacity. However, how the sedentary lifestyle and STS problem will change the life of elderly is reviewed.

A range of authorised questionnaires elucidate that elderly spend an average 10 hours in chair (sedentary behaviour) and many of them suffer from STS problem (could not rise unaided or at high risks of fall) (Matthews et al, 2008; Munton et al, 1984). Researches on sedentary lifestyle show that sitting for prolonged period of time is not a healthy living style. Apart from this, degeneration problems like metabolism, vascular health, and muscle skeleton can arise (Hvid et al, 2011; Tremblay et al, 2010), which could further elicit diseases including

osteoporosis, cardiovascular disease and type 2 diabetes (Warren et al, 2010; Hu et al, 2003; Nguyen et al, 2000; Davis et al, 2011).

Currently, sedentary behaviour has the possession of approximately 60% of people's total waking hours in the UK population, and over 70% in those with a high risk of chronic disease, especially among the elderly community.

In the perspective of this thesis, the sedentary lifestyle experienced by the elderly should be reviewed differently according to their social positions. Because aged people often have very limited participation in social activities, a passive sedentary lifestyle due to functional inadequacies will precipitate the situations. Therefore, depressed moods and decreased enjoyment of life can also be seen as consequent effects of living a prolonged sedentary.

Researchers investigated the term “sedentary” (physiology) in opposition to “active”. Whether the elderly people share sedentary problems is evaluated with a quantifiable figure called metabolic equivalents (METs). When the METs of an individual is lower than 1.5, his/her lifestyle is defined as sedentary while the active lifestyle, is defined with a METs greater than three. The METs is often computed through a list of guidelines for public health activity in different age groups (Tremblay, 2007). An “active” lifestyle reflects a well participation in both ADLs and IADLs. And it is the lifestyle the proposed robot chair should promote for the elderly with STS problems.

Being sedentary is harmful for cardio metabolic system, as the main effect of the levels of high-density lipoprotein cholesterol (HDL) as well as insulin sensitivity can significantly decrease. The reduction of these naturally produced substances would suggest high potential of cardio metabolic risk like type-2 diabetes (mainly caused by the fault when producing insulin) (Tremblay et al, 2010; Hu et al, 2003), which could also be classified as metabolic dysfunction and may subsequently deter physiological response and adaptation. Recent researches conducted in the UK have proved the acute cardiometabolic changes on the participants after short-term interventional experiments on adopting sedentary behaviours (Hedge et al, 2015).

In the long run, for those already defined as sedentary group, 10% higher risk of developing type 2 diabetes and 7.5% higher risk of developing cardiovascular disease with each additional hour of sitting (Biswas et al, 2015). Furthermore, studies have even reported a 5% increased

risk in premature mortality for those who spend more than 7h/day in seated positions with each additional hour of sitting (Chau et al, 2013). However, those who followed the recommended guideline (strategies to incorporate reduced sitting hours) have seen a drop in the risks of chronic disease.

In the past decades, the public awareness on STS difficulties has already been arisen along with the come into being of assistive chairs. In terms of the difficulties experienced by the elderly, standing up and sitting down rank in the top three on the list of the most expected homecare assistances in the robotic world (Qiu et al, 2012). This, following the trend of home based robots such as care-o-bot, brings promising opportunities for the development of a chair robot incorporating HRI techniques.

Therefore, an assistive chair that will assist the elderly in need is in demand, and could possibly delay age-related impairment and further change their lifestyle to reduce the risk of potential diseases. These concerns bring the survey further to the approaches that could enable assistive chairs to recognise the users' personalised features and ongoing intentions.

### 2.2.2 Biomechanics study on sit-to-stand mechanisms

STS ranked at Level 1 frequently performed activity by several health implication studies (Huge et al, 1996; Kaya, 1998; Tremblay, 2007). Moreover, STS movement is considered as the most biomechanically demanding movement than other ADLs, requiring lower limbs strength, range of motions at different joints and stabilising of HAT (Berger et al, 1988; Hodge et al, 1989; Huge et al, 1996).

The related work that target on why elderly adults are experiencing difficulties in STS can be allocated into the following two main aspects to demonstrate the determinant factors in STS performance: i). Deficit in physiological strength and range of motions and ii). Lack of postural control.

The biomechanics study on STS mechanisms is regarded as the most crucial subject of the literature review because without a thorough understanding on how the STS transfers are performed by different groups of humans, it is impossible to realise the key features should be extracted from the movement patterns, let alone recognise the STS intentions.

**i). Lack of lower limbs strength and range of hip flexion (physiological issues) ---- reflected by STS speed / lower angular momentum in sagittal plane**

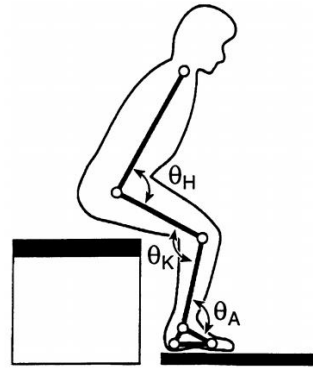


Figure 2.1 A simple biomechanical model of STS movement and in sagittal plane where the hip, knee and ankle ( $\theta_H$ ,  $\theta_K$  and  $\theta_A$ ), were configured as the angle between adjacent body segments (Lord et al, 2002).

The entire STS process can be described as 6 distinctive events through the measurement on ground reaction force (GRF). A test was conducted on 100 individuals to measure their GRFs under 4 possible postures (Etnyre & Thomas, 2007), in which average GRF (normalised to the percentage of body weight) were similar for the arms-free, arms-crossed, and hands-on-knees conditions in the 6 events: initiation ( $\approx 20\%$ ), counter ( $\approx 12\%$ ), seat-off ( $\approx 60\% - 70\%$ ), peak ( $\approx 116\%$ ), rebound ( $\approx 80\%$ ), and standing ( $\approx 100\%$ ), as shown in Figure 2.2. Note only vertical GRF is interested in the development of assistive robot chair because both Fore-Aft (longitudinal) and Lateral GRF are not in the scope of this study.

Under condition of hands-on-armrest, significantly less normalised GRFs were found comparing to other 3 conditions, especially in the event of seat-off.

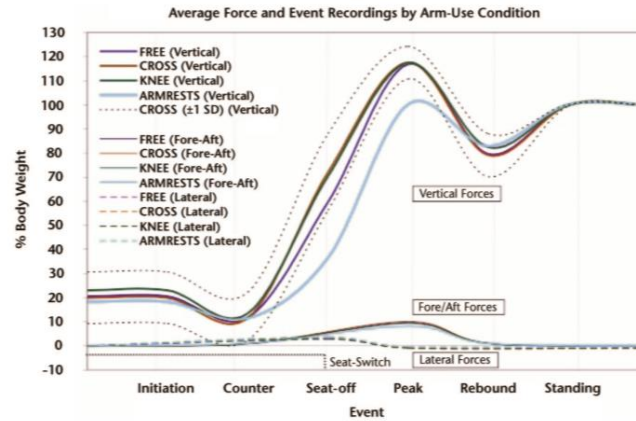


Figure 2.2 Distinctive events in STS through normalised GRF to the percentage of body weight  
(Etnyre & Thomas, 2007)

Table 2.1 Vertical GRF generated by able-bodied young subjects in corresponding STS events

Condition	Event					
	Initiation	Counter	Seat-off	Peak	Rebound	Standing
Arms free (AF)	20.6 (10.1) [7-60]	11.8 (10.2) [<1-53]	59.8 (9.7) [41-90]	116.2 (6.9) [104-140]	79.6 (6.7) [65-93]	100.0 (0.3) [99-101]
Arms crossed (AC)	20.0 (10.7) [2-60]	11.7 (10.6) [<1-56]	72.2 (15.9) [29-99]	117.0 (6.8) [104-139]	79.1 (9.0) [44-92]	99.9 (0.3) [99-101]
Hands on knees (HK)	23.0 (11.2) [3-60]	13.5 (11.2) [<1-56]	70.5 (18.1) [38-110]	116.4 (7.8) [103-142]	82.4 (6.7) [55-96]	100.0 (0.3) [99-101]
Hands on armrests (HA)	18.3 (10.3) [1-54]	11.5 (9.5) [<1-44]	36.6 (10.8) [8-69]	99.7 (6.7) [80-123]	82.9 (6.7) [69-101]	100.1 (0.4) [99-101]
Significant difference ( $P < .005$ )			HA < AF, AC, HK AF < AC, HK	HA < AF, AC, HK	AF, AC < HK, HA	

GRF has been a fever-topic and investigated by hundreds of research groups in the last decades. However, generalized standard is hardly achieved mainly because researchers tend to use their preferred measurement parameters and definition of stages. This might not be a huge handicap because when the on-chair measurement system attempts to deal with a familiar aged person continuously. After appropriate training procedure, an adequate model could be created eventually. This summarizes a resultant peak force measuring 118.7% of body weight, which clearly explains why a large amount of the elderly could stand still and walk without aided yet suffering STS problems. In the experiment on STS conducted by Etnyre & Thomas (2007), the 100 participants performed the STS movements when the sign of initiation was seen. It is noticed that each measurement was initiated by the direct view of the subject, where a consistent initiation (response) time were recorded. An improved triggering method might be in demand as a future work to limit the deviation of data. A detailed walk through on all STS events will be elaborated later in chapter 4.



The term STS speed is superficial but widely adopted by related work on STS movements of the elderly to describe the quickness of movement. It is also used as the criterion to assess the performance of STS transfers generated by the elderly (Yamada & Demura, 2009). The STS speed, in fact, is affected by a combination of physiological factors including above mentioned lower limbs strength, range of motion, postural control. In Lord et al.'s work, 12 subjects were selected with different level of physiological conditions. The reported study outcomes were mostly in consistent with the conclusions drawn by other studies (Yamada & Demura, 2009).

Strength training is highly recommended for those lacking of physiological capabilities. Functionally impaired elderly may regain strength of up to 174% after completing a strength training program. Personalised training regime is highly recommended to be well maintained in order to stay at the same level of motor function and encourage the regain of ADLs for independent living (Gross et al, 1998).

The seat height from which elderly subject is able to perform the STS transfer has significant influence on STS performance (Munton et al, 1981; Hughes et al, 1996; Schenkman, 1996). Transferring from a lower seated position is more biomechanically demanding in the sense of lower limbs strength, range of motion, and stabilisation. These make the determination of robot chair geometries (seat height, range of extensions) particularly crucial for the elderly with STS difficulties, hence are further elaborated in Chapter 3 with in-depth reviews.

In addition to the overall quickness of STS movements, the peak hip flexion velocity was measured to assess the performances elderly subjects generated with seat height purposefully varied (Demura & Yamada, 1997). In consequent, with the seat height decreased, the elderly subjects were observed to rely on more conservative strategy of STS with increased difficulty, along with decreased rate of success STS movements.

When performing STS movements, there are mainly 3 strategies used to control posture and body balance, including hip and ankle strategies, as well as the mixed strategy (Nashner and McCollum, 1985; Horak and Nashner, 1986). The hip strategy and ankle strategy are short for

ankle dorsiflexion strategy and hip flexion strategy, respectively. They were categorised in terms of which part of joint movement is more significant. Ankle strategy suggests an early and significant activation at ankle joints, unlike hip strategy where hip and thigh muscle play a more important role in the sense of generating the STS motion (Horak and Nashner, 1986). Although hip strategy tends to minimise muscle efforts when achieving the same amount of COG raise, proved by the monitoring of muscle activation, the functionally less capable elderly commonly suffer from hip trunk flexion issues that will significantly hinge the movements of hip joints, known as limitations of the movements. The use of different strategies is not only determined by the individual's physical conditions, but also postural goals and environmental constraints, for example the support surface and the height of seat (Kuo and Zajac, 1993).

However, separations of these strategies proposed by previous studies are arguable when being analysed through in-depth EMG examination on joints in sagittal plane (Runge Et al, 1997). Because many current studies explained the two strategies in STS transfers, hip and ankle, as compensatory strategies where the elderly trades off between both, regarding their own physiological conditions. According to latest research findings, more hip strategy tends to be used to counter-balance the limited range at ankle dorsiflexion. Hence when sufficient ankle dorsiflexion is available, less hip flexion is required (Rocha et al, 2015).

**ii). Lack of postural control (balance impairment and psychological issues)---- More efforts in terms of stabilising the HAT in STS movements.**

Apart from the significantly less GRF value and slower speed in STS transfers compared to that of the young people, the elderly are also discovered to spend extra efforts in terms of stabilising the locomotive ADLs (STS and gait). In contrast, able-bodied adults perform STS with little conscious effort needed to accomplish these movement patterns (Riley et al, 1997; Kaya et al, 1998). This phenomenon is further explained with anticipatory postural control (Klous et al, 2011), which is however out of the boundaries of this study.

Owing to the loss of balance, more than one third of the elderly living in community care

homes will fall or are at high risk of fall when performing STS transfers (Perry, 1982; Rubenstein et al, 1994). Comparisons were made between STS capable elderly and those elderly who suffered from STS difficulties due to bilateral vestibular hypofunction (BVH), the most typical balance-impairment among aged adults (Kaya et al, 1998). Suffering from BVH, the elderly may need to take a further corrective step sideward to regain balance after completing STS transfer (Riley et al, 1997). Although the elderly with BVH showed no significant deficits in lower limbs strength, the captured linear vertical momentum and GRF, were found significantly lower than the control group in this study. The subjects with balance impairment were suggested to avoid excessive momentums (both lateral and longitudinal) that may cause substantially increase of fall risks (Kaya et al, 1998).

The human body is inherently unstable because it involves the small support area, high center of mass, and multi-joint features. Voluntary movements to handle the instability are known as anticipatory postural control with the help of postural muscles. The further demonstration on this can be seen at (Massion, 1992). These voluntary movements are performed readily by able-bodied healthy elderly, but can be particularly difficult for the elderly with balance-impairment.

Most of balance-impairment owned to syndrome of post-fall, which can psychologically affect the elderly and worsen the postural control regimes by means of retropulsion. This stabilising disorder will result in a tendency to fall behind without compensation reactions, which is used by the capable elderly to restore balance (Riley et al, 1997; Médéric et al, 2004; Mak et al, 2011). Figure 2.3 shows how a subject is affected by retropulsion during STS transfer where his balancing fails to counteract the falling back motion and position his HAT (upper torso) to antepulsion postures.

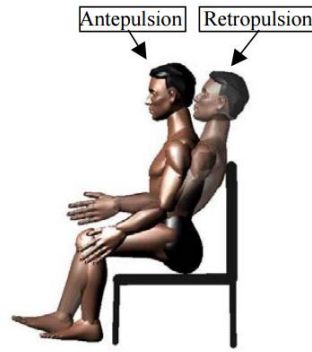


Figure 2.3 The Antepulsion and Retropulsion postures appearing in the initiation of STS transfer  
(Médéric et al, 2004)

Momentum strategy is often used by the able-bodied young adults in STS transfers as it uses the compound movements generated by the entire low limbs with upper body stabilisation. In contrast, the functionally impaired elderly use a stabilisation strategy (Schenkman et al, 1996) which may explain why the former finish STS movements significantly quicker.

M.M.Gross et al deployed the crucial factors that substantially affect the STS performance of the elderly. Significant weakness in hip and knee extensors were spotted, which are mainly caused by reduction in strength generated by lower extremities. Motions were captured in a sophisticated way using Motion analysis system (Motion Analysis Corporation) AMTI force plates as well as Electromyographic devices mounted on several muscle groups. This combination accommodated the acquirement of maximum torque around the lift-off (seat-off) instant at various crucial points, including hip extensor, knee extensor as well as ankle dorsiflexor. The maximum moment occurs shortly after lift-off from the chair, roughly 60 degree of knee angle.

The maximum torques at knees, buttocks and ankles are generated at the instant of buttocks separation from seatpan (seat-off), with the only physical contact becoming the feet against the footmat. Again, as previously mentioned in experiment setup, all seated movements are preceded under hands-free conditions. When designing the chairs for community uses, the seat height that lower than the knee level should be avoided, which would require higher momentum and longer distance to travel during STS movements for the elderly.

Also, to the best of related work suggest, few comprehensive analysis of the arm-supported STS transfer in healthy adults has been accomplished. The main reason is the lower limbs motor functions are more interesting when it comes to improving the unaided STS performance in the long run.

### 2.2.3 Commercial available assistive devices

Towards solving these STS problems, a wide range of assistive devices are introduced to the market, including the following categories, i). Standing-up frames, ii). Electric lift chairs and iii). pneumatic lift chairs. Critical reviews are presented after the demonstration of each device to illustrate the limitations, other problems might be induced and the potential latencies.

#### i). Standing-up frames

Standing-up frames are generally low-cost and widely adopted by most of the elderly whoever has difficulties in STS transfers. It has its main advantage of versatility because it assists the STS transfer from almost any seat surfaces. Also, as its name suggests, some of the frames can be used as sturdy walking frames to help the elderly with the outdoor ADLs.

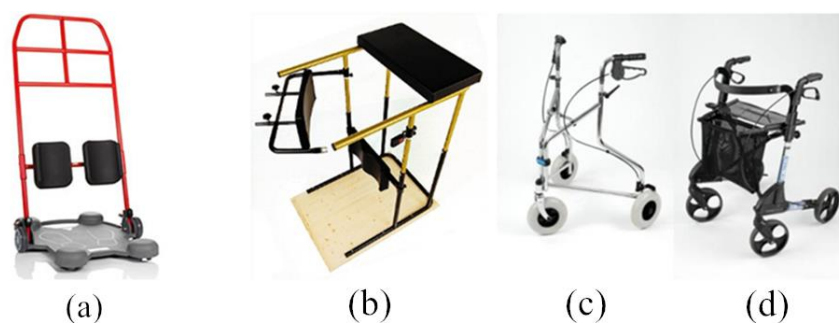


Figure 2.4 Variations of standing frames: (a) ReTurn7600 (SystemRoMedic, 2012); (b) Standing frame (Praschberger, n.d.); (c) Three-wheeler; (d) Four-wheeler (Rica, n.d.).

The first two variants of standing-up frames shown in Figure 2.4 are solely designed to provide STS assistance, offering stationary support whereas the rest two also supports walking and can be used as shopping carts. The first two variants, (a) and (b), are widely adopted by care-homes

and needed to be operated by specialised carers because the locking mechanisms have to be activated or released manually. This means the users can never be left unattended without carers around. Once stepped on the frames with knees against the knee pads, the users are not allowed to step off and must be transported by carers.

The last two variants, (c) and (d), are also known as walking frames from which the users not only receive STS aid but also walking aid. However, the extra walking assistance functions are not in the scope of this study because as previously explained, some elderly with functional declines are able to bare their BW and walk but still suffering STS problems. The walking frames require users to hold the braking level at the handle to activate the locking system prior to the STS transfer. This is regarded as a potential hazard especially in the events when the elderly forget to activate the braking mechanisms they will lose the balance entirely and fell with the walking frame.

In general, when applying the standing-up frame, users need to hold it with their upper limbs to lift-up the entire body. Sharing a similar concept with lift-up grab handles in disabled toilet, standing-up frame serve its purpose in aiding the subject to use his/her own motor function and rise from seated position. However, in the cases where their upper limbs are weak or the seats are too low, the users will have to ask their relatives or health care professionals to either give them a gentle pull or adjust the height of the frames. Even for those with capable upper extremities, using the standing-up frames excessively will accumulate pressures on other muscle groups that not meant to participate in STS movements, such as deltoids and triceps. After a prolonged period, the users may be confronted with shoulder risks and complications, suggested by Bromley (2006).

## **ii). Electric lift chairs**

Presently, there exist plenty of Electric lift chair manufacturers on the market, among which the market leading brands as suggested by disabled world are Pride lift chairs and Golden technologies (Disabled world, 2010). Disabled world is an organization that provides information and news to the general public and disabled people (Disabled world, 2010). Other

Electric lift chair manufacturers include La-Z Boy, Med-Lift and Maxi-Comfort. Electric lift chairs generally service home-use purposes but not limited to. This type of device can be easily integrated into a wheelchair (Aubert, 1987; Fontecchio, 1990) or automobile seat (Zalewski, 1991).

Market available lift chairs deliver all its functions manipulated by a control panel (Figure 2.5). The chair, acts like an elevator, moves back and forth to itself end points without virtual interaction with the user. It seems to be a ubiquitous solution to the elderly from the first glimpse. However, such chairs can hardly change how much assistance they provide regarding to users with different size and physiological condition.



Figure 2.5 Commercial available Electric lift chairs: (a) Restwell Seattle Intalift (Motionhaus, n.d.); (b) La-Z-Boy AVENGERluxury lift chair in operation (La-Z-Boy, 2010); (c)Pride C-30 in operation (U.S Medical Supplies, 2012)

However, two major problems and one hazard are highlighted to raise the awareness of those in need. Admittedly, Electric lift chairs enable users to perform STS motion easily with manual controller. These chairs are controlled manually by the subject seated and can merely provide fixed amount of assistant within the end-points. Comprehensive analysis suggests that most of lift chairs fail to offer sufficient muscle resistance exercises (Gross et al, 1998).This causes their physiological conditions to deteriorate faster especially when they become undue dependent on the chairs for standing up.

Moreover, latency may be induced by these electric lift chairs. As it can be seen in Figure 2.5 most electric lift chairs are operated using controller with a cable attached. This may develop an electric shock hazard as one was reported where the cable had got caught in the moving metal frame of the lifting mechanism without the awareness of the chair user. The Electric lift chair has operated repeatedly over a period of time until the outer insulation of cable peeled off, causing short circuit between power supply and the metal frame (Markowitz, 2012). The developed hazard, even though was recovered in time, could have killed the couple involved. In addition, even those advanced lift chairs with blind operating buttons may still have problems. Buttons being touched without conscious could cause an unwanted lift for the elderly. Also, functional failure due to fatigues or contaminations of the switches could also be a potential risk, especially under this circumstance abundant ADLs including drinking and eating are expected to be done while user seated.

### **iii). Pneumatic lift chairs**

As a low-cost alternative to electric lift chairs, pneumatic lift seat assists are promoted. Without the need of batteries and electricity, these seats can be easily attached to a bed or chair. The power of lifting stroke can be regulated by selecting the level of weight resistance. But, without professional clinical analysis, the user will never know the exact amount of lifting he/ she actually needs. The manufacturer claims the product will be activated with the user leaning forward and “acting as if he is getting up” (Stuffseniorsneed, n.d.), shown in Figure 2.6. This will become the most severe latency because the chair seat lift comes with no perceptive (sensory) system built-in, the lifting motion is very likely to be accidentally triggered, especially when the user needs to change the sitting posture by leaning forward. Besides, attaching this pneumatic device to existing chair will inevitably increase the seat height, which may have adverse influence on the elderly in ADLs. Additionally, using a gas spring to capture motion and store the energy, this device requires large amount of power every time the subject sits back. It can be particularly difficult for the handicapped elderly when the device has not been used for a while in which gas spring may become stiff.





Figure 2.6 The pneumatic chair seat lift (Stuffseniorsneed, n.d.)

These commercial available devices seem to solve the problem to some extent. However, being operated completely manually to move back and forth to its end points like an elevator, the systems fail to provide an appropriate level of assistance to the user in order to fulfil his/her actual need. Instead, in most of the cases, it is an overkill solution towards the STS problem in the sense of users always receiving the maximum output the lift chair could possibly generate. It could eventually be detrimental to the health conditions of the elderly if they excessively rely on lift chairs. In Gross et al's study, a guideline was proposed that effective strength training regimes for the hip musculature is necessary to maintain the STS ability of the elderly (Gross et al, 1998). This may further aggravate the functional decline of the elderly adults who spend too long in chair with increased disc degeneration or spine stiffness (Galumbeck, 2004).

The changes in motor function and body configuration of the user are not considered when designing these lift devices. Since the system is not able to adjust its output accordingly to overcome the user's changes in STS performances. In extremities, these lift chairs are providing inappropriate assistance, which could which could discourage potential condition improvements and actually worsen the condition of the user. Besides, in the circumstances when users have substantially gained their own BW, they would have to purchase a new lift chair of larger size to adapt to this change.

## 2.2.4 Experimental assistive devices

### **i). Standing frames**

Either based on or inspired by the previously demonstrated off-the-shelf assistive devices, a wide range of experimental prototypes was developed aiming to assist the STS movements using different approaches. At present, the prototypes involve powered walking frames, actuated lift chair/ seatpan powered by electric or pneumatic actuators, functional electric simulation (FES), and autonomous wearable robots. This taxonomy is based on the platform itself regardless of the sensing and assistance techniques implemented, which will be elaborated later in Section 2.2.

As briefly illustrated before, this type of protocols aims to provide the STS transfer assistance purely at upper torso, inspired by the off-the-shelf standing frames. Note some standing frame protocols may have the possibility of aiding the gait process after STS transfer from chair, which is not discussed here as it is beyond the scope of this study.

Médéric et al, (2004) aimed to tackle the STS problems from the aspects of postural control accompanied with risks of falling back. The study has successfully utilised the measurement at arm handles to compute the actual required force to apply to the subject through the STS movement. The assistive force was provided via two actuators mounted in parallel position onto the cantilevers of the standing frame protocol, as shown in Figure 2.7.

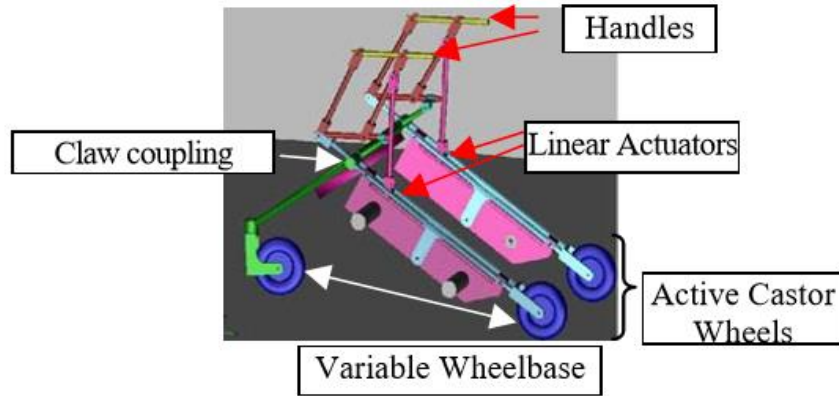


Figure 2.7 The EJAD Standing frame inspired by the assistive motion provided by care givers when aiding STS transfers (Salah et al, 2013)

Another standing-frame-based protocol, EJAD, was developed by Salah et al with a motorised 2-degree-of-freedom (2-DOF) robot arm controlled by soft computing techniques (Salah et al, 2013). It was inspired by the assistive motion that provided by the carers and aimed to imitate such motion shown in Figure 2.8. This typical motion proved by carer in helping STS transfer can be summarised as: Initially, a carer approaches the older user with 1. forward-back movement. The completion of assistance is provided as a compound movement with force generated at 2. hip joint, 3. shoulder joint and 4. wrist joint. Owing to the sensor fusion system (further explained in Section 2.2.2) and the computation of adaptive neuro-fuzzy inference systems (ANFIS), the EJAD managed to assist the older user throughout the STS transfer motion with the personalised level of assistance.

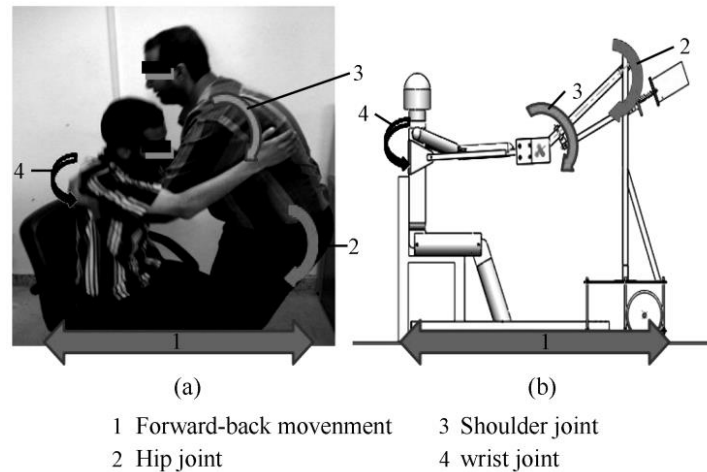


Figure 2.8 The EJAD Standing frame inspired by the assistive motion provided by care givers when aiding STS transfers (Salah et al, 2013)

## ii). Powered lift chairs

In the lifting chair designed by Bae & Moon (2010 & 2011), the mechanism aim to lift the seat at a certain angle using gas-spring actuator, rather than rise up the entire seat horizontally, as illustrated in Figure 2.9. The sensing techniques implanted in Bae & Moon (2010 & 2011) is further demonstrated in the later sections.

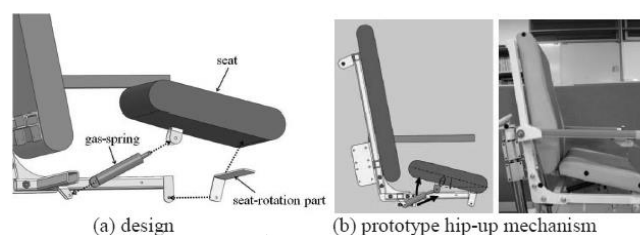


Figure 2.9 The lifting chair prototype with hip-up motion (Bae & Moon, 2010 & 2011)

The SIT & STAND™ assistive chair developed by Galumbeck et al (2004) featured a unique design with an electric actuator that is able to lift the main frame of the chair according to the length of the lower limbs of the subjects. When assisting the STS movements of the subjects, the front frame of the assistive chair can automatically fold down gradually to enable the feet of the subject to move backwards to a more posterior position. The effectiveness of this lift chair protocol was proved by 7 elderly individuals who experienced different kinds of

difficulties in STS in a clinical study. However, this assistive device failed to recognise the actual deficit in the strengths and range of motion of the subjects in order to generate adequate level of assistance.



Figure 2.10 The Ejector chair developed by (Munro et al, 1998) with the user seated and preparing to perform assisted STS movement

When performing assisted STS movements, subjects were positioned with their buttocks as far back as possible on the seat, their back resting against the backrest of the chair to establish a standard experimental condition (Figure 2.10). Each subject was verbally instructed to stand using a natural rising motion. Munro et al has used a self-rating system for the subjects to estimate their own efforts made to complete the STS transfer as well as the pain level experienced using the rating scale proposed by Borg (1970) and Huskisson (1974). However, the selection criteria of subjects were based on a group of elderly with rheumatoid arthritic problems who were actually capable of performing unaided STS transfers.

An assistive stand-up robot is developed featuring 3-DOF motion and advanced control algorithm (Kamnik & Bajd, 2004). This prototype can be recognised as a hybrid type with which the subject is able to perform STS with the seatpan and standing frame providing assistance simultaneously. In this work, an innovative data fusion framework has been built up

which integrates sensing data acquired from seat, arm, feet reaction force sensor and Infrared markers (position capture). Early experimental stage as it might be, the robot successfully detects subject's intention with the integration of sensory data from multiple channels, which will be expanded in the next sections.

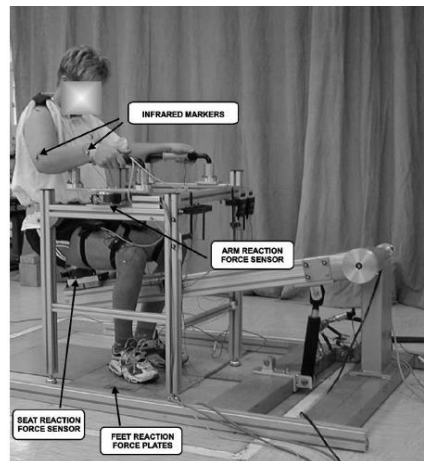


Figure 2.11 The standing up robot equipped with integrated sensor networks (Kamnik & Bajd, 2004)

### **iii). Functional electric simulation (FES)**

Confirmed by (Barrett et al, 2009), functional electrical stimulation (FES) has been recently recognised as an effective routinely (long-term) treatment towards functional regain for adults with paralysis or significant strength deficits caused by multiple sclerosis (stiffened muscle tissue) because of SCI. FES activates the nerves in affected muscles by exerting small electrical impulses directly onto targeted nerve system so as to assist the locomotive ADL of both STS and walking for the paraplegic subjects (Lynch & Popovic, 2008).

An example of study incorporating FES to assist the elderly SCI patients in STS movements was conducted by (Hussain et al, 2014) with a successful simulation on a 3D body segments model of one degree of freedom (considering single joint movement at knee joints). The FES targeted quadriceps muscles group with the response to both natural activations exerted by the subjects and FES passive activations.

FES, however, is an intrusive technique that is not suitable for the home-use scenario in this study. Furthermore, this remedy only helps STS movements of those who suffer from lower limb paralysis caused by spinal cord injury (SCI) because it emulates the way how human brain controls the muscles (Lynch and Popovic, 2008). It is clearly not applicable for the elderly who are able to activate their lower limbs muscles however not able to perform STS owing to the deficit in motor function of muscles.

#### **iv). Autonomous wearable robots**

The autonomous wearable robots, also known as exoskeleton devices, aim to follow the human motion trajectories when performing STS movements. Some are capable of delivering assistance-as-needed according to the actual movements performed by the subjects. The Purposefully designed exoskeleton devices concentrate on different muscle groups: upper limbs (Kiguchi & Hayashi, 2012), lower limbs (Jamwal et al, 2014; Taslim et al, 2014) and the entire body (Tsukahara et al, 2010).

A wearable robot was developed by Jamwal et al (2014), aiming to provide strength the range of motion exercises for subjects with ankle injuries like sprain. This ankle-based Exoskeleton robot has incorporated lightweight but powerful pneumatic muscle actuators (PMA) in the design to emulate the movement of skeletal muscles.

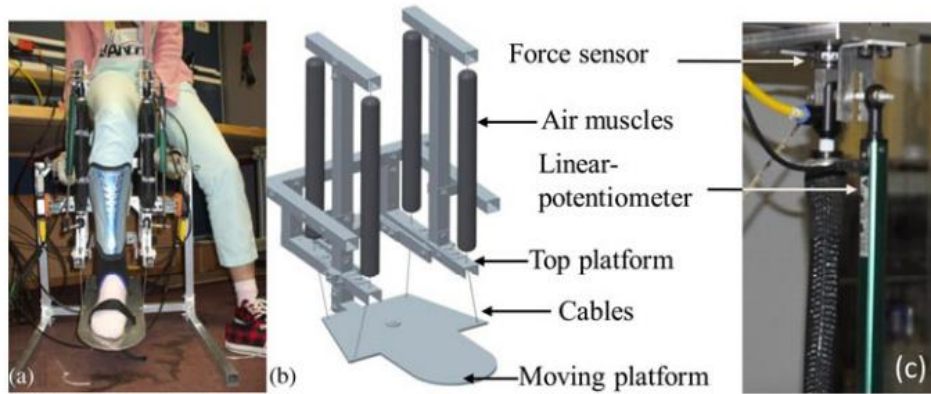


Figure 2.12 Wearable ankle robot proposed by Jamwal et al (2014) (a) Robot in use after construction. (b) 3-D solid model of the final concept. (c) Positions of force sensors and linear potentiometers.

A complete wearable assistive device named PAL has been developed (Tsukahara et al, 2010) which harnesses the entire mechanical as well as the complicated mathematical modelling on geometric parameters in locomotive movements, including STS transfers.

These assistive devices mainly target on incomplete and complete paraplegic patients which are not discussed in the content of this research. However, the concept of exoskeleton robot has its significant contributions in terms of rehabilitating lower limbs motor functions (joint(s) motion and strength). The HRI relationships are achieved as though the actuators are orthosis of human bodies.

### 2.3 Sensing techniques for human-robot interactions

The objective of intention recognitions implemented by the related work are summarised as: improve the sitting habits from posture wise (e.g. Tan et al, 2001; Xu et al, 2012), utilising the extracted intention to drive assistive devices (e.g. Yokota, 2009). This part is then followed by a critical analysis with adverse effects and problems might incur when applying these techniques and the reasons why they may not be suitable for this study.



### 2.3.1 Introduction of HRI

The fundamental paradigms of human-robot interaction (HRI) can be epitomised as: physical interaction and cognitive interaction on the basis of home-use proximate scenarios (Breazeal, 2004). The physical interaction between chair user and robot chair is achieved by the seatpan, seat back footmat as well as the lifting mechanism of the chair, which is demonstrated in Chapter 3. The cognitive interaction is carried out through the extraction of useful features on users' on-chair behavioural patterns and the implications (manifestations) behind. Sections 2.2.2 and 2.2.3 introduce the related work on the feature extraction techniques.

### 2.3.2 A variety of on-chair sensory implementations

The taxonomy presented here is purely allocated by the genre of sensing techniques themselves, regardless of the computing algorithms used. Note some studies have incorporated more than one sensing channel (technique) to fulfil the requirement of HRI, which is known as sensing fusion (e.g. Kamnik & Bajd, 2004; Tao et al, 2007; Bae & Moon, 2010; Salah et al, 2013).

#### **i).Force plate approaches**

#### **ii).Flexible sensing approaches**

#### **iii).Miniature sensing approaches (IMUs, Force transducer, Binary sensors)**

#### **iv).Optical (camera) monitoring approaches**

#### **i).Force plate approaches**

Yamada & Demura, (2009) successfully confirmed the relationships between GRF and STS stages by combining a power platform Gravicorder G5500, also known as stabilometer. The experimental setup incorporates a sheet switch system to capture the hip separation from chair. This helps identify GRF value at the moment when subject's buttock leaves the bearing surface. The work separates the entire STS process to three phases, i) from the initiation to seat-off, ii) from seat-off to the appearance of peak GRF and iii) from the peak GRF moment to the completion of STS movement. This research has its significant in terms of justifying the correlation between GRF values at different phases and level of physiological lower limbs

motor functions as well as the falling risk of the elderly.

A multichannel force platform manufactured by Kistler (Kistler, Switzerland, type 9281B) was used in the work of Munro et al (1998) to capture the reaction force in 3D, namely, vertical, anteroposterior (as shown in Figure 2.10). and mediolateral, generated by each subject. The force plate was placed in front of the assistive chair prototype to avoid force interferences.

## **ii).Flexible sensing approaches**

In the study of manipulating a motorized wheelchair with the patient's own upper body inclination (Yokota, 2009), inexpensive pressure sensing films are mounted on the seat pan and seat back respectively. The sensing system contributes to recognise the behavioural pattern where the shifting of COG can be extracted, implying the patient's degree of indication. In addition, by moving upper body back and forth the user can drive the wheelchair along longitude direction, while leaning left and right functions as a steering wheel.

However, the pressure sensing films applied in the study of Yokota suffers from poor resolution issues which might not be a concern when it comes to mapping the behavioural pattern of users into the direction of the wheelchair prototype (Yokota, 2009).

As shown in Figure 2.13, a haptic sensing chair equipped with BPMS (body pressure measurement sensor) flexible mats from Tekscan is introduced in capable of classifying the sitting postures into a pre-defined model, termed as an Eigen-posture space (Tan et al, 2001), also known as pattern recognition. Such a classification has a reported accuracy of 96% for the "familiar" subjects when fitting up to 14 Eigen-postures, including leg crossing, slumping, leaning, etc. However, for those who haven't used the system before, the accuracy would drop to 79%. However, when investigating the minimum distance from posture space method, the accuracy could still reach 93% encapsulating 1st & 2st choice of posture. It is speculated that when applying to the home based assistive chair, the training data can be continuously gained from the aging couple. Another scenario is presented as an input device for computer games. The sensing chair approach as a dynamic interactive input device to manipulate computer

games can be pivotal from the perception point of view. The control signal is thoroughly retrieved through occupant's position, movement and weight shifting, indicating subject's intention (Tan et al, 2001). However, with a system cost at approximately 2000 GBP, current BPMS sensors can hardly be applied on home-based assistive chairs.



Figure 2.13 BPMS mats placed on chair (Tan et al, 2001)

### **iii).Miniature sensing approaches (IMUs, Force transducer, Binary sensors)**

In the work conducted by Tanimoto (1998), an evaluation was conducted through the study of pressure distribution on 5 types of commercial available cushions, which are dedicated to relieving the pressure sores mainly experienced by patients with spine cord injuries (SCI). The measurement was conducted pressure films mounted on seatpan. The device used in this study has a spatial resolution of merely 16x16 mm. Although more generous resolution could be obtained with other more advanced devices, the results were considered valid because the research interest was mainly on identifying areas (of interest) of risk for developing pressure ulcers rather than the specific pressure values. Both the amplitude of excessive pressure points and the area of substantial pressure concentration were extracted through pressure pattern.

Besides, as an affordable alternative to BPMS, another study on posture classification is carried using merely 4 force transducers (Schrempf et al, 2011). With the help of biomechanical model of seated person, Schrempf et al used a simple biomechanical model to estimate and measure the lumbar joint moment, flexion/extension angle, foot-support, force acting on the foot-

support and back rest usage using four force transducers embedded in an office chair. This was done aiming to develop future posture guidance algorithms in order to improve office worker sitting behaviours.

Another project that uses a converted arm chair is the SenseChair project by the Massachusetts Institute of Technology. It is an ordinary armchair fitted with pressure sensors in the seat, armrests and seatback. This chair is also fitted with vibration motors, lights and speakers in order to provide a variety of “personalities” to the elderly. The chair uses a pattern of motor vibrations, light oscillations and sounds to help an elderly person sitting in the chair. For example, if the elderly is sitting in an ergonomically uncomfortable position, the chair would vibrate using the embedded motors to alert the elderly. If the elderly is unsettled, sounds could be used to soothe the elderly so that he or she falls asleep. Using the time of the day, the chair could wake the elderly up to go to bed for a more comfortable sleep whilst using its light to illuminate the room (Forlizzi et al, 2005). Investigating the on-chair sensor with vibration feedback clearly shows some significance. Since although in some occasions sedentary behaviour for the elderly is inevitable, it is advisable for the elderly to shift positions from time to time in order to encourage blood circulation and reduce stress on the lumbar. This could be done through dynamic seating in which the chair senses the changes in the posture of the user in real time and give feedback to the user in order to encourage changes in position or exercises.

Similarly, researchers fitted a normal office chair with 7 force-sensitive resistors for posture detection and 6 vibrotactile actuators for haptic feedback as shown in Figure 2.14 (Zheng & Morrell, 2010). The vibrotactile actuators were miniature pager motors enclosed in a housing resulting in a low cost feedback system. By providing feedback via the vibrotactile actuators, they were able to guide people sitting in a chair to a correct posture. It was discovered in their study that after the vibrotactile feedback was disabled without the subject’s knowledge, the subjects still continued to sit in a correct upright or near-upright posture. These findings suggest that the use of haptic feedback is an effective way of providing the human sensory-motor system with correction cues or commands.

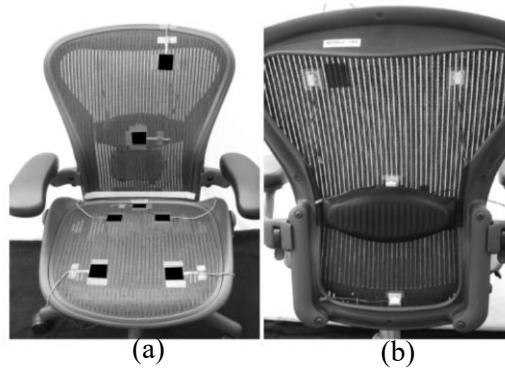


Figure 2.14 (a): Placement of the 7 Force Sensitive Resistors (b): 4 vibrotactile at the back of the seat  
(Zheng & Morrell, 2010)

As an even more simplified approach, to classify the sitting patterns into 9 defined postures, Xu et al (2012) used 7 binary valued force sensors attached to a causal office chair. These binary valued force sensors can be functioning properly once the applied forces trigger the threshold. Similar to others studies, cover sheets consisting of 64 binary sensors are placed onto the cushion and seatback respectively. Novelty could be found in the classification methods used in the study. Several naïve Bayesian classifiers are integrated into a hybrid cascade structure. The first stage is defined as coarse classifier, only the sensors mounted on seat pan are taken into account, providing a relatively rough clue of classification. Later on, seatback sensors take their role as fine classifier, computing the final judgment. The reported accuracy is achieved by 82.3%, confirmed by cross-validation. With merely 6 subjects selected for the entire training procedure, the sample pool is considerably low (Xu et al, 2012).

Inertial measured sensors (IMUs) are another genre of wearable miniature sensor for the compact in size and light weight. It is aimed to solve both stationary and dynamic problems of high complexity. The components of a typical IMU include accelerometer, gyroscope and magnetometer to capture angular speed, linear acceleration as well as spatial position (Lin et al, 2010). The IMUs generally require easy setup and calibration, which makes tracking human motions particularly handy. The applications of IMUs are known as non-affecting rehabilitative body segments tracking solutions, which can be seen from work of (Tao et al, 2007; Zhou et al, 2008). A parallel setup, namely IMU motion positioning system and camera 3D sensor, was incorporated by Tao et al (2007). This camera-based monitor was used as a motion reference

system to verify the 3D positioning measured by IMUs after corrective algorithms. The credibility of employing IMU system was assessed in this manner. Rooted mean squared errors (RMS), coefficients and nonparametric tests have proved that both systems have generated similar results.

From the EJAD assistive standing frame developed by Salah et al, two IMUs were attached to the trunk and leg of the subject so as to capture the motions during STS transfer (Salah et al, 2013). This IMUs sensory system was used in conjunction with an infrared camera and a foot-based force sensor plate to present a multi-channel sensory system for motion capture.

The following related work on STS research makes use of Electromyogram (EMG) capture system as a manner of signal extracting from the actions that the subjects performed but may not directly link or contribute to STS process for understanding the effort experienced by the subject.

Bae & Moon (2011) successfully matched the EMG signal to the extension of knee joint during STS transfers. Dry-type active electrode (DE-2.1, Delsys Co.) was used to collect anioigst signals from subjects' rectus femoris muscle. This largely contributed to determination of assistance level offered by the hip-up mechanism, shown in Figure 2.9. The effectiveness of the lifting motions provided to the subjects was also confirmed by EMG, in contrast to the figures gathered at the initial position.

Kiguchi & Hayashi (2012) used the EMG signals obtained from 16 positions to understand the level of assistance required by the subject in various upper limbs movements.

However, how exactly can EMG be harnessed to assist the research has long been a problem due to different physiological conditions of subjects. Lee et al (2008) has attempted to solve the challenge of relating the captured EMG to the actual joint moments in STS transfers, which is explained in Section 2.3.2.

#### **iv).Optical (vision) monitoring approaches**

The optical approaches commonly used in monitoring STS movements are in the form of reflective (Infrared) sensing (with markers attached on subject body, as shown in Figures 2.10 and 11) or optical camera. However, the motion capturing system solely relies on vision sensors may suffer from focal length and lens distortion. These problems can be attenuated with an appropriate environmental setup and calibration process, or the usage of other sensing channels, such as inertial (IMUs) sensory system (Randeniya et al, 2008) and EMG sensors (Bae & Moon, 2010 & 2011; Taslim Reza, 2014).

The motion capturing system developed by Salah et al (2003), VICON, utilised 8 infrared (IR) cameras with LEDs bands as emission device. The emitted IR light was reflected by various makers attached to the hip, head, trunk, leg, and ankle of the subject. This, in conjunction with the use of IMUs, formed a sensing fusion system that is capable of monitoring as well as measuring features (accelerations and torques) of trunk flexion, momentum transfer, hip joint extension, movement stabilization.

Taslim Reza et al (2014) used an inexpensive camera-based motion capturing system Kinetic, developed by (Microsoft, 2010). It features an innovative depth information which would normally require a transformation algorithm from 2D to 3D. Such system is known to be well suitable for indoor environments as it performs well even with poor illumination. The system captures STS movements which can be difficult to achieve with the usage of single channel EMG measurement (Figure 2.15).

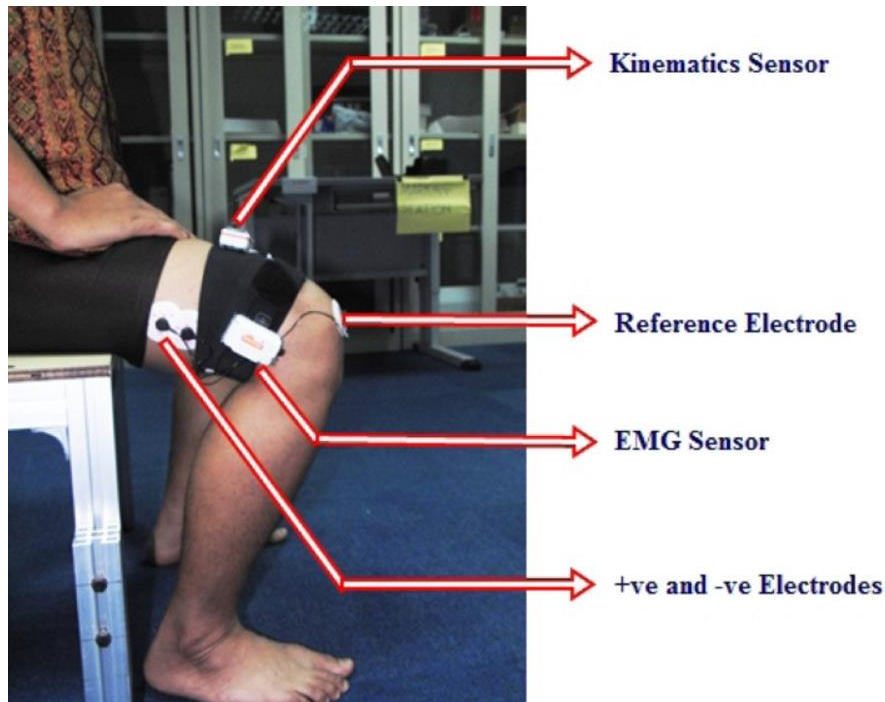


Figure 2.15 A hybrid sensing system incorporating vision sensor as well as EMG sensor (Taslim Reza, 2014)

Claus and his fellow researchers took the advantage of an optical tracking system to investigate the STS spine postures (Claus et al, 2016). Unlike other studies on STS postures, they stressed on the three postures defined by sagittal plane spine angles at thoracolumbar and lumbar spinal, specifically. Spontaneous Gender differences were up to 1/3 the magnitude of posture differences (in terms of angles in sagittal plane) from 10-minute measurement tests on STS conditions.

### 2.3.3 Critical analysis

Japanese researchers (Yamada & Demura, 2009) successfully tackled this problem by combining a power platform Gravicorder G5500, also known as stabilometer, to justify the correlation between GRF and level of physical activity as well as the falling risk of the elderly. Later on, comparison was also made between healthy young individuals and the elderly to identify the difference in STS movement. Consequently, the study suggests that GRF has a strong bond with physical activity ( $|r| = 0.27-0.28$ ). Falling risk is a sign of decreasing in ambulatory and balancing ability, which was found significantly correlated with GRF ( $|r| =$



0.26–0.41). Consequently, the STS movement speed and the stomping force of the elderly were indicated to be considerably slower and weaker than that of the young.

The force plates used to acquire GRF by the studies so far, e.g. Kistler type 9281B and Gravicorder G5500, come with the systematic costs well over 2000USD. Not only it is a high-cost solution of GRF caption, the thickness of the force plate was omitted by the researchers, which will clearly affect the actual seat height from which the STS performance was investigated (Munro et al, 1998). As suggested by another work using the identical force plate, type 9281B, the thickness was measured at 150mm (Franklyn et al, 2008).

Besides, the other components of the reaction force, anteroposterior and mediolateral (lateral in horizontal plane), which can be measured by the expensively built force plates, has significantly less correlation with biomechanical STS performance, according to the recent researches standardisation of GRF in STS transfers (Etnyre & Thomas, 2007; Yamada & Demura, 2009).

Aside from the well-known privacy issue it might induce, the main drawback of incorporating a vision motion capturing system is that most of the experimental setups have to be fixed and calibrated each time before usage (Moeslund et al, 2006).

The Tekscan flexible pressure sensors from Tekscan, are widely used in biomechanics research for the sake of its capability of yielding pressure measurements of high resolutions on complex surfaces. Although they are generally manufactured at a high precision level, extra caution should be taken when using these pressure sensors to evaluate the pressure at different contact area. The typical accuracy of Tekscan pressure sensors have reported accuracies ranging from 5% to 27%, which could be effectively reduced to 1% with the filtering algorithm applied (Drewniak, 2006). Moreover, the accuracy of BPMS is significantly affected by the curvature of measurement surface (Tekscan). Generally, a high curvature of sensing surface is prone to incur errors.

However, the main reason flexible sensing was not adopted in this study is its expenditure. The cheapest variation in BPMS series, CONFORmat 5330, costs in average of 1300 GBP, according to the quotations offered by UK suppliers. The cost of sensor matrix itself is affected by the number of sensing elements, known as Sensels, ranging from 1024 to 16128. However, the entire systematic solution typically costs well over 10, 000 USD, including the sensing matrix, readout electronics and software (Yip et al, 2009).

As IMUs are built with 3-axial gyroscopes as well as 3-axial accelerometers, the the properties of micro-electro-mechanical systems (MEMS) are inevitably inherited. Inaccuracies caused by drift effects and accumulation of erroneous over time. The error will accumulate because the spatial positioning is derived through computation of the sensory outputs at all axes at certain duration of measurement time. The integration of the measurements of gyroscopes and accelerometers requires precise analogue algorithm to compute. This sees a difference in characteristics between navigation grade IMU and low-cost IMU (Randeniya et al, 2008).

Due to the intrinsic characteristics of IMUs sensor, the spatial positioning accuracy (in world coordinate system) can be rather poor without calibration or effective corrective algorithms, hence this inertial sensing technique is often used in conjunction with camera-based (visual) tracking system to enhance the robustness (Tao et al, 2007; Randeniya et al, 2008). This type of inertial sensory system may also suffer from other issues caused by the experimental configurations. For example, the movements of the targeted muscle tissue itself may affect the initial measurements performed by IMUs and such error will accumulate when it comes to a multi-body-segment positioning measurements (Tao et al, 2007).

For some applications with the use of a single camera, the error generated in a 2D image measurement will significantly affect the systematic accuracy when it is necessary to reconstruct the 2D visual system to a 3D scene (Tao et al, 2007).

EMG monitoring system has been widely adopted by related studies (Bae & moon, 2007; Taslim Reza, 2014) for its capabilities of gathering sub-conscious signals throughout STS

transfers. However, the ideas of using EMG and 3D are not practical for a lifting chair, especially for the home-based ones that serve multi-users as in STS detection applications it requires the signal to be captured from subjects' rectus femoral muscle.

## **2.4 Machine learning technologies for intention recognition**

Regarding to the nature of interactivity, the assistance provided by this chair robot should be comfortable and acceptable to human whereas robots should be able to study and familiarise with specific human behaviours. However, in spite of the big advancement in sensory techniques, present robots are still struggling to benefit from its merits simply because of the challenging in cognitive capabilities (Dautenhahn, 2007).

This cognitive interaction is stressed here as it provides the ability to recognise the intentions or implications of certain human behaviours that are difficult to be parameterised (modelled) using conventional mechanical and mathematical knowledge. Machine learning, also well known as soft computing, has long been used to tackle with inherently complicated problems. The machine learning methodologies are demonstrated with related work on STS movements (locomotive ADLs) or other inspirational applications.

### **2.4.1 ANN and time series prediction**

Artificial neural network (ANN) has been on fever for the recent decades on movement classification (identification) as well as time series prediction. Related work involving a wide variety of applications can be seen at areas such as water flow forecasting (Wang et al, 2007), wind mill power prediction (Saroja and Aggarwalhas, 2014), glucose level monitoring (Zeccin et al, 2010), life span prediction of gearbox (Tian and Zuo, 2010), financial time series prediction like stock market and foreign exchange rate (Kuan and Liu, 1994; Brezak et al, 2012). Only a walkthrough of these ANN applications is presented here whereas the structure and training of ANN are thoroughly demonstrated in Chapter 6.

Time series predictions with ANN have also played crucial roles in representing complex relationships between its inputs and outputs in human locomotive ADLs movement prediction (Zhang & Zhu, 2004; Zhang et al, 2005).

As one of the forerunners who successfully employed ANN on STS study, Gioftsos and Grieve (1996) developed a classifier that is able to recognise whether the subject has experienced lower back pains during STS transfers. The network used the forces and COPs at knee and ankle, as well as the lower back movement trajectories as inputs, in order to compute a binary output (lower back pain or not). To test the performance of this ANN classifier, 36 subjects with different physical conditions were invited to conduct a cross-validation test with one of them after training process undertaken by the rest subjects. The study has a reported accuracy of 86.1%, which was encouraging compared against the classification results provided by professional physiotherapists.

By using GRF features as the inputs of ANN, Zhang et al, (2005) were able to accurately (>97%) identify the type of activity as well as predict the speed of walking and running after effective training process.

Unlike the other related work on using FES to assist STS movements, Zhang & Zhu (2004) has developed a robust ANN-based controller to deliver the appropriate signals according to the movement conditions. The  $\theta_h$ ,  $\theta_k$  and  $\theta_a$  representing the angles at hip, knee and ankle, respectively, were used as the input variables of the ANN. Through effective training, the ANN was able to generate PWM signals targeting on several lower limbs. Such system was evaluated through the efforts of upper limbs that can be reduced when performing STS transfers.

Su et al (2013) concentrated on a three DOF exoskeleton arm that uses the users' upper limb motion to assist STS movements. Although this is a different approach to overcome STS difficulties, the ANN modelling has its novelty in terms of computing the assistance-as-needed through STS movements. The assistive motion was provided through harmonic drive transmission which offers precise positioning of the exoskeleton harness. However, the control

process was complex owing to the unknown parameters of the harmonic drive and its oscillation characteristics.

An ANN model was developed to bridge the captured EMG signal with the moment at knee joints during STS movements (Lee, 2008, October). The network in use is inherently a feed forward network (FFNN) with exogenous EMG values as input. The work was validated with the corresponding knee moments acquired through kinematic measurements at certain EMG values with two systems performing in parallel configurations.

Tian and Zuo (2010) have developed an extended recurrent neural network (ERNN) incorporating Jordan recurrent network together with Elman recurrent network. The innovative technique was applied on the life span prediction of gearbox based on the experimental findings between usage conditions and year of failure, which has largely contributed to condition based maintenance (CBM).

Zeccin et al (2010) has conducted a time series prediction based on glucose data extracted through continuous glucose monitoring (CGM) in clinical environments. They combined conventional ANN together with first-order polynomial extrapolation algorithm, with ANN primarily served its function handling non-linear components of glucose data. Experiments have proved a significant advancement in both accuracy and time of prediction ahead, compared against the existing short-time glucose prediction techniques.

Kuan and Liu started an era of using ANN, including FFNN and RNN to investigate financial time series like foreign exchange rate and stock market (1994). The study successfully optimised the suitable network based on the performance criteria. They confirmed different networks achieved varying results dealing with various exchange rate series. Brezak et al, (2012) have validated the capability of both FFNN and RNN for handling financial time series using benchmarking Mackey-Glass non-linear chaotic test series. Applications of implementing ANN on foreign exchange rate prediction can also be seen at related work from (Yao et al, 2014; Oancea & Ciucu, 2014).

However, the generalisation of has been the most challenging concern when training the ANN. A properly formed network that is suitable for training data with very satisfying performance may suffer overtraining (overfitting) issues with test data. Hence efforts have been made to mitigate this with different techniques, which will be further expanded in Chapter 6.

A comparison model among Bayesian regularisation (BR), early stopping (ES) and no-stop training has been developed with the variance being the ratio of training sets over the number of weights (Wang et al, 2007). ANN was constructed aiming to predict hydrologic variants of several rivers through different training approaches. Unlike other related work which often uses MSE to verify performance, a particularly seasonal adjusted coefficient of efficiency was introduced as evaluation index. When ratio between training sets and weights was lower than 10, both BR and early stop outperform the early stop training however little credit could be given to separate the both. When ratio was above 20, BR outperforms the rest two in most cases. When such ratio exceeded 50, no overfitting was observed albeit network gave poor results. It was also discovered that early stop training shown an incomparable training speed against the rest two. ANN was later extended to enable a 1-to-5 time steps ahead prediction, BR and ES training generated similar results through same performance measure. However, the performance of early stop approach was found to be inconsistency hence was not used in the multi-day-ahead prediction.

#### 2.4.2 Fuzzy logic system

As to the exoskeleton robot developed by (Taslim Reza, 2014), fuzzy controller was designed to deal with the ambiguity of EMG signals. The status of STS movement was used gathered. The two exacted variables, EMG signal and acceleration angle were used as the fuzzy controller inputs. The output of such controller was the status of the motor, namely, “anti-clockwise rotation”, “no rotation” and “clockwise rotation”. The combinations of both inputs established the following 6 fuzzy rules:

**Rule 1:** If Acceleration angle = “Low” and EMG readout = “Negative High”, then actuator output is “Anti-clockwise Rotation”.

**Rule 2:** If Acceleration angle = “Low” and EMG readout = “Low”, then actuator output is “No Rotation”.

**Rule 3:** If Acceleration angle = “Low” and EMG readout = “Positive High”, then actuator output is “Clockwise Rotation”.

**Rule 4:** If Acceleration angle = “High” and EMG readout = “Negative High”, then actuator output is “Clockwise Rotation”.

**Rule 5:** If Acceleration angle = “High” and EMG readout = “Low”, then actuator output is “No Rotation”.

**Rule 6:** If Acceleration angle = “High” and EMG readout = “Negative High”, then actuator output is “Anti-clockwise Rotation”.

The corresponding truth values (weights) for all Rules were all set as 1 in Taslim et al’s work. The rules were constructed in a way that contradictory action (of the actuator) was avoided.

However, this work did not account the level of assistance the subject actually requires, as previously discussed. The level of assistance could be defined by i.e. the rotational speed of the actuator and the angle of rotation. The exoskeleton device was controlled with the desired direction of motor spinning according to the capturing of movements.

#### 2.4.3 Adaptive neuro-fuzzy logic system

As demonstrated before, although the functional electrical stimulation (FES) has its effectiveness in terms of improving the mobility of the lower limbs, the amount of stimulation amplitude to be applied has long been an issue because it is complicated to describe the relationship between the gain of error in (lower limbs) mobility and system output. The nature of this technique has hindered its usage in home-use conditions because a therapist has to be at present throughout the routine process of the treatment. However, the ANFIS algorithm harnessing the subject’s movement trajectory to control the FES shows encouraging results.

The FES treatment developed by Hussain et al for the elderly suffering SCI, has incorporated

a parallel system with ANFIS and proportional-integral-derivative (PID) controllers, as shown in Figure 2.16. The latter has a conventional fixed parameter design as feedback controller handling the difference between target (reference) movement trajectory in need and the actual one. Meanwhile, such difference and its derivative were fed into the ANFIS controller. When trained properly, the ANFIS controller is capable of learning the mapping between amount of stimulation required by the quadriceps muscles and the difference of knee movement trajectory needs to be generated (Hussain et al, 2014).

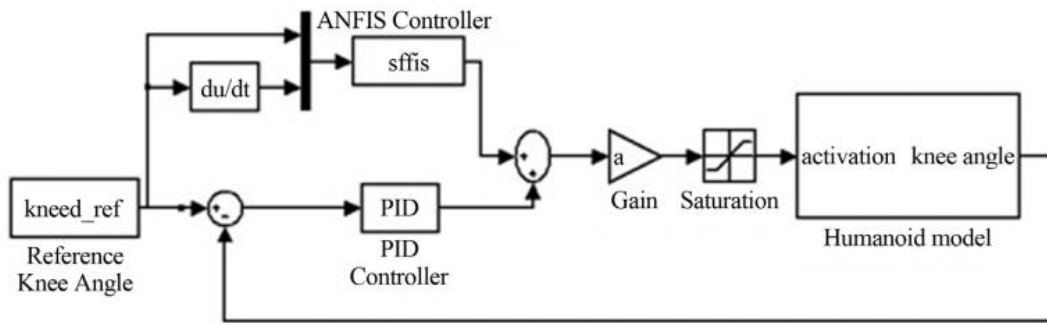


Figure 2.16 ANFIS-PID control system configuration developed by (Hussain et al, 2014)

This study has successfully coped with such a non-linear and highly complex system that is difficult to be mathematically modelled. This soft computing technology sees its advantage in non-parameterised fields or complicated environmental conditions with disturbances (Hussain et al, 2014) where traditional methods are difficult to model. Based on fuzzy logic system, it does not anymore require the knowledge of the designer or trial-and-error process. Instead, such relationships (parameters in membership functions) are obtained through the training process based on the obtained personalised mappings between inputs and outputs, which will be further elaborated in Chapter 5.

Consequently, through the comparisons with ANFIS alone and traditional PID controllers, this parallel ANFIS-PID control system has achieved the best results with reported errors of  $\pm 0.0873$  rad in terms of angular movement trajectory at knee joints. The overall performance of this parallel controller is considered to be better than the similar studies on the use of FES to assist STS movements, developed by (Zhang & Zhu, 2004) and (Abu Bakar & Abdullah, 2011).



Another ANFIS was prompted to handle the uncertainties and the geometric complexity, especially when used by subjects of different physiological abilities and biomechanical features (Jamwal et al, 2014). With the foot of subject placed onto the platform. Such a platform requires to be positioned by the actuator throughout the desired trajectories. ANFIS was adopted because this positioning of the platform is purely controlled by inflation and deflation of PMA (Figure 2.12) where traditional proportional-integral-derivative PID was not applicable. The output yielded by fuzzy controller is pressure value that needs to be applied, which is then converted into pulse width modulation (PWM) to control the pneumatic actuators. The experimental result was confirmed as the trajectories of motions provided were consistent to those generally adopted by therapist. With the help of fuzzy controller, safety actions are also provided so that the foot platform can be brought back to its initial configuration in time.

The effectiveness of applying ANFIS to control upper-limb exoskeleton was demonstrated by Kiguchi & Hayashi (2012). The construction of robot has seven DOF achieved by seven motors, which is particularly complex to control using traditional parametric modelling methods. The system utilised the joint angles of the subject, captured with either the encoders on the motors or the potential meters attached, as the inputs of the ANFIS controller. Through training with multiple subjects, the controller was able to manipulate the motors that need to be activated for the movement performed by the subject. Meanwhile, multichannel EMG signals were used to estimate the actual assistance-as-needed of the subject.

In Kiguchi & Hayashi's work, four levels of assistance were defined according to the assistance-as-needed with the minimal amount of assistance being merely a follow-through of the subject's upper-limb movements. The safety issues were also considered in the study. This was achieved from both algorithm and mechanical design with the former computing limitations on torque and speed according to the actual movements and the latter incorporating physical stoppers.

## 2.5 Summary

The chapter briefly introduced general STS problems and related physiological conditions of the aged adults. Later, how the reduced lower limbs strength and sensory capacity of the elderly will affect their STS transfers was thoroughly explained in the biomechanics of STS. More importantly, reviewing the biomechanical largely contributed to the design of the mechanical structure and lifting mechanisms of the robot chair.

Afterwards, the contemporary treatments were investigated, including market available assistive devices and experimental prototypes. The current off-the-shelf devices serve their functions to some extent but are problematic for many reasons. Especially, they have hardly adopted any sensors to help recognise or monitor the users' STS movements, albeit the majority of them incorporate actuators that assist the STS motion in a simple on-and-off manner. The efforts made by previous studies incorporated a wide range of sensing techniques, which were elaborated in a way which may inspire the come into being of sensors used by the robot chair.

To deal with the complexity of mechanical modelling of the systems, along with the actual STS movements performed by subjects, a series of machine learning techniques were used by the related work.

## **CHAPTER 3 THE DEVELOPMENT OF ROBOT CHAIR ASSEMBLY WITH INTEGRATED SENSING FOOTMAT**

The development of the chair assembly as well as its sensing foot prompts a platform to physically achieve the STS assistance. The essential features of movements can be also captured during the STS transferring process of the elderly.

### **3.1 Design of chair mechanics**

#### **3.1.1 Biomechanical concerns**

Kinematics of human biomechanical model for STS movement is taken into account when designing the structure of assistive chair, especially the seat height, tilting angle and endpoint of the assistive motion. Ng et al (2015) have proved the significant influence of seat height on STS performance of elderly female using five-time-STS tests, which is in line with the findings of other studies (Bohannon et al, 2010). In terms of STS strategies, the elderly would have to use more stabilising strategies in STS transfers from a lower seated position. Owing to a higher chair seat, the moments at knee level as well as hip level can be lowered up to 60% and 50%, respectively (Janssen et al, 2002). However, in order to validate the effectiveness of the assistive chair, the initial seat height should refer to that of general purpose chairs, such as office chair and those used for canteen sitting, reception waiting. These chairs are commonly designed considering human biomechanical model of human in chair to optimise the essential features like seat height.

It is also interesting that the anthropometric database defining optimal seat height shows demographic preference due to body configuration. The corresponding ranges are set as 430-510 (British standards), 420-540 (German standards) and 390-540 (European standards). Nevertheless, Korean database recommends an optimal seat height of 428mm for the elderly (Bae & Moon, 2010 & 2011). These are referred for different standards used by different countries.

The nature of optimal seat height is commonly set by popliteal height (PH) plus the shoe thickness. The corresponding PH of male and female elderly are 425 and 395 in mm (at 50<sup>th</sup> percentile), suggested by British anthropometric expert (Pheasant, 1998). Fifty-five Finnish elderly were asked to perform simple tasks at home to find out the most suitable seat height. A scoring system was introduced where ergonomic specialists and participants both gave the chair of 450mm the highest score at  $\alpha=0.05$  and 0.01 significant level (Kirvesoja et al, 2000). Nevertheless, similar study in UK suggests a height of 450mm is preferable by 100 elderly participants covering a range of physical capabilities (particularly in disabled elderly) (Gyi et al, 2004).

Thus, a seat height of 440mm is finalised in the actual design with a seat cushion of 30 mm in thickness mounted parallel to the ground. The opportunity of changing seat height could be achieved by simply replacing the seat pan cushion.

Tilting the seat with a certain angle is the key to help the subject substantially reduce the required muscular effort in STS movement. In the measurement of EMG signal for rising motion, an average peak signal of 50.34 mV was captured without lift assistant. When the participants were provided with lift angle of 14 and 21 degree, the average peak signal was reduced to 37.4 and 25.42 mV (Bae & Moon, 2010 & 2011). In reality the maximum lift angle of the robot chair is set as 22.8 degree considering the space constraints set by the chair structure.

The following specifications should be the foremost when carrying out the design of chair mechanics.

- The maximum tilting angle (MTA) can be reached by the lifting mechanics is 22.8 degree.
- The corresponding maximum rising height (MRH) is 87.78 mm.
- For safety reasons, mechanical stoppers are designed to ensure the end positions when MTA and MRH are reached

### 3.1.2 2D sketch and 3D CAD sketch

The chair structures have been constructed through computer aided design (CAD) and manufacturing process. Due to its unique structure and articulation functions, some parts of the chair frame require CNC machining. The 3D modeling of assistive chair is constructed with CREO Parametric 2.0, which can be seen at Figures 3.1, 3.2 and 3.3. The technical drawings are also generated by the software with manufacturing tolerances and notations, as shown in Figure 3.4. The sketch shown in Figure 3.8 is generated by Office Visio 2007.

In order to fulfil the design criteria stated in Section 3.1.1, a quad-pivot design is carried out so that both rising and tilting motions are provided. The quad-pivot structure is core part of mechanical design, which enables a lifting height and angle simultaneously. To follow the motion contour of the chair users' lower limbs, the combination of both rising and tilting motions is in demand. Synchronisation is assumed in the proposed chair where the relative time variants between each motion could be eligible owing to the time and expenditure boundaries of this study. Otherwise a linear mechanism serving vertical feeding and a tilting mechanism should be manufactured separately and controlled by at least 2 actuators.

On top of the quad-pivot a trapezoid structure is placed to support the seat pan, so that the top surface is parallel to the ground at the initial position, as shown in Figure 3.1 (b) and (c). The parameters in Figure 3.1 (a) and 3.2 (a) indicate the corresponding lengths of the 4 pivots together with the crucial dimensions in mm and the reference angle that controls the tilting motion. The orange lines in Figure 3.1 (a) and Figure 3.2 (a) represent the quad-pivot structure highlighted in Figure 3.1 (b) and Figure 3.2 (b). At the end position of the assistive motion, this mechanism provides the MTA of 22.8 degree, which can be seen in Figure 3.2 (a). This means the trapezoid structure is tilted at such angle, as seen in Figure 3.2 (b) and (c).

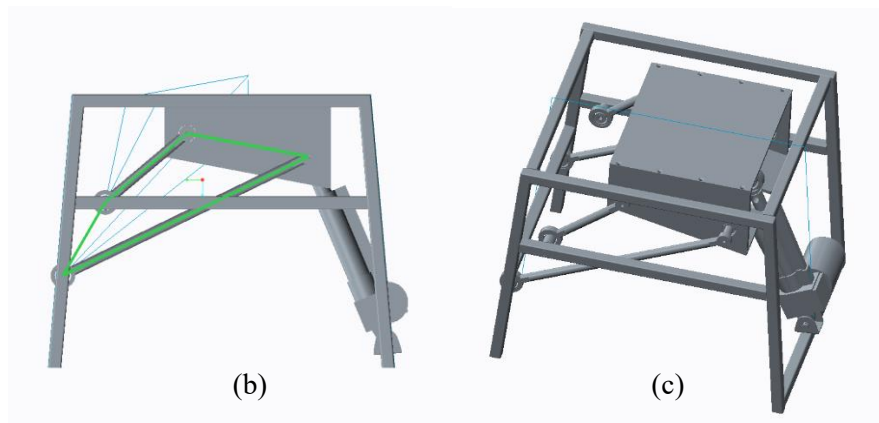
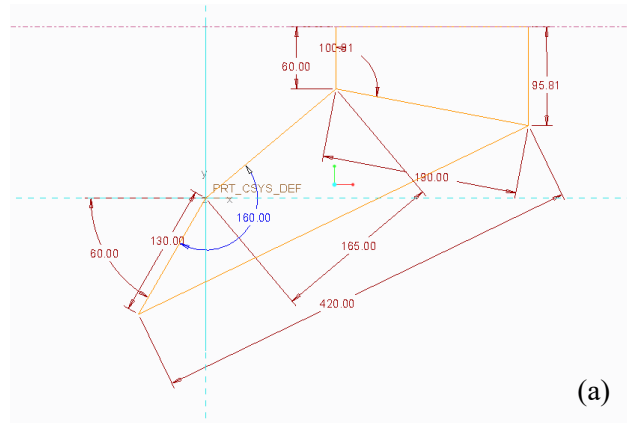
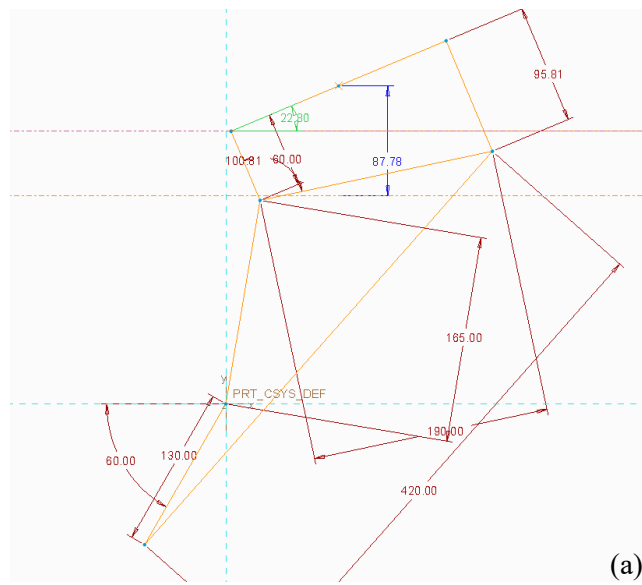


Figure 3.1 Initial position of quad-pivot structure (a) principle 2D sketch (b) side view of the chair mechanism (c) 3D view of the chair mechanism



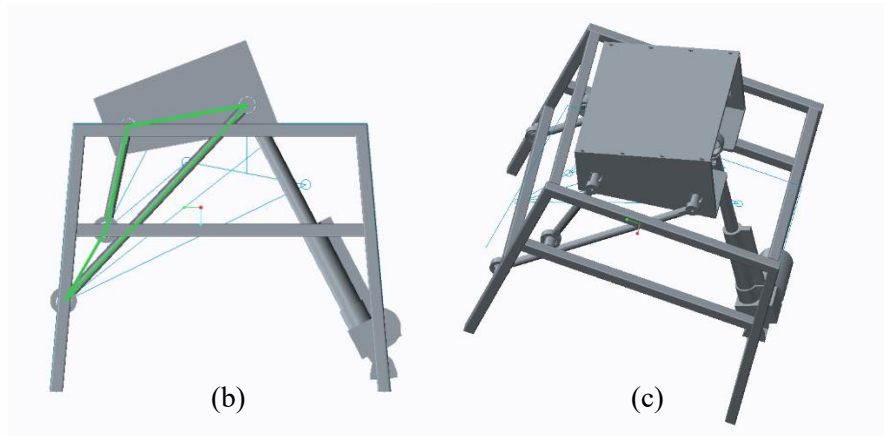


Figure 3.2 End position of quad-pivot mechanism (a) principle 2D sketch (b) side view of the chair mechanism (c) 3D view of the chair mechanism

The MRH is determined as 87.78mm, when the end position of lifting motion is reached. This will entitle the chair a maximum seat height of 527.78mm, This is still considered as a safety seat height by the above mentioned European standards while effectively assisting the elderly's STS movements. A seatpan is selected to provide sufficient support and confort. Eligible chair users will not experience huge deformation at the seatpan when the assistive motion is applied. The seatpan is fastened on top of the trapezoid structure with a 3D sketch shown in Figure 3.3.

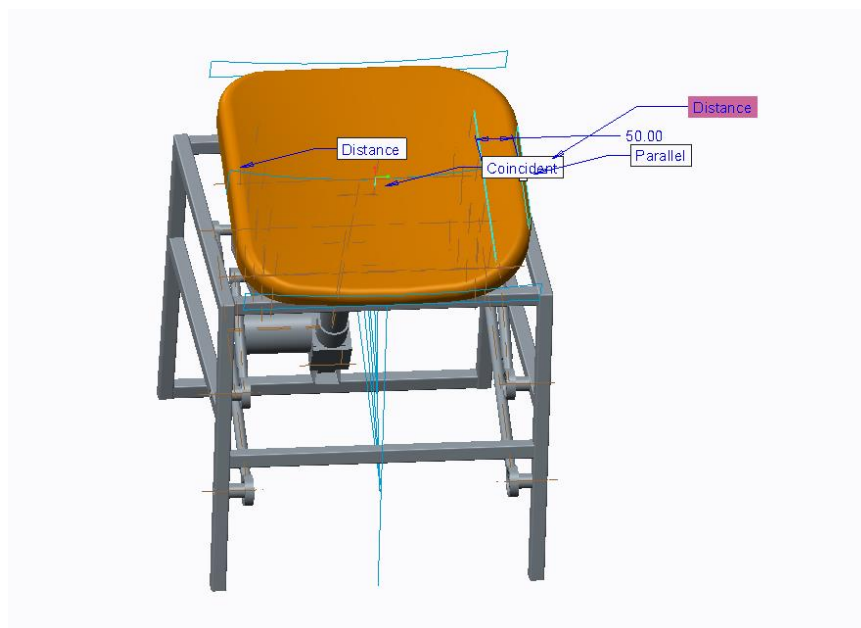


Figure 3.3 The placement of seatpan (graphics generated by CREO Parametric 2.0)

With tilting angle provided along with the raise in height, the subjects experience an easier seat-off transition than those high-chairs with the same designed seat height. Although there was no available elderly subjects with STS difficulties due to ethical concerns, 10 subjects with different demographics and biomechanical features were invited to test the lifting motion and describe the experience subjectively. Consequently they have reported a reasonably comfortable and smooth transition process with the lifting motion provided by the robot chair, where noticeably less effort from lower limbs is required during STS movements. This preliminary test was conducted in an on/off manner, regardless of the soft computing techniques introduced later. Note the purpose is simply to determine whether the travel of the lifting motion is suitable for the eligible chair users of different gender, height and physical conditions.

More importantly, safety concerns are achieved a combination of mechanical stopper and the accordingly adjusted lockout from the actuator side. Owing to the unique design of the quad-pivot mechanisms, the bearing housings on both sides will get in touch with the long rods (Figure 3.2),. This acts as a mechanical stopper as the rigidity of CNC machined alloy rods ensure the structure will not deform even with the maximum actuator power applied. The lockout of the actuator will be explained in Section 3.1.3. The combination of both, in addition to the high-level intention recognitions later used as safety precautions, introduced in Chapter 4 and 5, will provide a comprehensive and safety prioritised HRI for the chair users.

Afterwards, discussion has been taken place with veteran engineers to figure out the manufacturing difficulties appearing in the design of chair. This helps reengineering process with the functionality features retained. For instance, in initial model the side beam of the main frame was designed in a curved shape to realise the desired stability and ascetics. Feedback was given that it is hard to achieve unless the chair is going to be mass produced. Therefore, these beams were redesigned with a tilt angle of 95 degree respecting to the top rectangular structure to facilitate welding process, as shown in Figure 3.4.



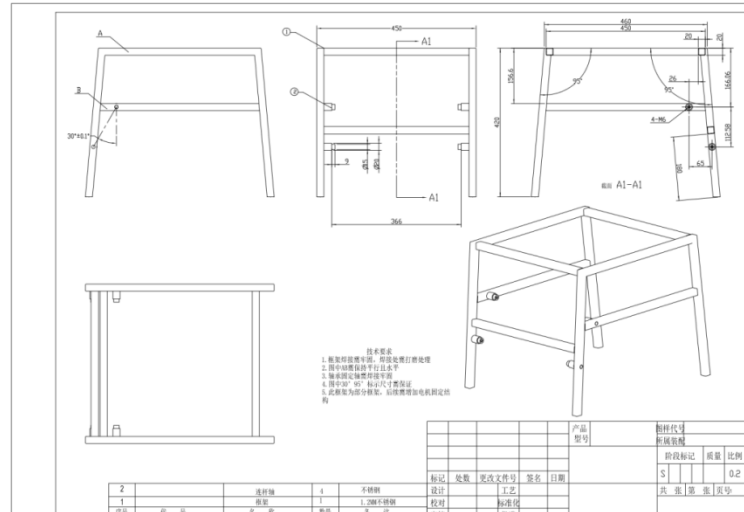


Figure 3.4 Technical drawing of the main frame

The mechanic parts of assistive chair were manufactured by Beijing Shizhi Hongyuan Technology due to cost-efficient. At first, the main frame was designed with aluminium to be as light as possible to facilitate overseas transportation. However, the factory had difficulties in welding aluminium beams together. The strength calculation was adjusted to stainless steel so as to minimize the net weight without sacrificing the functionality and robustness.

Meanwhile, when welding the main chair frame, one has to assure the stability considering possible thermal expansion, in that the chair will not wobble when the motor is in operation. This is particularly critical to provide a sense of security for the subject seated.

The backrest of chair is positioned similar to common office chair for the simplicity since no significant influence of backrest has been found by other scholars in STS studies (Janssen et al, 2002). Note in assembly process the backrest brace of the chair is bended in a way to make sure it does not interfere with movement provided by lifting mechanics, which can be seen in Figure 3.5.

Similarly, few researches have conducted on the influence of the armrest height and horizontal position respecting to seat height on performance of STS movement, albeit pressing on armrest can reduce up to 50% the moment on lower hip extension (Arborelius et al, 1992). Mount

adaptors are installed on both sides for future armrest replacement, in case adjustable armrest is in demand to verify such a determinant.



Figure 3.5 The final assembly of the robot chair mechanics

## 3.2 Design of sensing footmat

### 3.2.1 The sensing footmat

In order to extract the essential features without affecting the elderly users' STS performance, the following specifications of the sensing footmat were proposed.

- The sampling rate is set as 10Hz (refer to Section 3.2.2), which ensures that the obtained data will not omit the sudden change of GRF, indicating imbalanced STS transfers, the trend of falling back to seated position (retropulsion postures), etc.
- The design features a 7 by 8 matrix of FSR-400 sensing cells connected to 7 channels of analogue input of Arduino processing board via 7 multiplexers.
- A fixed 40mm cell to cell distance was set between adjacent FSR sensing cells. A spacer was attached underneath each FSR cell.
- The dimensions of the footmat are 294.68mm in width and 372.69mm in length (refer to longitudinal and lateral directions in Chapter 4). Based on such dimensions, the sensing

area is 280mm X 360mm.

- The main casing of the footmat was made by sheet steel after galvanisation.

On the basis of the above design specifications, a simplified schematic circuit design is carried out (Figure 3.6), followed by the structural design (Figure 3.7)

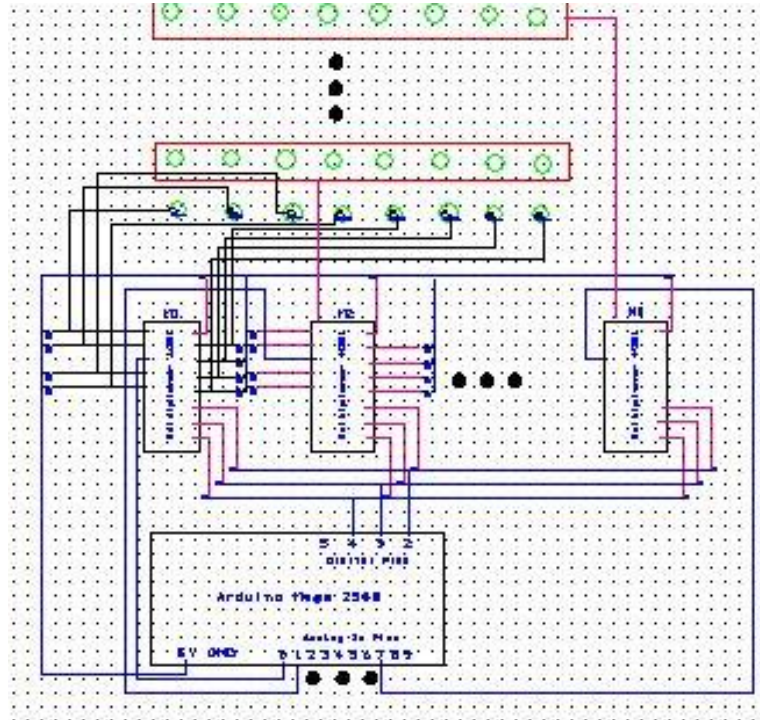


Figure 3.6 The schematic circuit design of the sensing footmat



Figure 3.7 Preliminary experiments on prototyping footmat with evenly distributed FSRs to test out the geometric layout and optimal number of cells

Based on the electric diagram, a simplified sketch of footmat is shown in Figure 3.8. In total

of 56 FSR sensing cells are individually labelled as F11, F12,...,F18,..., F78. Seven multiplexers are positioned accordingly as U1-U7, enabling 7 rows of sensing cells in parallel configurations. Port P1 is the channel of power supply. Considering the power consumptions of multiplexers and 56 sensing cells, it is not recommended having the power directly sourced from Arduino board. Hence a constant voltage of 5V was supplied from one channel of a power supply unit. The power is distributed to multiplexers, accordingly. In this way, the terminal voltage ( $V_{cc}$ ) at each FSR cell is ensured. The auxiliary ports, J1, J2 and J3 were created so that all digital inputs of all seven multiplexers are accessible without the need for disassembling the sensing footmat. This facilitates an easy verification if any problem occurs.

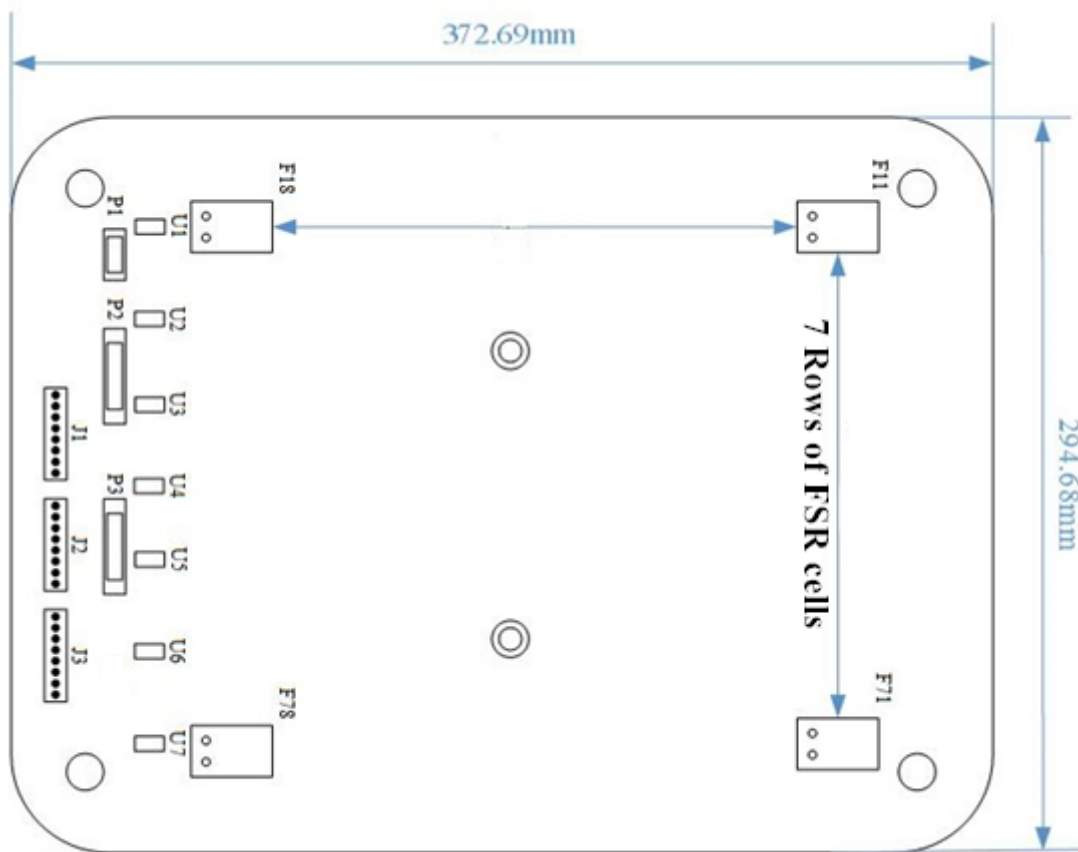


Figure 3.8 Construction sketch of sensing footmat (sketch generated by Office Visio 2007)

Thanks to the specifications, the designed footmat is able to fulfil the following design criteria,

- The primary goal of the sensing footmat should be precisely capturing the GRF values respect to the subject's body weight (BW). However as shown in Figure 2.2, the GRF curves also consist of transit peaks appearing at "counter" and "rebound" stages, the

sampling rate should be determined so that the complexity of the complete GRF curve is captured without omitting important information.

- The complexity of sensing matrix needs to be achieved for the reasons of two: the footmat should be able to i) precisely capture the change in centre of pressure (COP) and ii) reflect the contour of subjects feet for further exploitations. The reaction force should be purely exerted on the sensing cells. Otherwise with a rather sparse distribution of force-sensitive resistor (FSR) cells, circumstances where part of the subject's foot touches the non-sensing area will lead to significantly inaccurate results in GRF capturing. For the cost-effective reasons, the number of cell employed to fulfil the two requirements has been minimised. Therefore, the distribution of FSR sensing cells is confirmed as a matrix containing 7 rows of 8 cells, through prototyping experiments on the setup shown on Figure 3.7.
- The cell to cell distance was set close enough through the preliminary tests using prototype footmat. In addition to the usage of spacers under the sensing cells, it ensures no contact can be made between the chair users' feet and the non-sensing area.
- The dimensions of the footmat facilitate an easy placement of the eligible subjects' feet regardless of wearing shoes or not.
- The base of the footmat should feature a sturdy design. The contact surface with subjects' feet should not deform throughout the STS transferring process. This ensures the subject can perform the STS movements without paying additional attention to the existence of the footmat.

The final construction of the sensing footmat is shown in Figure 3.9.

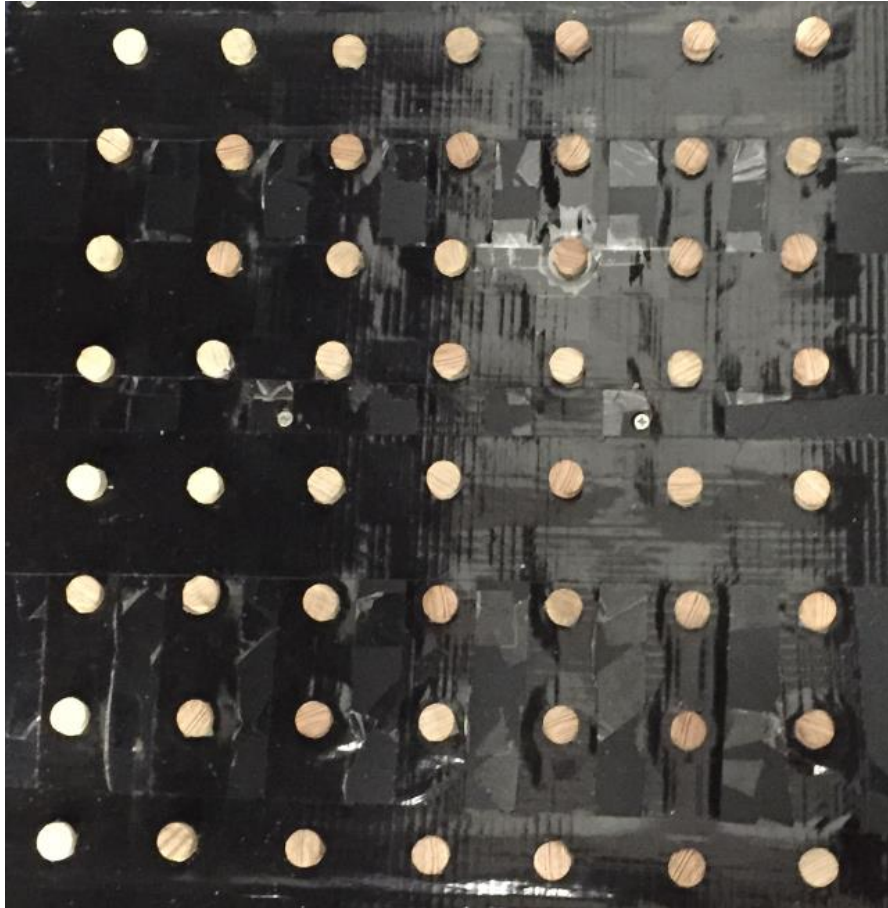


Figure 3.9 The sensing footmat that forms a robust structure to ensure robust force transition onto FSR cells

### 3.2.2 Data acquisition and software implementation

Arduino Mega 2560 is chosen as data acquisition (DAQ) module of the sensing system, which enables fast synchronisations between sensors and computer with simple IDE (integrated development environment) programming interface.

As shown in Figure 3.10, because Arduino Mega 2560 has merely 16 analogue inputs while 56 FSR cells are required, a set of 7 multiplexers CD4051B is introduced. With the binary rules applied, the input A, B, C on multiplexer are connected to the three digital inputs of Arduino, featuring a  $2^3 = 8$  channels of selection among analogue inputs. The Out/in pins of the 7 multiplexers, are connected to 7 analogue inputs of the Arduino, respectively. By that, one channel of analogue input on Arduino is able to collect the readouts of the 8 FSR cells in a sequential manner.



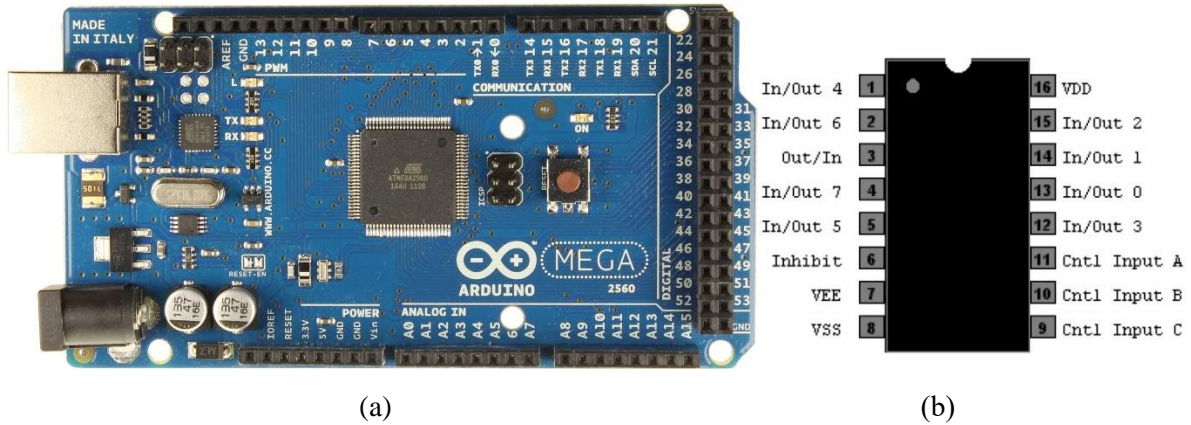


Figure 3.10 (a) Arduino Mega 2560 (b) Schematic diagram of CD4051B multiplexer

Figure 3.11 demonstrates the basic structure of a FSR sensing cell, the principle of voltage divider and the resistance-force characteristics provided by the manufacturer.

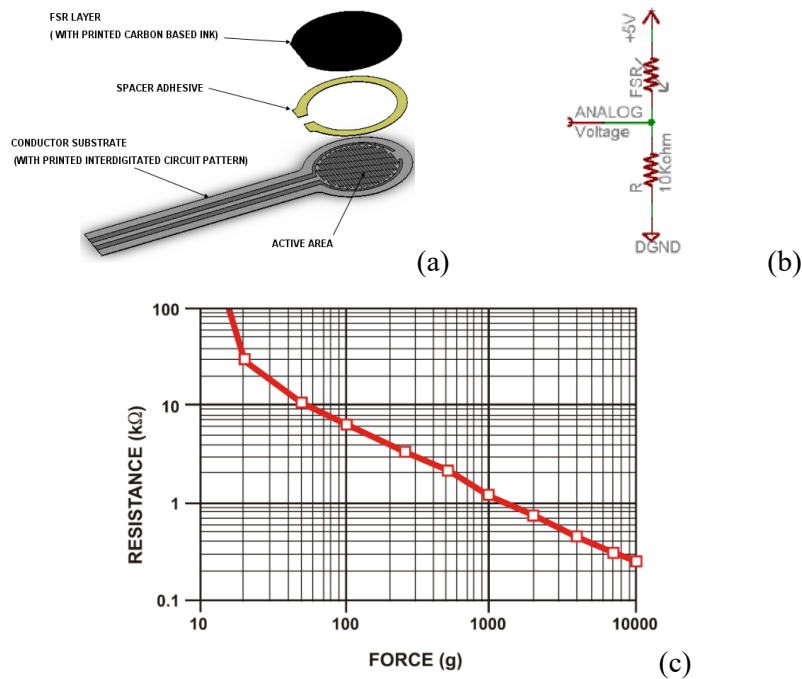


Figure 3.11 (a) Construction of FSR-400 sensing cell (b) Simplified voltage divider with FSR cell tied to measuring resistor (R=10Kohm) (c) Resistance-force characteristics of FSR-400 (Interlink electronics, 2006)

When collecting GRF values, the sampling rate should be properly determined. Because the desired GRF curves also consist of rather transit peaks appearing at “counter” and “rebound” stages, suggested by Table 3.1, the GRF curves of the complete STS movement should be captured without omitting important information.”

In Table 3.1, only arms free (AF) and arms crossed (AC) were investigated in this study. However, the transition time between counter and seat-off events is the shortest, with an average time of 0.28 seconds. From the previous knowledge, seat-off is the most demanding event of the all six, in terms of the requirement on subject’s lower limbs motor functions. This defines the upper limit of the sampling period, which must be smaller than 0.26 seconds.

Table 3.1 Average event times (Etnyre and Thomas, 2007)

Condition	Event					
	Initiation	Counter	Seat-off	Peak	Rebound	Standing
Arms free (AF)	0.28 (0.16) [0.10–0.85]	0.60 (0.18) [0.24–1.15]	0.88 (0.25) [0.31–1.42]	1.14 (0.23) [0.75–1.9]	1.65 (0.28) [1.11–2.43]	2.26 (0.30) [1.67–2.90]
Arms crossed (AC)	0.28 (0.13) [0.06–0.82]	0.61 (0.17) [0.26–1.18]	0.90 (0.24) [0.44–1.87]	1.14 (0.21) [0.71–2.03]	1.66 (0.28) [1.08–2.64]	2.19 (0.34) [1.38–2.99]
Hands on knees (HK)	0.28 (0.12) [0.12–0.79]	0.60 (0.18) [0.21–1.18]	0.87 (0.24) [0.43–1.85]	1.12 (0.22) [0.71–2.03]	1.66 (0.29) [1.04–2.49]	2.30 (0.31) [1.57–2.99]
Hands on armrests (HA)	0.26 (0.14) [0.05–0.85]	0.56 (0.19) [0.12–1.13]	0.82 (0.28) [0.24–1.55]	1.36 (0.32) [0.81–2.7]	1.64 (0.33) [1.03–2.8]	2.22 (0.35) [1.4–3.0]
Significant difference ( $P < .005$ )				HA > AF, AC, HK		

<sup>a</sup> Values are averages, standard deviations (in parentheses), and ranges (in brackets). Significant differences among arm-use conditions are indicated in bottom row.

However, the instinct downside of employing the multiplexers to expand the number of inputs is that a delay of data propagation should be taken into consideration. This limits the minimal sampling period. The limit of sampling is defined by the bandwidth of available analogue channels, which is restricted by the propagation delay of the multiplexers, 760ns (Texas Instruments, 2000). Therefore, the sampling period  $T_s$  is restricted by the upper limit and the lower limit, which is,

$$T_{lower} < T_s < T_{upper} = T_{event} \quad (3.1)$$

where  $T_{lower}$  suggests the delay of AD converter caused by the multiplexer,  $T_{event}$  is the duration of the shortest event in STS movements. For the computational reasons, the sampling period was finalised as 0.1 seconds, suggesting a sampling frequency of 10Hz.



### 3.2.3 Data processing

The primary goals of the data processing are 1) convert the collected raw data (serial) to GRF values, 2) normalise the GRF values with respect to subjects' body weights (BW). Based on the cell-wise force values, pressure patterns can also be obtained for further exploitations, referring to the implementations in Chapters 4 and 5.

A pre-processing block is developed prior to the following feature extraction step. In this block, framed serial output captured from footmat is collected through bridging between Arduino IDE and Matlab 2014a. As Figure 3.12 suggests, each line of serial data encapsulates the entire readouts generated by 56 FSRs, which is refreshed at the sampling rate. This resolution of 0.1s enables a fairly smooth GRF curve yet without triggering (interfering) the previously explained time delay issue brought by multiplexers.

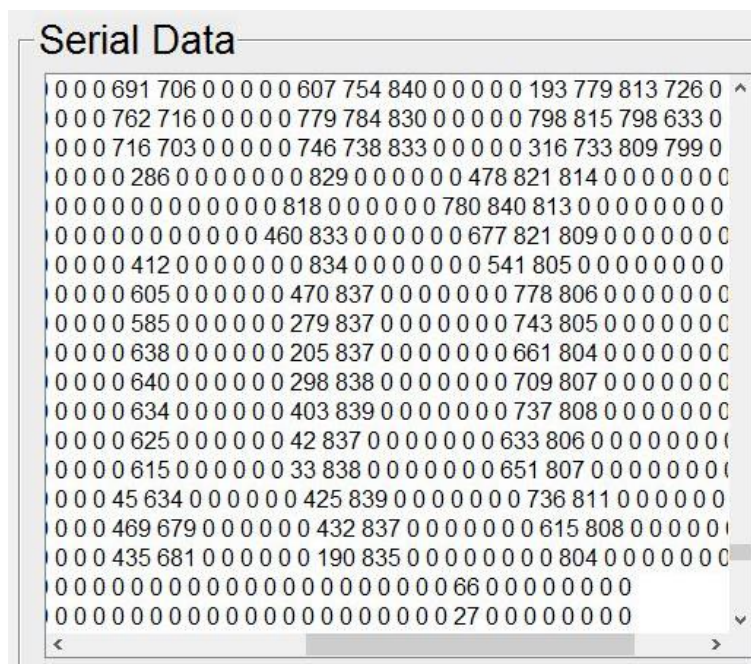


Figure 3.12 On-time serial output displayed on Matlab

However, initial measurements generated by footmat are considered inaccurate. This is proved by placing a fixed weight ranging from 100g to 5kg onto single cell, the derived measurement value varies from 2% to 20%. This clearly does not fall into the guidance claimed by

manufacturer instructions, which suggests the drift is expected to be less than 5% under a constant load of 1kg added for 35 days (Interlink electronics, 2006).

Therefore, an initial calibration process was arranged prior to the GRF capturing experiments. The calibration places 4 weights, 100g, 500g, 2kg and 10kg onto a random sensing cell. The calibration is valid under the presumptions that 1) the measurement readouts provided by single FSR has good repeatability, 2) multi-FSR will perform consistently under the same conditions, suggested by Interlink electronics (2006). The above two presumptions have also been approved by experiments.

The primary reason is discovered that in the initial setup the foam base board shown in Figure 3.7 will significantly deform with subjects stepping on it, resulting indirect force transition to FSR cells. It was also realised that systematic error was introduced by both feet stepping onto the non-sensing area. Because the initial design of the footmat attempted to trade off the resolution with sensing area in real-life scenario, considering in daily living, both feet of a seated subject are supposed to be randomly placed within a certain region in front of the chair. Also the amount of FSR sensing cells are rather fixed due to cost-efficient reason, the distance between adjacent two cells is set at 35mm.

The following Equations (3.2, 3.3 and 3.4) are introduced to achieve voltage-to-GRF conversion that minimises 1) operating temperature, 2) hysteresis, 3) drift effects of the FSR sensing cells.

Thus the GRF value was derived as,

$$GRF = \sum_{i=1}^{N_{activated}} F_{cell} \quad (3.2)$$

where  $F_{cell}$  is the force readout on each FSR sensing cell. In the summation of Equation 3.2, it counts the number of FSR cells being activated (under loads greater than the pre-defined threshold). This is added to the equation to attenuate the intrinsic problems of FSR cells.

Equation (3.3) depicts the voltage-to-GRF relationships of with the DAQ module which is derived from experimental result. Note such an exponential relationship is in line with the resistance-force characteristics provided by (Interlink electronics, 2006).

$$F_{cell} = \omega \times e^{-i\omega V_{out}} + Dev \quad (3.3)$$

of with  $\omega$  and  $i$  are resistance-related coefficients that are subject to changes as such characteristics vary upon the load durations, load area, operating temperature, hysteresis, etc.  $Dev$  represents the resistance-related zero order deviation. These coefficients are determined by initial calibration.

With the concept of voltage divider applied, the single cell readout  $V_{out}$  can be represented as,

$$V_{out} = \frac{V_{CC} \times R_{FSR}}{(R_M + R_{FSR})} \quad (3.4)$$

where  $R_M$  denotes the resistance of measuring resistor, which is 10Kohm.  $V_{CC}$  is the supplied voltage, which is 5V.

Based on the derived GRF value (Equation 3.2), the normalised GRF value regarding body weight (BW),

$$GRF_N = \frac{GRF}{BW} \quad (3.5)$$

of which the BW is measured as the average of GRF readouts at the standing event, recorded for a period of 0.5s.

Stem from the load on each sensing cell  $F_{cell}$  the pressure pattern of the entire sensing footmat was also derived through the reconstruction of sensing matrix (transforming single-row  $F_{cell}$  values to 7x8 matrix). Based on such pressure patterns, the other related STS features, such as change of COP in various directions and distance between both feet can also be acquired, which are further demonstrated in Chapters 4 and 5.

### 3.3 Actuation

Linear actuator was chosen to feed the desired motion at a controlled pace. These actuators feature a compact size which allows easily-fit within a confined structural boundary, as shown in Figure 3.13. A commonly seen market available rise-recliner chair takes approximately 12-20s to achieve the entire movement.



Figure 3.13 Limited space for the actuator

As to the robot chair, the requirement on stroke time depends on the actual STS time finished by the elderly and the time before they start to sit back when they struggle in STS transfers. However, two aspects, the length of stroke and the actuation force, were taken into account when selecting eligible actuator.

- The length of stroke, 126.1mm, determined by the structural design of the chair, set the requirement for the extension of the linear actuator.
- The maximum actuation force has to be delivered to ensure a smooth and consistent lifting motion. The maximum actuation force required by the system, denoted as  $F_{act}$ , appears at the initiation of the lifting motion thanks to the designed structural configuration (Figure 3.1). In this position, actuator has to be capable of delivering sufficient force to bare the whole BW of the chair user. Hence, the calculation as below was carried out,

$$F_{act} = \frac{F_{Load} \times K_c \times K_s}{\eta} \quad (3.6)$$

in which the  $F_{Load}$  consists of 2 components, the BW of the subject and the upper mechanism (including seatpan), 85kg and 9.75kg are taken respectively, referring to the maximum allowed BW of eligible chair user and the weighted lifting mechanism with seatpan mounted.

$K_c$ : the equivalent gravity centre with respect to the rotation point, referring to the bottom left joint of the quad-pivot shown in Figure 3.1 (b). However, the combined gravity centre of both the upper frame and subject seated on, is hard to predict as it depends not only on the structural configuration, but also on how the chair user is seated. Note the sitting posture can affect the gravity centre significantly. Thus  $K_c$  could be hard to predict. A value of 0.91 was estimated in the situations where the subject was seated with his back firmly against the seatback of chair.

$K_s$  : the safety factor that takes deformation of structure, wear and sudden change of force into account. A value of 1.2 was used.

$\eta$  : the mechanical efficiency of the lifting mechanisms, considering friction loss between moving parts. Considering the typical mechanical loss of a quad-pivot mechanism, an efficiency factor of 0.95 was taken.

Hence the maximum actuation force can be calculated as,

$$F_{act} = \frac{F_{Load} \times K_c \times K_s}{\eta} = \frac{(85+9.75) \times 9.81 \times 0.91 \times 1.2}{0.95} = 1068N \quad (3.7)$$

Supplied at its nominal voltage (24V DC), the linear actuator has a feed force rating of 1200N, greater than  $F_{act}$ .

However, at this stage, a low cost linear actuator that meets the above criteria was installed to demonstrate the lifting motion. A rather steady and smooth assistance were provided by the actuator during preliminary experiments. The operation characteristics are further discussed in Chapter 6.

The extension stroke was also adjusted to mechanically fulfil the requirement of the safety concerns. The end position has been securely fixed in addition to a mechanical switch mounted to the end of travel. It ensures in no way the actuation motion will pass beyond the defined limit.

### 3.4 Summary

In this chapter, the mechanical design of the robot chair was first carried out. It features a quad-

pivot structure that can enable a tilting motion together with the rise-up assistance with the usage of single actuator. The initial seat height, tilting angle and rising height were determined based on the biomechanics in STS movements, which played fundamental roles in chair design.

The sensing footmat features in total of 56 sensing cells with the help of multiplexers expanding the number of analogue channels. The structure of footmat was built on a solid platform placed in front of the chair frame. Afterwards, certain calibration and transformation algorithms were applied to determine the actual force readout of single FSR cell. This was followed up by a summation of the entire 56 cells to gain the desired GRF. Later, a dynamic force matrix in every frame was also reconstructed for further exploitations.

The actuator fulfils the requirements on feed force and stroke length. In conjunction with the mechanical stoppers of the chair frame, the actuator also features a lockout switch at the end of the stroke to ensure the safety concerns.

A series of preliminary tests have proved the functions of the robot chair as a capable platform delivering smooth and comfort STS assistance, through manual operations.

## CHAPTER 4 INTENTION RECOGNITION

The previous chapter presented the design and the manufacturing process of both chair mechanics and sensing footmat. They are the major physical components of the robot chair and also serve a platform on which subjects can perform STS movements for the purpose of data collection. Essential features can then be identified and captured from the data to gain deeper understanding on STS process and to facilitate the robot chair to recognise its human users' intentions.

This chapter emphasises on human intention recognition, aiming to enable the robot chair to understand the envisaged intentions at seated position and to predict if assistance is required by human users from their behaviours. The followings need to be taken into account in the intention recognition and the prediction:

- Safety is primarily critical to the intention recognition. In cases where human users do not intend to stand up, if the robot chair mis-interprets subjects' behaviours and actuates the lifting mechanism, it could drive the elderly users into panic situations and potentially cause injuries.
- Accuracy is another issue. The robot chair aims at supporting subjects' STS movements at the point where they are not able to perform unaided STS. Although assistance provided at the time when not needed can also help the subject to stand up, it will discourage them from using own motor functions, leading to lose of function eventually.
- Robustness is the third concern. Human users, even the same user, will not follow the same pattern when performing STS movements. A certain amount of uncertainties need to be dealt with.
- Timing also plays a critical role. Intention recognition has to be completed within a limited time scale. STS process commonly takes from 1.91s to 2.30s for completely able-bodied healthy adults to perform in natural speed depending on several related studies (Kerr et al, 1997; Schlicht et al, 2001; Etnyre and Thomas, 2007). Although STS duration is proved to be longer for able-bodied elderly users, some will not resist more than 3.00s until they sit back to seated position. In both cases, the first about 1.00s is the period

when STS is initiated and hence the intention recognition must be done within this period to support the followed-up motion of stand up. Otherwise incapable subjects will not reach the point of seat-off without any external assistance.

To achieve a safety-critical, robust, accurate and timely intention recognition, a 2-stage recognition process was developed in this research, namely, a fuzzy inference system (FIS) based classification as well as an ANN based predictor. The FIS-based classifier aims at ruling out all unintended random movements out at the early stages of STS process.

#### **4.1 Background Knowledge**

In the study conducted by Etnyre and Thomas (2007), the entire STS process can be separated into 6 distinctive events according to vertical ground reaction force (GRF), namely, initiation, counter, seat-off, peak, rebound and standing, which are shown in Figure 4.1.

The six events are defined as the following:

- i) Initiation ( $\approx 20\%$  BW) refers to the period from subject being informed to initiate the STS, until the first deviation of GRF greater than 10N captured. This event commonly represents the duration it takes for the subject to get mentally prepared for oncoming STS from the neuro-musculo-skeletal system point of view.
- ii) Counter ( $\approx 12\%$  BW) is mainly caused by early lifting of the thighs from the seat by contracting the hip flexor muscles while upper torso mostly remains in its original position.
- iii) Seat-off ( $\approx 60\% - 70\%$ ) is signified by the moment where subject's buttocks separate from seatpan. It is also worth noting that captured GRF increases dramatically in this event which is reported to appear after 1.0s from the beginning of STS.
- iv) Peak ( $\approx 116\%$ ) is simply denoted as the event captured GRF reaches its maximum.
- v) Rebound ( $\approx 80\%$ ) represented by a less-than-body-weight GRF observed after the peak event which can also be understood the tendency of both feet leaving the ground.
- vi) Standing ( $=100\%$ ), apparently.



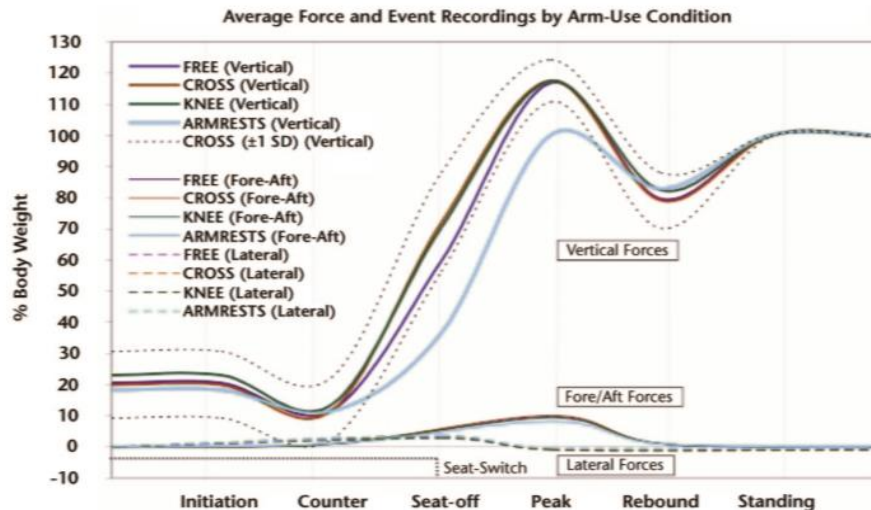


Figure 4.1 Distinctive events in STS through normalised GRF to the percentage of body weight  
(Etnyre and Thomas, 2007)

This standardised curve suggests a resultant peak force measuring 118.7% of body weight, which clearly explains why a large number of the elderly could stand still (bearing the whole body weight) and walk without aid yet suffering sit-to-stand problems.

They conducted tests on 100 individuals to measure GRF under four possible postures, namely, arms-free, arms-crossed, hands-on-knees and hands-on-armrest conditions. In consequence, they found that the average normalised GRFs were similar for the first three conditions in the 6 events.

In contrary, under conditions of hands-on-armrest, significantly less normalised GRFs were found, especially in the event of seat-off. This is mainly because the pushing off force exerted on armrest will contribute to vertical lifting motions hence reducing the GRF, which is further confirmed by related work conducted by Yamada and Demura (2009). However, most of functional limitations and deficits will be spotted under the hands-free conditions, where subject has to primarily rely on lower limbs to provide the strength and stability to complete the STS transition. Therefore all the experiments are arranged under arm-crossed conditions to eliminate the use of hands providing extra assistance to STS movements. It is also realised that some of the original data set are found to be badly executed because of the ununiformed sitting

postures as well as different shoes worn. For the follow-up experiments, 2 Unintended and 2 Intended movement samples were updated under the same conditions of posturing as the rest movements. The performed STS tests should be taken under the presumption that the back of the subject should stay reasonably close to the back rest. Although it is not obligatory for the subject to lean the back firmly against the backrest, used is not a recommended position for the elderly users to prevent from falling (Alexander et al, 1996).

Referring to the previously mentioned human biomechanical model (Figure 4.1) for STS movements, the maximum torques at knees, buttocks and ankles are generated at the instant when buttocks separated from seatpan (seat-off), with the only physical contact being the feet against the ground (hands-free conditions) (Huges et al, 1996). This clarifies the necessity of the 1st stage-classifier that is able to differentiate the cases where the users intend to stand up and where they do not before this critical point from which subject may experience the greatest difficulties if assistance is required.

Fuzzy inference system (FIS) is a system that uses fuzzy logic theory to map input features to crisp output values or classes (Zimmermann, 2001). By definition, a fuzzy constraint  $\tilde{A}$  is a fuzzy subset of  $U$ ,  $\forall u \in U$ , a value  $\mu_{\tilde{A}}(u) \in [0, 1]$  is defined as the membership degree of  $u$  to  $\tilde{A}$ , ranging from 0 to 1. Given the mapping,  $\mu_{\tilde{A}}: U \rightarrow [0, 1], u \mapsto \mu_{\tilde{A}}(u)$  is the membership function of  $\tilde{A}$ .  $U$  is the domain of discourse (Zimmermann, 2001).

Sugeno type of FIS is implemented in the early-stage classification for its simplicity and also the classification output being countable and crisp classes (Abraham, 2001). This type of FIS shares the similar architecture with the most popular Mamdani FIS (Mamdani and Assilian, 1975), with the only difference being the way data gets fed in and fuzzification. The output of Sugeno FIS is typically either constant or linear. Specifically, zero-order Sugeno type is applied here to verify the Unintended movements against other types of Intended STS movements in the early stages, as previously mentioned. Such a fuzzy controller output comprises of singleton spikes as output, which are crispy defined constants representing Unintended and Intended STS movements, accordingly.

The algorithm is simply multiplication which could significantly save the computational time while retaining a compact structure. This will also facilitate the follow up inter- subject adjustment by introducing a dynamic FIS, which will be further elaborated later.

**Rule number  $i$ :** If input = A, then the output function

$$Z_i = ax + c \quad (4.1)$$

This suggests in Sugeno FIS, how the output generated by rule number  $i$  is related to input  $x$ . On the RHS of the equation,  $a$  is the first-order parameter whereas  $c$  is the zero-order parameter, also known as the scalar vector in (Tagaki and Sugeno, 1985). In the selected zero-order Sugeno FIS, the RHS of equation is just constant  $c$ .

The final output of the FIS, denoted as  $Z_f$ , is computed as,

$$Z_f = \frac{\sum_{i=1}^N w_i Z_i}{\sum_{i=1}^N w_i} \quad (4.2)$$

Where the truth degree  $w_i$  is also known as firing strength, suggesting the weight of impact when rule number  $i$  is applied (Tagaki and Sugeno, 1985).

## 4.2 Feasible Features for Intention Recognition

Being the key to successfully meet the four requirements as stated at the beginning of this chapter, intention recognition must be done based on feasible and reliable features that distinguishing different intentions.

Subjects' on chair intentions can be sorted as the following three:

- A). The subject has a clear intention of rising up from seated position and he/she is capable of proceeding the entire STS movement, denoted as Successful STS movement.
- B). The subject generates an intention of rising up despite his/her physiological condition does not allow him/her to do so, denoted as Unsuccessful STS movement.
- C). The subject is not intended to rise up, denoted as Unintended movement.

A study on feasible feature was carried out here to figure out whether GRF can be the eligible feature to distinguish the three intentions. Data were collected from experiments where a subject performed following movements using the prototype described in Chapter 3 and a data collection unit.

- 10 Successful STS movements, denoted as test No.1-10
- 10 Unintended movements by rolling or buttock-off to change seated postures randomly, denoted as test No.11-20
- 10 Unsuccessful STS movements, denoted as test No. 21-20

Because the primary design purpose of the robot chair is to encourage the users to use their own lower limbs motor functions, all movements on STS are conducted under hands-free conditions, eliminating the supports from hands. Meanwhile, in order to avoid any ethical breaches, it is difficult to invite elderly or handicapped people with any risks when seated in the chair prototype. Therefore, unlike the incapable elderly with either functional or structural constraints, the healthy subject was asked to simulate the elderly adults who are lack of lower limbs strength to perform Unsuccessful movements. Namely, flex his upper trunk to bring it closer to seatpan before seat-off point to generate more momentum, and meanwhile elevates much slower than he normally does. As a consequent, Unsuccessful STS is defined when subject is not able to stand straight without external aid although efforts have been made to maximise the effectiveness of motor action (Papa and Cappozzo, 2000).

#### 4.2.1 Data analysis on GRF curves

The data collection has framed serial output captured from the footmat as input through Arduino IDE to an Matlab based pre-processing algorithm. Please note each line of serial data encapsulates the whole outputs generated by 56 sensing cells -- force sensitive resistors (FSRs), which is refreshed at a frame rate of 10Hz. This resolution of 0.1 seconds enables a fairly smooth GRF curve yet without triggering the previously explained time delay issue brought by multiplexers. Afterwards, calibration and transformation are applied to determine the actual force output of single FSR cell. This is followed up by a summation of the entire 56 cells to

gain the desired GRF. Meanwhile, the derived GRF is normalised against subjects' body weight derived under same circumstances (refer to Section 3.2.3).

Six sets of normalised GRF curves are randomly selected from 60 successful STS movements performed by the subject, respecting to STS movement No. 8, 15, 26, 31, 44 and 59. These examples are illustrated in Figure 4.2. From the diagram, it can be readily seen that the captured GRF curves are generally in line with the theoretical GRF curves discovered by related work shown in Figure 2.2.

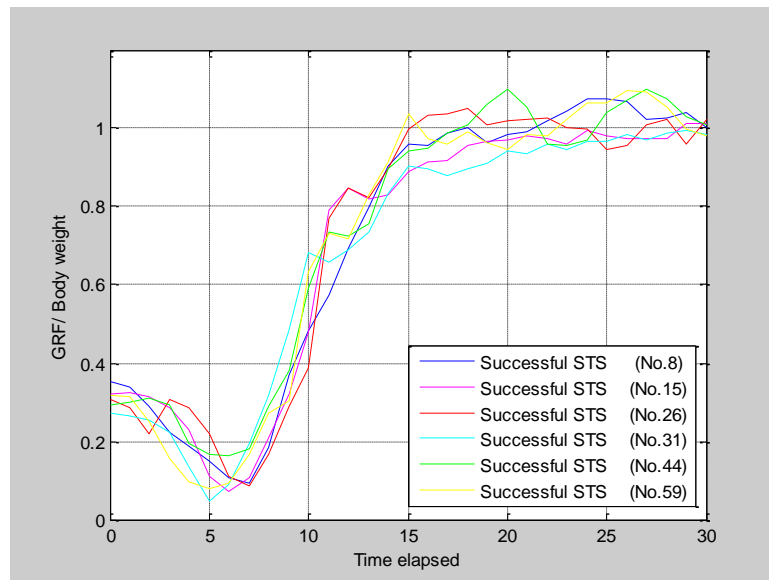


Figure 4.2 Normalised GRF respecting to body weight from Successful STS movements

The processed data from the experiments show that GRF is not able to convey adequate information to classify the type of movement. Because all three types of movements share similar patterns of GRF curves, particularly at the early stages such as initiation, counter and part of the seat-off event, where the movements need to be differentiated as seen in Figure 4.3. Especially between Unintended and Intended STS movements, there is not much deviation in GRF curves that is able to distinguish between the both, even via human interpretation.

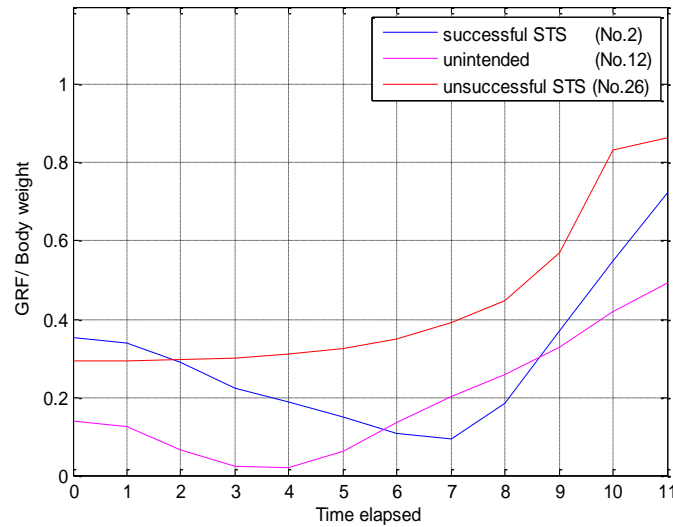


Figure 4.3 Normalised GRF in three cases over first 1.1 seconds

The first 1.1 seconds is set as a critical period for distinguishing situations of A, B, and C, known as the 1<sup>st</sup> stage classification. As discussed in Section 3.1, this period, before pivotal seat-off event, is the most demanding period for subjects to generate sufficient GRF, which should reflect very different efforts the subjects made in different situations. The 1.1 seconds from initiation of the movement is also the point from which assistance must be applied if it is needed, otherwise the subject would not be able to complete the STS movement.

Figure 4.3 confirms Unintended movements can be similar to Unsuccessful or Successful movements in terms of GRF captured, which may cause issues where posture changing scenarios are still mis-classified as the rest two.

From biomechanical model in 3D point of view, the captured GRF merely depicts subjects' function of neuro-musculo-skeletal system in vertical directions. In reality, even some able-bodied elderly struggling with STS are mainly because of lack of stability and motor control while rising, elucidated by the work of Carr (1998).

In summary, exclusively relying on the GRF curves to predict subjects' intention has the below shortcomings,

- i) The summed GRF response does not realise the full potential of design purpose of sensing

footmat.

- ii) The GRF curve is insufficient to identify the corresponding intention.
- iii) It is also not compatible with the time requirement, previously proposed as criteria of intention recognition.
- iv) It is not able to examine subject's STS performance in non-vertical directions.

#### 4.2.2 Centre of Pressure

In the related work on biomechanics of STS, because the centre of body mass is posterior, the Centre of Pressure (COP) transiently shifts backward after the initiation of STS movement. Afterwards, the COP shifts forward for the sake of the dominating upward movement. Before the completion of STS movement, the COP again shifts slightly backward. Meanwhile, ankles are consistently generating longitudinal and lateral motions, named ankle strategies, to adjust and maintain the balance along with the entire STS process. At last, a stable standing position is achieved following a postural adjustment (Hughes et al, 1996).

Therefore, the study on shift of COP is conducted from three aspects, a) Magnitude of change in COP, b) Longitudinal shift of COP, c) Lateral shift of COP. Because all the sensory data is collected from footmat, any sort of COP captured here does not directly imply Centre of Gravity (COG) of the subject.

COP is defined as the gravity centre of pressure subject exerted on footmat. With the COP captured at the very first time instance of each movement counted as the origin, oncoming shift of COP is computed with respect to this origin. Additionally, when plotting any sort of the shift of COP, the origin of the first 1.1 seconds of movements is omitted as there is no comparison against previous point. Hence only 10 meaningful points are shown on these graphs.

While performing the Unsuccessful STS movements, subject had to simulate a less capable person lack

ing of lower limbs strength, hence being conservative in terms of generating GRF. This may

result in a slower shifting of COP than he/she commonly does while performing any seated movements. The step diagram of how COP was computed from raw data is shown in Figure 4.4

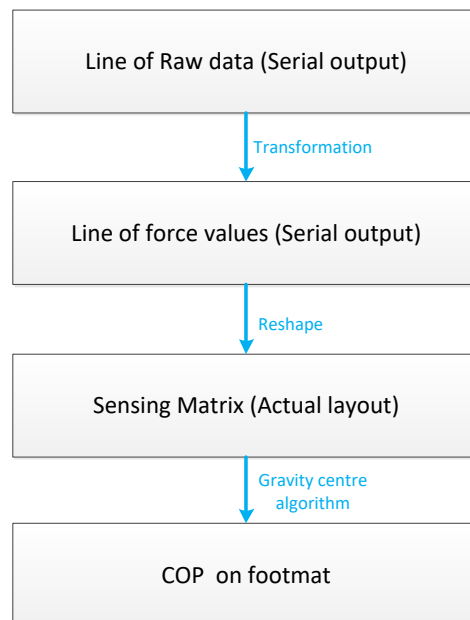


Figure 4.4 Procedure of computing COP from the sensing footmat

Figure 4.4 demonstrates the approach to obtaining the COP on footmat. On top of the diagram, the transformation process is computed the same way as obtaining GRF with the output being force per FSR cell rather than summed GRF. Because of the use of multiplexers the raw data is captured line by line with each line representing all sensors' information per frame. The lined serial output is then reshaped back into the matrix that corresponding to the actual shape of the footmat. Afterwards, COP of this sensing matrix is computed through gravity centre algorithm.

Magnitude of change in COP, Longitudinal shift of COG and Lateral shift of COP obtained through the above procedure are shown in Figures 4.5 to 4.7, respectively.

Proofed by electromyogram (EMG) Magnitude of change in COP shows muscle activation in the sense of determining the intensity of activity over a period of time (Bae and Moon, 2010). However, it can be seen from Figure 4.5 that Unintended random movements is not



significantly different from the rest two at early stages. Therefore it is not considered as the optimal feature for intention recognition.

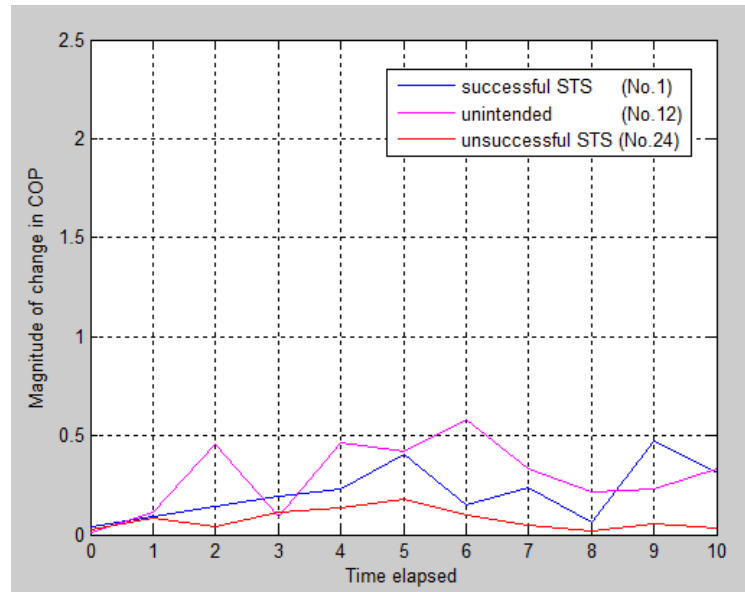


Figure 4.5 Magnitude of change in COP from three previously selected movements

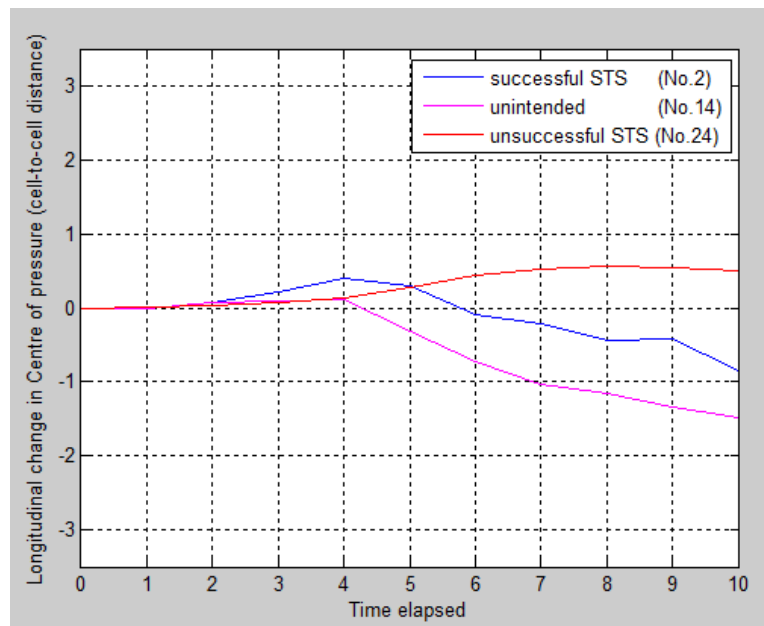


Figure 4.6 Plot of Longitudinal shift of COP in three cases

As related work (Kerr, 1997) suggested, a smooth transition of COG in Longitudinal directions is supposed to be observed from the Successful STS movement. Longitudinal shift of COG is minimal as the force applied to footmat is primarily vertical GRF to generate upwards motion, with the follow-up leaning forward motion given by upper torso. After this, with the upper

torso straightening after leaning forward in first 4 STS events, initiation, counter, rebound and seat-off. Again, neither forward motion nor COG of subject is able to be manifested by trend of Longitudinal shift appearing on footmat. Although similar pattern is hard to be found from the rest two types of movements, it is almost impossible to distinguish them at early stages.

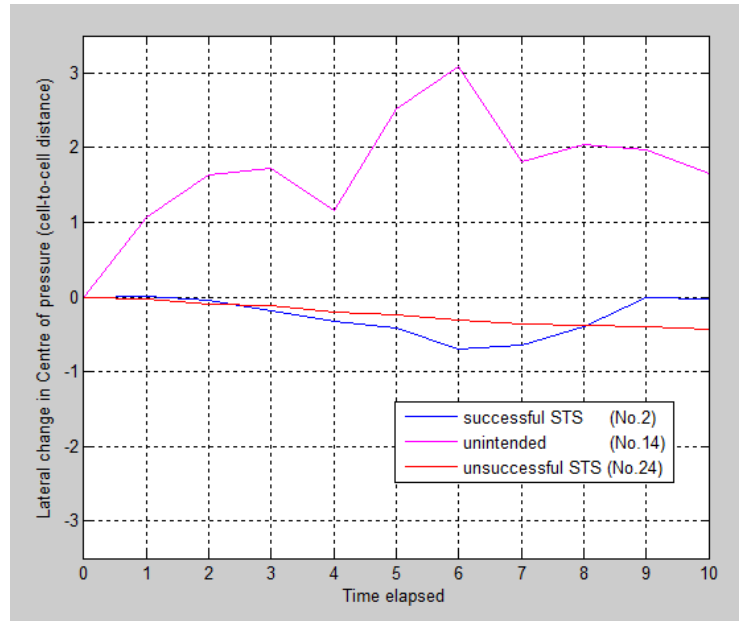


Figure 4.7 Plot of Lateral shift of COP in three cases

Figure 4.7 clearly demonstrates that Lateral shift of COP captured in Unintended movements shows significantly greater absolute values when compared against the rest two. To further confirm this, the lateral shift of COP from all recorded data on the three types of movements are plotted respectively as Figures 4.8 to 4.10. With the vertical axis fixed at same range, it is obvious that subject's feet shift laterally far more frequently when performing Unintended movements.

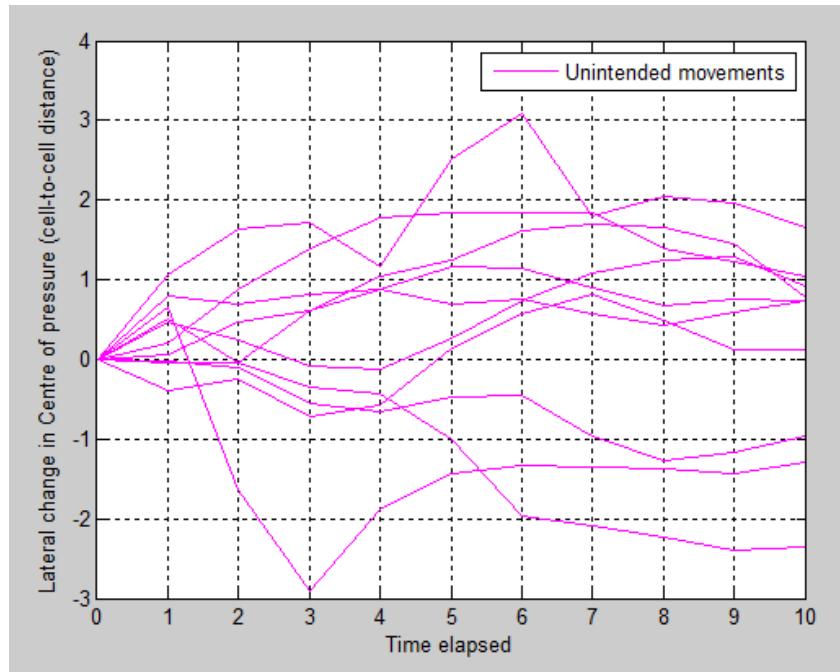


Figure 4.8 Lateral shift of COP in all Unintended movements

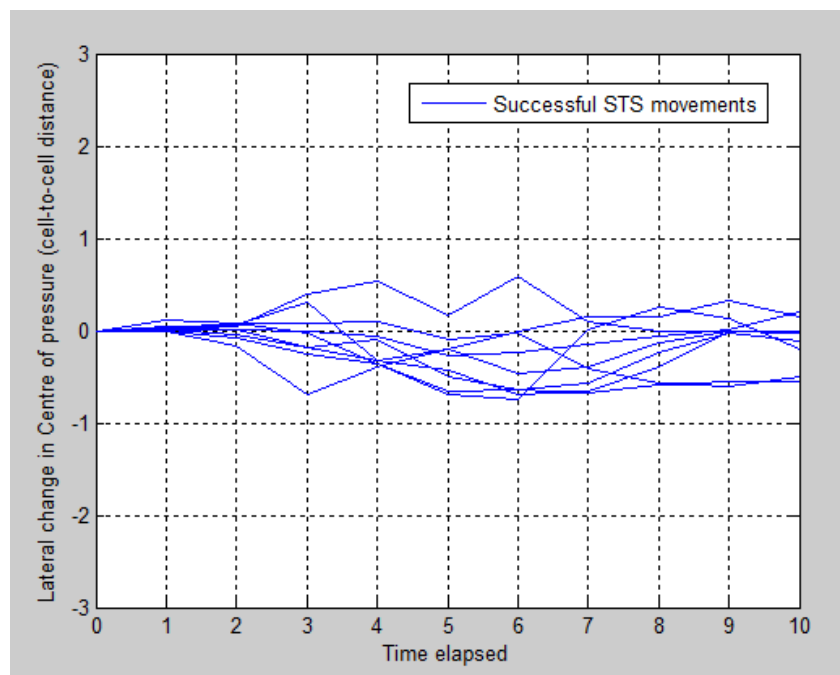


Figure 4.9 Lateral shift of COP in all Successful STS movements

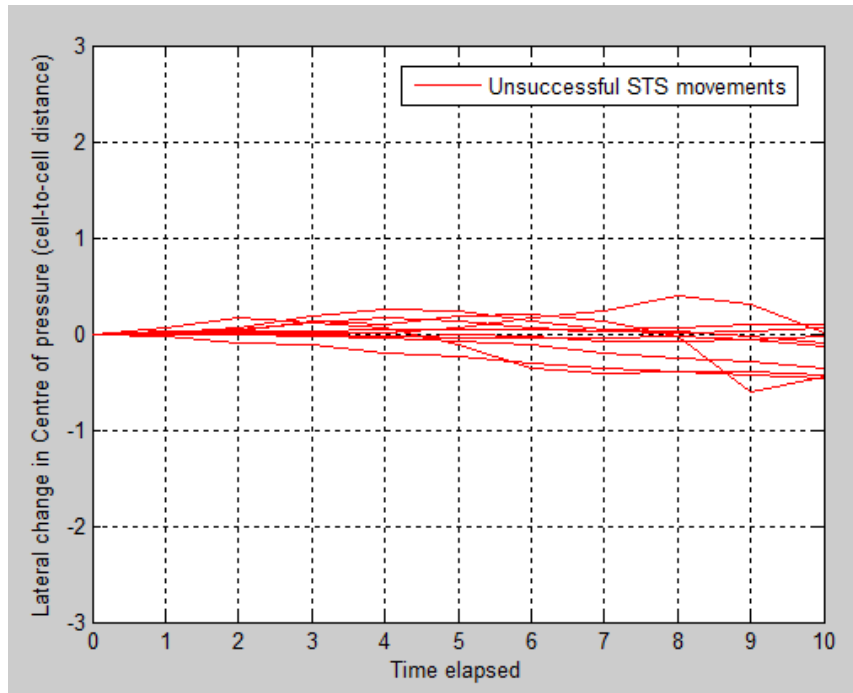


Figure 4.10 Lateral shift of COP in all Unsuccessful STS movements

Theoretical background can be found from clinical research where the concept of peak pressure and the seated self-repositioning are brought in. NHS suggested that it is necessary for every seated person to take self-repositioning movements every 15 to 30 minutes to relieve the pressure, to prevent pressure ulcer and enable blood regulation as well as tissue oxygenation (Trumble, 1930; Coggrave and Rose, 2003). Rolling laterally is considered one of the most effective and easy-to-achieve movements in terms of repositioning one's body, in which the seated person moves from side to side, lifting each buttock off the seatpan to encourage tissue reperfusion at the lifted side. It is also commonly seen a seated person may lean leftwards/ rightwards to grab items fell on the ground, without the need of standing up to reach it. In other scenarios, the subject may intend to lean sideways to take a nap.

From all of these descriptive phenomenon, it could be discovered, especially at early stages of each movement, change of Lateral shift of COP in Unintended motions is distinctively higher, comparing to the Successful STS and Unsuccessful STS movements. This signifies if there exists a fuzzy logic that could possibly rule out the case of Unintended movements from the very beginning, so that there is no need to get the control algorithm and actuator involved to

assist the subject. All of these brought in the come into being of the FIS.

Meanwhile, it is confirmed that intuitive relationships are difficult to find through Magnitude of change in COP and Longitudinal shift of COP.

In summary, Lateral shift of COP has shown significantly better results than the other envisaged features in light of its ability of distinguishing the Unintended movements from the rest two at the early stage. Therefore the essential feature is targeted on lateral shift of COP for the 1<sup>st</sup> stage classifier to distinguish the intention of STS, typically before 1.1 seconds from initiation of movement. Moreover, this study on shift of COP could also be used to examine the performance of subject in both static and dynamic stability during STS movements, which will be carried out later.

#### **4.3 Fuzzy Inference System Based Classification**

In human robot interaction (HRI), fuzzy inference system (FIS) has long been recognised as effective in intention recognition from human behaviours in the sense of handling uncertainties especially when direct mathematical modelling is difficult to achieve.

In the development of the robot chair, FIS is employed to implement the classification aiming to recognise human intention via differentiating Intended and Unintended movements due to the following reasons:

- i). Lack of access to exact modelling of human biomechanical model as well as mechanical geometries
- ii). Uncertainties existing in human behavioural data of STS movements. The Lateral COP distributions displacement, will not be exactly the same among different users considering vast difference in health conditions. Even for the same user, health condition can vary from time to time and will not keep the same positioning and posture prior to standing up. All of these contribute to the uncertainties of Lateral shift of COP. Certain uncertainties have been observed through experiments carried out in this research, which can be found

in Figures 4.8-10.

The following three strategies have been developed to feed Lateral shift of COP to Sugeno-type FIS-based classifier. They are point-wise, accumulation and max-diff classifications.

#### 4.3.1 Point-wise classification

The point-wise classification approach makes decisions in the sense of fuzzification at each sampling point. Of the 200 data of Lateral shift (LS) of COP regarding to Intended STS movements, no matter subject succeeds or not, the majority have the value ranging from -0.5 to 0.5 units. On the other hand, as to the 100 data regarding to Unintended movements, many land outside this region, either surpass 0.5 or below -0.5 units. This distinct phenomenon guides the research interest of designing fuzzy sets for the different types of movements.

The distribution of actual data on LS of COP is shown in the following diagram with separation respecting to the type of movements, Unintended and Intended STS.

Among 200 Intended movement samples, which were double the amount of points extracted from Unintended movements, there were merely a minority of points (22 out of 200) having an absolute LS of COP larger than 0.5 units. These ranges of lateral displacement not only help define the realms of fuzzy set, but also contribute to the truth degrees (weights) of fuzzy rules. Specifically, of all the Intended movements, 20 out of 200 points of ranged between -0.5 and -0.75 units, 2 out of 200 points lied between 0.5 and 0.75 units. According to this discovery, the fuzzy sets of A, B and C for LS of COP are defined as shown in Figure 4.12.

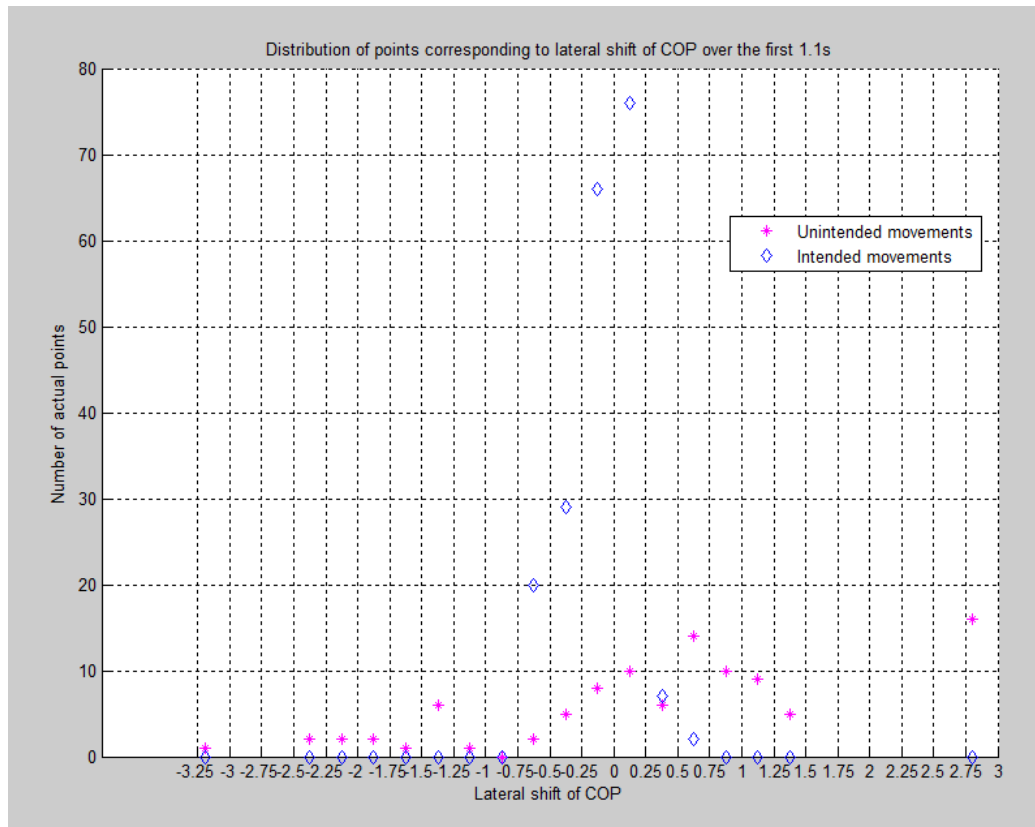


Figure 4.11 Distribution of LS of COP in Unintended (100 points) and Intended (200 points) movements over the early stages

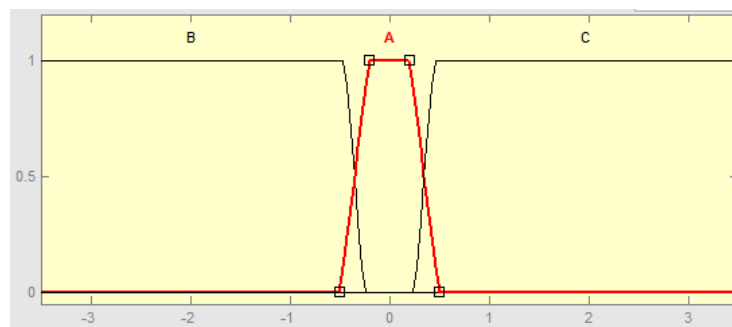


Figure 4.12 Fuzzy sets of A, B and C regarding to LS

Fuzzy rules were defined in an intuitive way. For a change in lateral direction that is outside of  $[-1, 1]$ , it is more likely the movement to be classified as “Unintended”. Therefore, the following fuzzy rules were obtained to classify intention into “Intended” and “Unintended” according to the Lateral shift of COP (LS).

Note when it comes to labelling the input data set as Unintended and Intended, the previously

defined “Successful” and “Unsuccessful” STS movements were combined.

**Rule 1:** If LS = A, then intention = “Intended”, with a truth degree of 0.89 (178/ 200).

**Rule 2:** If LS = B, then intention = “Unintended”, with a truth degree of 0.76 (37/49).

**Rule 3:** If LS = C, then intention = “Unintended”, with a truth degree of 0.67 (34/51).

**Rule 4:** If LS = A, then intention = “Unintended”, with a truth degree of 0.11 (22/ 200).

**Rule 5:** If LS = B, then intention = “Intended”, with a truth degree of 0.24 (12/49).

**Rule 6:** If LS =C, then intention = “Intended”, with a truth degree of 0.33 (17/51).

The truth degree of the Rule 1 was considered based on the rate of the number of Intended samples that were in the range of  $[-0.5, 0.5]$  (178) over the total number of Intended samples (200). The truth degree of Rule 2 and 3 were computed in the similar fashion, shown in Figure 4.13. Rule 4, 5 and 6 can also be understood as the negation part of the first three rules with significantly less degree of impact.

The final output of the system will be the weighted average of all rule outputs, computed as equation (4.1).

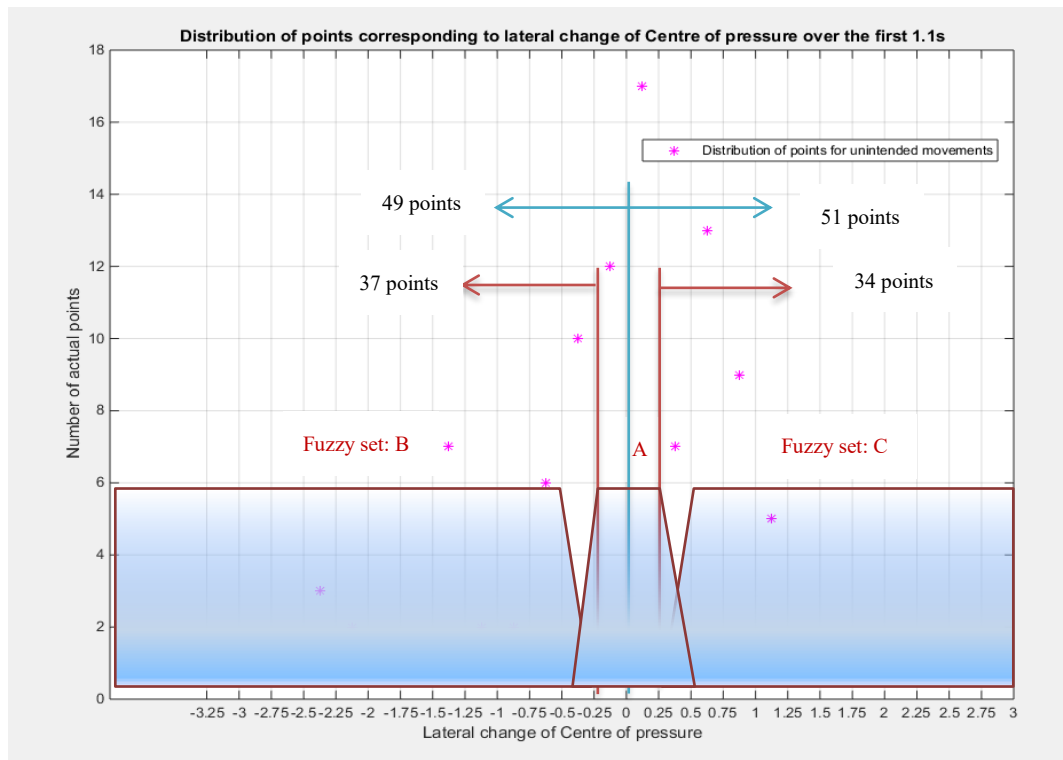


Figure 4.13 Criteria used when determining the truth degree of Rule 1, 2 and 3



**Example 4.1:**

The following shows how point-wise classification works based on the fuzzy sets and rules. Given the value of LS as 0.43, which is the sampled value at a point of 0.9 seconds of an Unintended movement. Fuzzy rules of 1, 3, 4 and 6 were fired, as shown in Figure 4.13.

According to the zero-order Sugeno FIS, the output of each of fired rule can be calculated as:

Rule 1 (Intended),  $\frac{0.5-0.43}{0.5-0.25} \times W_{mfpA} = 0.28 \times 0.89 = 0.255$ , where  $\frac{0.5-0.43}{0.5-0.25}$  is the fuzzification of sample value on fuzzy set A.

Rule 4 (Unintended),  $\frac{0.43-0.25}{0.5-0.25} \times W_{mfpA'} = 0.72 \times 0.11 = 0.079$ ,

Rule 3 (Unintended),  $\frac{0.43-0.25}{0.5-0.25} \times W_{mfpC'} = 0.72 \times 0.67 = 0.482$ ,

Rule 6 (Intended),  $\frac{0.5-0.43}{0.5-0.25} \times W_{mfpC} = 0.28 \times 0.33 = 0.092$ ,

where  $W_{mfpA}$ ,  $W_{mfpA'}$ ,  $W_{mfpC'}$  and  $W_{mfpC}$  are corresponding truth degrees of the fired rules.

The weighted sum of corresponding rules:

Probability of classifying the sample point as “Unintended” is  $0.48 + 0.079 = 0.569$

Probability of classifying the sample point as “Intended” is  $0.092 + 0.23 = 0.322$

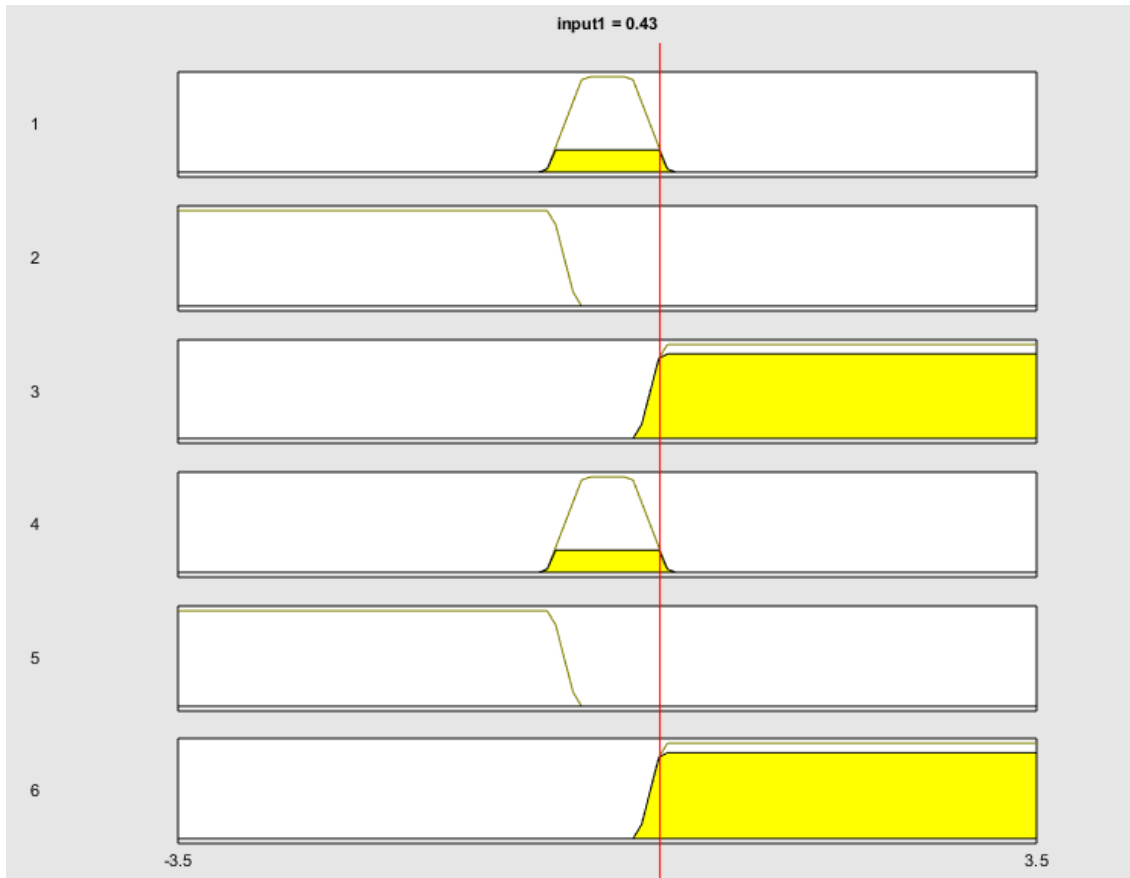


Figure 4.14 Rules fired by Example 4.1

Table 4.1 Complete point-wise classification of all sample points for Example 4.1

Sample points No.	Unintended	Intended
1	0.11	0.89
2	0.11	0.89
3	0.11	0.89
4	0.11	0.89
5	0.11	0.89
6	0.3622	0.3528
7	0.4918	0.318
8	0.4456	0.3314
9	0.569	0.323
10	0.6523	0.2493
Classification outputs	3.0709	6.0245

With the same algorithm applied to the rest sample points of this specific movement, the final outputs of point-wise classifier are generated as 0.307 for “Unintended” and 0.602 for “Intended”. Hence the classification result is given as Intended, correctly matching the nature of Unsuccessful movements.

#### 4.3.2 Accumulation change-based classification

Accumulated change-based classification looks into the summation of absolute values of the shift of COP over a period of time, which represents the amount of changes relative to the initiation of an STS movement.

**Definition 4.1:** Accumulated shift of COP

Let  $f$  be the lateral shift of COP, the accumulated shift of COP within a period of time,  $\varepsilon f$ , is defined as:

$$\varepsilon f = \sum_{1}^{T=11} |f_T - f_{T-1}| \quad (4.3)$$

where  $f_T$  is the feature captured at sampling time step  $T$ , of a STS movement, and  $f_o$  is that captured at the first sampling step (origin). It can be seen the absolute differences between the adjacent values are accumulated.

In this approach, the accumulated shift of COP in lateral directions is highlighted because it reflects the overall intensity of lateral shift of COP (LS) within a fixed period of time. Figure 4.15 shows the distribution of accumulated shift of COP (ACLS) of the respecting Unintended and Intended movements. It can be seen that discernible variations of the feature regions signify the different types of movements. The feature values of Intended movements are mainly in the range of  $[0, 3]$  whereas the feature values of Unintended movements lie above 4. In the distribution plot, it can be easily observed that there is merely one sample with accumulated LS lower than 4 units appearing of all Unintended movements. And only one Intended movement at No.9 shows accumulated LS greater than 3.5 units. This distinctive difference signifies two fuzzy membership functions.

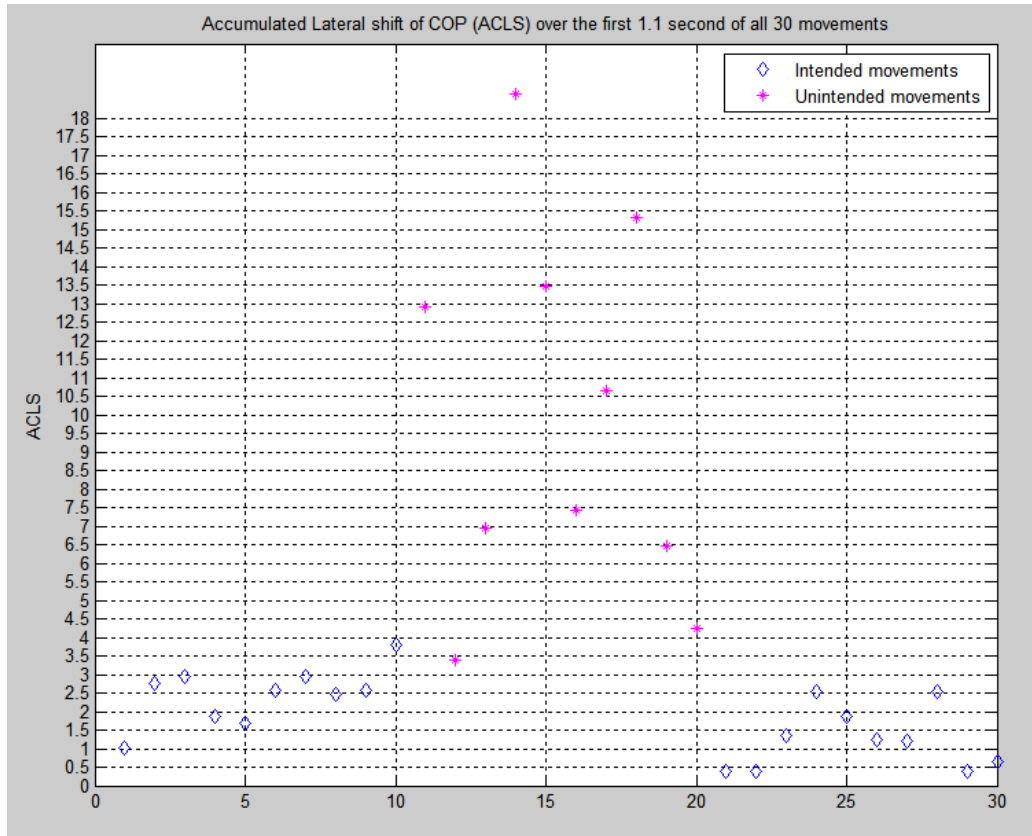


Figure 4.15 Distribution of accumulated LS of the respecting Unintended and Intended movements

As ACLS (unit: time step) has positive values only, two fuzzy sets A and B were defined, as shown in Figure 4.16. Fuzzy set A represents Unintended movements, with boundaries set as  $[0, 3, 3.5]$ . Fuzzy set B represents Intended movements, with boundaries set as  $[3, 3.5, 20]$ . Both membership functions of A and B were designed in trapezoid shape for its simplicity. The region between 3 and 3.5 is where both fuzzy sets collapse, suggesting uncertainties.

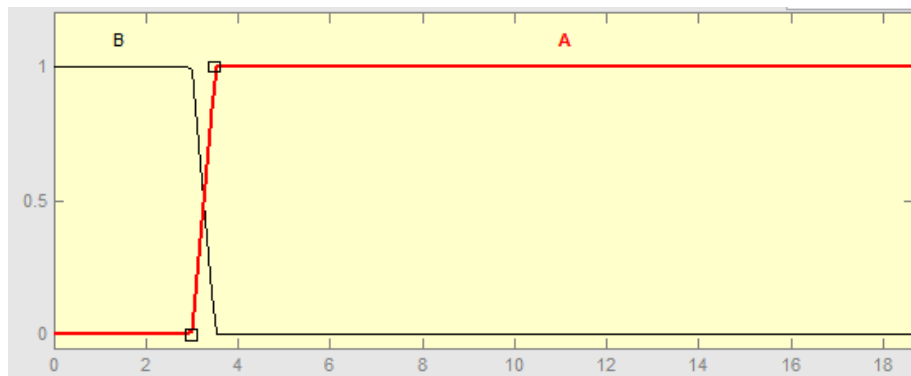


Figure 4.16 Fuzzy sets of A and B respecting to the accumulated LS

Four fuzzy rules were composed on the basis of antecedent data sets of both Intended and Unintended movements, according to the distributions shown in Figure 4.15.

**Rule 1:** If ACLS = “A”, then intention = “Unintended”, with a truth degree  $W_{mfaA}$  of 0.9 (9/10).

**Rule 2:** If ACLS = “B”, then intention = “Intended”, with a truth degree  $W_{mfaB}$  of 0.95 (19/20).

**Rule 3:** If ACLS = “A”, then intention = “Intended”, with a truth degree  $W_{mfaA'}$  of 0.1 (1/10).

**Rule 4:** If ACLS = “B”, then intention = “Unintended”, with a truth degree  $W_{mfaB'}$  of 0.05 (1/20).

The truth degrees of the Rule 1 and 2 were determined by all the samples with ACLS within the realm of membership functions, which were 19 out of 20 and 9 out of 10 respecting to Unintended and Intended movements. On the contrary, Rule 3 and 4 were derived based on the outliers appearing out of the boundaries of the fuzzy sets. Specifically, one outlier of both Intended and Unintended movements were spotted.

#### **Example 4.2:**

Taking the same sample movement in Example 4.1 as the example for this classifier, the ACLS was captured as 2.55 units.

According to the zero-order Sugeno FIS, the output of each fired rule can be calculated as:

$$\text{Rule 2 (Intended), } 1 \times W_{mfaB} = 1 \times 0.95 = 0.95$$

$$\text{Rule 4 (Unintended), } 1 \times W_{mfaB'} = 1 \times 0.05 = 0.05$$

Hence the final outputs of point-wise classifier are 0.05 for “Unintended” and 0.95 for “Intended”. Hence the classification result is given as Intended.

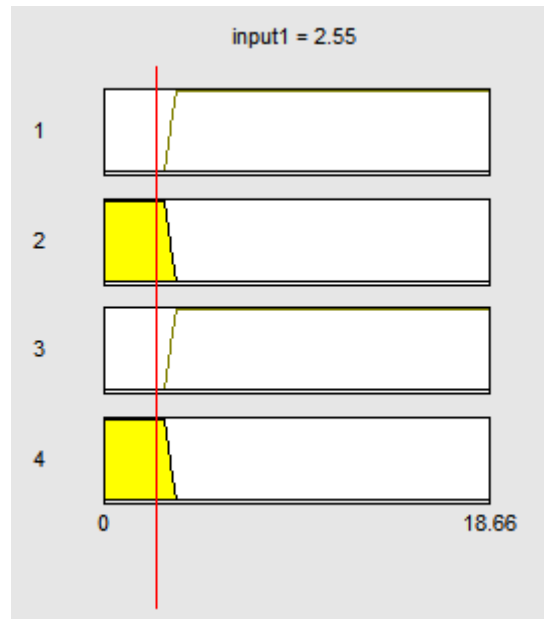


Figure 4.17 Rules fired by Example 4.2

#### 4.3.3 Max-difference based classification

Max-difference based classification was developed considering the difference between the maximum and the minimum, including negatives if applicable, change in Lateral shift of COP recorded in the first 1.1 seconds of each sample movement. Positive indicates lateral COP shift to the right, whilst negative indicates left.

As seen from the previously extracted Lateral shift of COP from STS process, a substantial increase of magnitude could be spotted at the beginning of movements, followed by a gentle rebound at the following about 3 time intervals. When approaching the last few tenths of seconds, typically from 0.7 to 1.1 seconds, the magnitude tends to decrease and stabilise, unlike the Unintended random movements, which shows no alignment with certain phenomenon. Take the sample No. 3 of Successful STS movements as an example, LS of COP started to increase from -0.26 at 0.3 seconds, reached its peak value of -0.67 at 0.6 seconds, referring to Table 4.2. The magnitude then dropped back to 0.02 at 1 second. Similar pattern could be found in the No.4 movement of Successful STS. This observation inspired the development of the Max-difference Lateral Shift of COP (MDLS) classification.

Table 4.2 LS of COP captured from No. 3 of Intended STS movements

Time steps	Lateral shift of COP
1	0
2	-0.002
3	-0.072
4	-0.261
5	-0.367
6	-0.663
7	-0.637
8	-0.578
9	-0.230
10	-0.024
11	-0.119

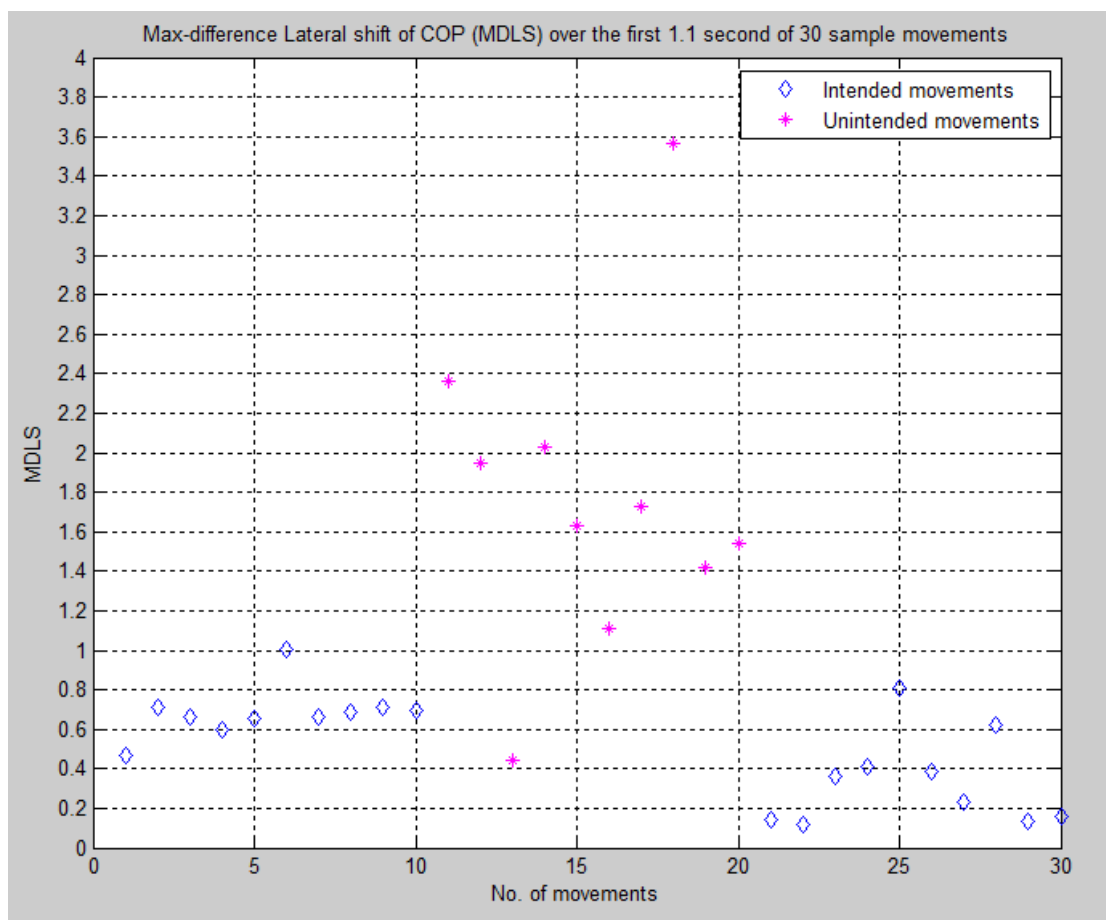


Figure 4.18 Distribution of MDLS of the respecting Unintended and Intended movements

Figure 4.18 shows the distribution of MDLS of the same sample Unintended and Intended movements. The majority of Intended movements show MDLS ranging from 0 to 1 with only 1 out of 20 points lie above 1. As to Unintended movements, values of captured MDLS were all greater than 1 expect one outlier being less than 0.5. Such separation suggested the design of 2 fuzzy sets with A representing Unintended movements and B representing Intended

movements. The shape of membership functions were both defined as trapezoid to handle the uncertainties close to boundaries.

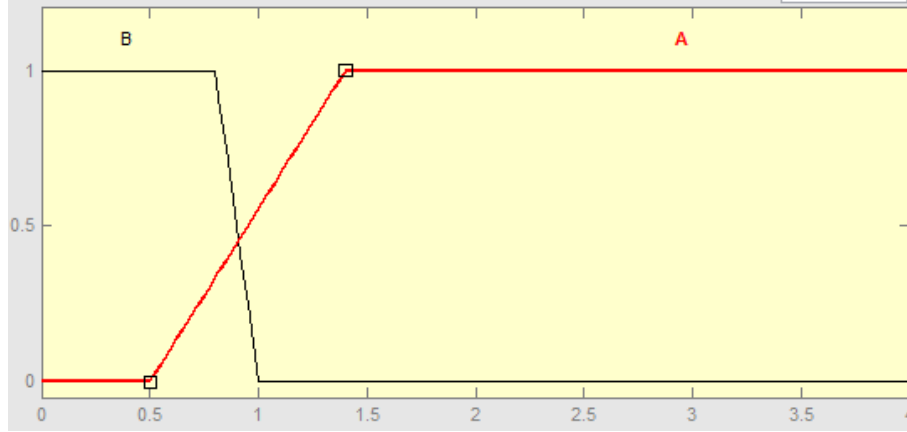


Figure 4.19 Fuzzy sets of A and B respecting to the MDLS

According to Figure 4.18, it can be readily seen that 8 out of 10 Unintended movement samples have MDLS greater than 1.4 units. However, 1 outlier was captured with MDLS just above 1 unit whilst the other one was spotted near 0.4 units. Therefore the boundaries of fuzzy set A in trapezoid shape were determined to be  $[0.5, 1.4, 4.5]$  (Figure 4.18). And because of the outlier closing to 0.4, the truth degree of classifying set A as “Unintended” was computed as 0.9 (9/10). As to 20 sets of Intended STS movements, 13 out of 20 show MDLS less than 0.5 and 8 have values greater than 0.5 yet smaller than 0.8. Therefore the boundaries of fuzzy set B were set as  $[0, 0.8, 1]$  so that these 19 samples can be encapsulated. Considering the outlier that was slightly above 1, the truth degree of classifying fuzzy set B as “Intended” was derived as 0.9 (9/10). In contrast, when classifying A as “Intended” and B as “Unintended”, stated as Rule 3 and 4, truth degree computed as 0.1 (1/10) and 0.05 (1/20), respectively.

Thus, rules were composed as follows,

**Rule 1:** If MDLS = “A” then “Unintended”, with a truth degree of 0.9 (9/10).

**Rule 2:** If MDLS = “B” then “Intended”, with a truth degree of 0.95 (19/20).

**Rule 3:** If MDLS = “A” then “Intended”, with a truth degree of 0.1 (1/10).

**Rule 4:** If MDLS = “B” then “Unintended”, with a truth degree of 0.05 (1/20).



**Example 4.3:**

Taking the same sample movement in Example 4.1 and 4.2 as the example for this classifier, the corresponding MDLS was captured as 0.63 units. Rules shown in Figure 4.20 were fired given the MDLS value as input value.

According to the zero-order Sugeno FIS, the output of each fired rule can be calculated as:

$$\text{Rule 1 (Unintended), } \frac{0.63-0.5}{1.4-0.5} \times W_{mfmA} = 0.14 \times 0.9 = 0.13,$$

$$\text{Rule 2 (Intended), } 1 \times W_{mfmB} = 1 \times 0.95 = 0.95,$$

$$\text{Rule 3 (Intended), } \frac{0.63-0.5}{1.4-0.5} \times W_{mfmB'} = 0.14 \times 0.1 = 0.01,$$

$$\text{Rule 4 (Unintended), } 1 \times W_{mfmB'} = 1 \times 0.33 = 0.05,$$

where  $W_{mfaA}$ ,  $W_{mfaA'}$ ,  $W_{mfaB}$  and  $W_{mfaB'}$  are the truth degrees of the corresponding fuzzy rules.

Thus, the probability of classifying the sample movement as “Unintended” and “Intended” are 0.18 and 0.95, respectively.

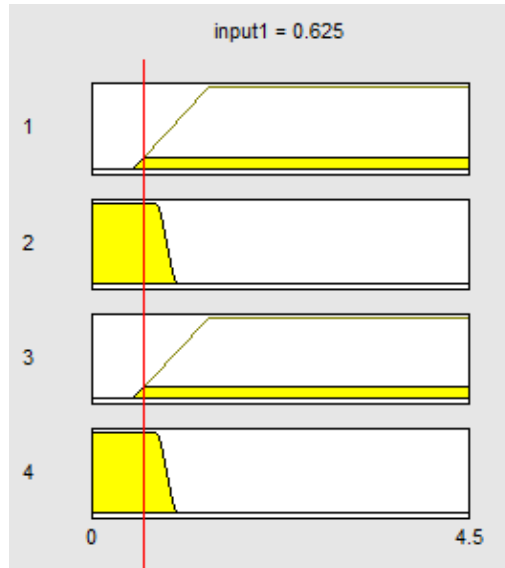


Figure 4.20 Rules fired by Example 4.3

#### 4.3.4 Discussion

The following measures are defined to compare the three approaches of classification:

- False matching rate of Unintended movements to intended ones (FMR) is measure for the safety. The rate should be minimised as the false matching will cause the assist actions of the robot chair to take place, which may force the user who has no intention to stand up and lead to a fall.
- True matching rate of intended to intended (TMR) is the measure for the accuracy. This should be maximised as the aim of the classification is to find out the user's need for assistance in STS process.
- Variety in sample data (VD) in conjunction with FMR and TMR are used to measure the robustness. High variety means high uncertainty level in sample data. Together with FMR and TMR, they reflect the capabilities of handling the uncertainty.
- Responding time of the classification (RT) reflects the time criterion. The classification must be done at the end of first 1.1 seconds period.

Tests with 2-fold testing data and with pure testing data were undertaken for the purpose of comparison of the three classification approaches. The 2-fold test data splits the data set into two halves. The first half is used for modelling the fuzzy classifier whereas the second half is taken for testing. The “pure” test data is fresh data sets fed into the build FIS-based classifier, which is independent of the data that is used to build the FIS. It is used to test how well the modelled FIS-based classifier can be applied to fresh new data.

For the point-wise classification, the test results with 2-fold data are shown in Table 4.3. In each section of the table, the first row records the results regarding to Unintended movements while second row shows outputs for Intended movements. Despite all the Intended movements being successfully classified, No. 14, 15 and 17 are supposed to be Unintended movements however were classified as Intended STS movements. Tests were also performed with pure test data. The results are recorded in Table 4.4. Of all Intended movements, No. 1, 2, 3, 5, 6 and 8 were incorrectly classified as Unintended. As to the Unintended movements, No. 15 and 19 were classified as Intended.

Table 4.3 Results of point-wise classification with 2-fold data

	1	2	3	4	5	6	7	8	9	10
1	0.2484	0.3141	0.2832	0.3327	0.4918	0.0884	0.3198	0.3141	0.2422	0.1186
2	0.5622	0.5036	0.5241	0.5348	0.4475	0.7107	0.5094	0.5036	0.6460	0.5890

	11	12	13	14	15	16	17	18	19	20
1	0.6032	0.6132	0.7510	0.4248	0.4209	0.5607	0.1654	0.6521	0.6700	0.6093
2	0.3703	0.3794	0.2490	0.4253	0.4019	0.3539	0.5269	0.3212	0.3300	0.3483

	21	22	23	24	25	26	27	28	29	30
1	0.1322	0.0834	0.2860	0.1012	0.0960	0.1018	0.1014	0.1182	0.2295	0.2054
2	0.6705	0.6746	0.4534	0.8189	0.7766	0.8237	0.8205	0.6464	0.4422	0.6101

Table 4.4 Results of point-wise classification with pure test data

	1	2	3	4	5	6	7	8	9	10
1	0.5933	0.6347	0.5654	0.2044	0.6700	0.6999	0.4355	0.5380	0.4754	0.3652
2	0.3346	0.3366	0.3466	0.7242	0.3300	0.2575	0.5035	0.4620	0.4930	0.5619

	11	12	13	14	15	16	17	18	19	20
1	0.5945	0.5237	0.5808	0.6087	0.4685	0.6700	0.6700	0.7600	0.4076	0.6700
2	0.3630	0.3286	0.3241	0.3429	0.3897	0.3300	0.3300	0.2400	0.4045	0.3300

	21	22	23	24	25	26	27	28	29	30
1	0.0926	0.4748	0.2806	0.1474	0.3750	0.4370	0.0974	0.0974	0.3776	0.3615
2	0.7493	0.3221	0.4865	0.6019	0.4393	0.4977	0.7881	0.7881	0.4928	0.5616

The test results of ACLS classification with 2-fold data is shown in Table 4.5. Of all 2-fold datasets, sample No. 5 was supposed to be Intended movements however was classified as Unintended movements. With pure test data fed in, 10 Unintended movement samples were classified as “Unintended” (100%), whereas 14 data sets of Intended movements were classified as “Intended” (70%).

Table 4.5 Results of ACLS classification with 2-fold data

	1	2	3	4	5	6	7	8	9	10
1	0.0500	0.1971	0.0500	0.0500	0.9000	0.0500	0.0500	0.1971	0.0500	0.0500
2	0.9500	0.7420	0.9500	0.9500	0.1000	0.9500	0.9500	0.7420	0.9500	0.9500

	11	12	13	14	15	16	17	18	19	20
1	0.9000	0.7733	0.9000	0.9000	0.9000	0.9000	0.9000	0.9000	0.9000	0.9000
2	0.1000	0.1337	0.1000	0.1000	0.1000	0.1000	0.1000	0.1000	0.1000	0.1000

	21	22	23	24	25	26	27	28	29	30
1	0.0500	0.0500	0.0500	0.0500	0.0500	0.0500	0.0500	0.0500	0.0500	0.0500
2	0.9500	0.9500	0.9500	0.9500	0.9500	0.9500	0.9500	0.9500	0.9500	0.9500

Table 4.6 Results of ACLS classification with pure test data

	1	2	3	4	5	6	7	8	9	10
1	0.6366	0.0500	0.9000	0.0500	0.0500	0.0500	0.0500	0.0500	0.0500	0.0500
2	0.2780	0.9500	0.1000	0.9500	0.9500	0.9500	0.9500	0.9500	0.9500	0.9500

	11	12	13	14	15	16	17	18	19	20
1	0.9000	0.9000	0.9000	0.9000	0.9000	0.9000	0.9000	0.9000	0.9000	0.9000
2	0.1000	0.1000	0.1000	0.1000	0.1000	0.1000	0.1000	0.1000	0.1000	0.1000

	21	22	23	24	25	26	27	28	29	30
1	0.0500	0.9000	0.2380	0.0500	0.9000	0.9000	0.0500	0.0500	0.0500	0.8397
2	0.9500	0.1000	0.6988	0.9500	0.1000	0.1000	0.9500	0.9500	0.9500	0.0933

Tests were also carried out to verify the results of MDLS classification, with 2-fold and pure test data. In spite of 10 Unintended movements being accurately classified, 7 out of 20 Intended movements were wrongly classified as “Unintended”, which can be seen in Table 4.7 showing 2-fold data. When feeding the MDLS classifier with pure test data, one in both Unintended and Intended were incorrectly classified opposite to their movement types.

Table 4.7 Results of MDLS classification with 2-fold data

	1	2	3	4	5	6	7	8	9	10
1	0.0500	0.2608	0.2108	0.1491	0.2028	0.5025	0.2108	0.2365	0.2640	0.2431
2	0.9500	0.9500	0.9500	0.9500	0.9500	0.0558	0.9500	0.9500	0.9500	0.9500

	11	12	13	14	15	16	17	18	19	20
1	0.9000	0.9000	0.0500	0.9000	0.9000	0.6110	0.9000	0.9000	0.9000	0.9000
2	0.1000	0.1000	0.9500	0.1000	0.1000	0.0679	0.1000	0.1000	0.1000	0.1000

	21	22	23	24	25	26	27	28	29	30
1	0.0500	0.0500	0.0500	0.0500	0.3115	0.0500	0.0500	0.1750	0.0500	0.0500
2	0.9500	0.9500	0.9500	0.9500	0.0435	0.9500	0.9500	0.9500	0.9500	0.9500

Table 4.8 Results of MDLS classification with pure test data

	1	2	3	4	5	6	7	8	9	10
1	0.3277	0.0684	0.0620	0.1497	0.3522	0.6311	0.0594	0.5137	0.8450	0.2250
2	0.1053	0.9500	0.9500	0.9500	0.1984	0.0701	0.9500	0.8119	0.0939	0.9500

	11	12	13	14	15	16	17	18	19	20
1	0.9000	0.9000	0.9000	0.9000	0.9000	0.9000	0.8175	0.9000	0.9000	0.9000
2	0.1000	0.1000	0.1000	0.1000	0.1000	0.1000	0.0908	0.1000	0.1000	0.1000

	21	22	23	24	25	26	27	28	29	30
1	0.3140	0.0500	0.0500	0.5532	0.8822	0.0500	0.9000	0.3220	0.3379	0.9000
2	0.0532	0.9500	0.9500	0.0615	0.0980	0.9500	0.1000	0.0836	0.1440	0.1000

The corresponding confusion matrices for the 3 classification approaches with 2-fold and pure

test data are given in Figure 4.21- 4.26, respectively.

		Classification		Results	
		<i>Unintended</i>		<i>Intended</i>	
Actual Datasets	Unintended	70%	True Positive	30%	False Negative
	Intended	0%	False Positive	100%	True Negative

Figure 4.21 Confusion matrix of point-wise classification with Two-fold input data

		Classification		Results	
		<i>Unintended</i>		<i>Intended</i>	
Actual Datasets	Unintended	80%	True Positive	20%	False Negative
	Intended	30%	False Positive	70%	True Negative

Figure 4.22 Confusion matrix of point-wise classification with pure test data

		Classification		Results	
		<i>Unintended</i>		<i>Intended</i>	
Actual Datasets	Unintended	100%	True Positive	0%	False Negative
	Intended	5%	False Positive	95%	True Negative

Figure 4.23 Confusion matrix of ACLS classification with 2-fold test data

		Classification	Results
		<i>Unintended</i>	<i>Intended</i>
Actual Datasets	Unintended	100% True Positive	0% False Negative
	Intended	30% False Positive	70% True Negative

Figure 4.24 Confusion matrix of ACLS classification with pure test data

		Classification	Results
		<i>Unintended</i>	<i>Intended</i>
Actual Datasets	Unintended	100% True Positive	0% False Negative
	Intended	30% False Positive	70% True Negative

Figure 4.25 Confusion matrix of MDLS classification with 2-fold test data

		Classification	Results
		<i>Unintended</i>	<i>Intended</i>
Actual Datasets	Unintended	100% True Positive	0% False Negative
	Intended	35% False Positive	65% True Negative

Figure 4.26 Confusion matrix of MDLS classification with pure test data

As introduced in the beginning of Section 4.3.4, FMR is primarily highlighted for safety concerns of the robot chair. It will cause safety issues in the scenarios where subject is intended to simply change his/her posture but the actuator mechanism arises the entire seatpan due to the false matching of intention. The top-right corner of each confusion matrix above shows the

FMRs of the different approaches. With 2-fold test data FMR were recorded as 30%, 0% and 0%, for point-wise, ACLS and MDLS classifications. When fed in with pure test data, the FMRs became 20%, 0% and 0%, respectively. Consequently, it is readily concluded that both ACLS and MDLS classifications outperform point-wise classification in terms of minimising the FMR. Referring to the weakness of point-wise classifier as Table 4.2 suggested, it will considerably affect the FMR of this approach. Owing to the rebound phenomenon of LS at early stages of STS movements, some sample points captured from Untended movements would be classified as Intended only owing to the lack of sample points with LS values surpassing the threshold of fuzzy sets B and C.

TMR is used as another critical measure to benchmark the accuracy of the 3 classifiers. Referring to the bottom-right corner of the above confusion matrices, the TMRs of the 3 approaches with 2-fold input test data were recorded as 100%, 95% and 70%, respectively. With pure test data, the TMRs became 70%, 70% and 65%, respectively.

As the nature of MDLS demonstrates, this approach takes the registered maximum and minimum over the period of first 1.1 seconds, which will be subsequently sensitive to the ambiguities brought in by the following scenarios in Intended movements: randomly reposition of arms while standing up, difficulties when stabilising body motion in a significant torque. All of these will change the captured LS in a rather short time span. Nevertheless this negative effect can be minimised when taking ACLS into account, which can potentially be the reason why it outperforms the MDLS considering the TMR.

VD is another measure of performance of the classification approaches. VD refers to the different ways in which COP shifts. The LS of COP is related to the sitting postures such as positions of feet and arms, buttock position on seatpan the subject used while conducting each type of test movements. These positions determine what strategy subject uses to stabilise his/her body when standing up. As previously discussed in Chapter 2, subjects tend to adapt his/her STS strategies to environments and conditions to perform STS movements. According to findings derived by (Nardone et al, 1990; Kuo and Zajac, 1993; Kuo, 1995), ankle positioning

and subjects' functional capability are correlated to strategies used for postural control and upper torso stabilisation, proved by the extraction of joint torques. For example, subject appears to use ankle strategy when upper torso movements are restricted, which will affect the captured LS appearing on footmat. In contrast, when STS is performed based on a rather wide stance the stabilisation motion will require less muscle activation hence results in different shift of COP. When generating data for defining and testing the classifiers, subject was advised to avoid retaining the same foot, arm or buttock positions. It can be summarised that VD is high in the datasets as movements were executed naturally to introduce realistic uncertainties. The same datasets were applied to all three classification approaches. Testing with VD guarantees the robustness of the classification.

According to the measure of criteria proposed to examine the performance of the classifier, all 3 approaches were characterised to be timely efficient and capable of handling different kind of uncertainties to some extends. The RT is considered through 2 aspects, the captured time span of input data and processing time of FIS function. The time duration of input data is limited to 1.1 seconds. In addition to this, the average processing times of FIS function for 3 classification approaches were recorded as 0.077, 0.003 and 0.001 seconds. With the processing time of both ACLS and MDLS classifications rather negligible comparing to the 1.1 seconds of input data capturing.

#### **4.4 Summary**

This chapter first reviewed the biomechanics of STS process in order to seek possible features for intention recognition at early stages of STS process. The extracted LS was verified as the feasible feature in capable of distinguishing Unintended movements from Intended ones within the time constraints. Three fuzzy logic based classifiers, point-wise, ACLS and MDLS, were then designed and tested via 2-fold and pure test data. The performance of these classifiers was examined through criteria proposed to meet the requirements of intention recognition. Consequently, ACLS was verified to outperform the other two in terms of handling uncertainties and recognising subjects' STS intention at early stages.





## CHAPTER 5 SELF-ADAPTIVE FUZZY CLASSIFIER

### 5.1 The need for self-adaptive classification

In Chapter 4, fuzzy logic based classification approaches have been developed, namely point-wise, ACLS and MDLS classifiers. ACLS was proved the most successful one, reaching 100% TMR in terms of classifying Unintended movements.

However, in real-world applications, more than one family member will use the robot chair and expect the same assistance to the STS movements if experiencing difficulties in STS movements. This requires the robot chair to be able to support different users with different biomechanical features such as body weights, heights (measured with shoes on instead of stature heights) and thigh lengths, as well as sitting habits. To simulate this home-use scenario, Subject B was introduced to further develop the robot chair.

It is essential to examine how the classifiers perform on Subject B with the fuzzy logic based classification with fuzzy sets determined for Subject A. In order to obtain representative experimental results, Subject B was purposefully chosen with completely different biomechanical features (Table 5.1) and preferable sitting postures (Table 5.2). This can not only create a wider span of the targeted features but also shed light on the STS patterns often used by the elderly. Although owing to the above mentioned ethical issues (Section 4.2) the elderly subjects suffering STS problems are not available, it would be more convincing to introduce a subject with similar STS features and behaviours.

Table 5.1 The biomechanical features of Subject A and B

Subject A				Subject B			
Body weight	Height (w/ shoes)	Length of thighs	Shoe size	Body weight	Height (w/ shoes)	Length of thighs	Shoe size
85 kg	185 cm	49 cm	UK 10.5	49 kg	156 cm	42 cm	UK 3.5
*mid-knee to hip bone				*mid-knee to hip bone			

Table 5.2 The recorded sitting postures of both subjects when performing STS movements

Subject A			Subject B		
arms-free	arms-crossed	hands-on-knees	arms-free	arms-crossed	hands-on-knees
47	2	11	27	7	26
Total No. of Movements		60	Total No. of Movements		60

Subject B was informed to go through all three types of movements as performed by Subject A, namely Successful STS, Unsuccessful STS and Unintended. The key feature, Lateral shift of COP (LAT) over the first 1.1 seconds, was extracted from these three movements as the same as what was done with Subject A. The tests were then performed on two contender classification approaches, ACLS and MDLS, with the classification results shown in Figure 5.1 and 5.2, respectively.

		Classification		Results	
		<i>Unintended</i>		<i>Intended</i>	
Actual Datasets	Unintended	70% True Positive		30% False Negative	
	Intended	5% False Positive		95% True Negative	

Figure 5.1 Confusion matrix of the original ACLS classification applied on Subject B's test data

		Classification		Results	
		<i>Unintended</i>		<i>Intended</i>	
Actual Datasets	Unintended	65% True Positive		35% False Negative	
	Intended	0% False Positive		100% True Negative	

Figure 5.2 Confusion matrix of the original MDLS classification with test data only applied on Subject B's test data

The above confusion matrices show a significant drop in TMRs, which are 70% and 65% for ACLS and MDLS, respectively, comparing to an accuracy of 100% for both approaches when

the tests were performed by Subject A. It was speculated that the well-defined fuzzy based classifier in Chapter 4 may not be directly applicable to other chair users with great variations in biomechanical features.

It was found that the extracted magnitude of lateral shift (LAT) of Subject B is much smaller than that of Subject A. Variations in biomechanical features and sitting postures of the two subjects can be the reasons that caused such differences in LAT. This is because when conducting the Unintended movements by random movements, different subject will yield different buttock movements due to the vast difference in subjects' biomechanical features (length of thighs), LAT will not remain the same. Also, owing to the different sitting postures the subjects adopted when performing STS movements, the resultant LAT will be different.

In addition to the difference in biomechanical features between Subject A and B, they were also observed to perform the STS movements with different habits in terms of sitting postures. As previously explained, the posture of hands-on-armrest was not considered within the scope of this study, as the main design objective of the chair is to encourage the motor functions of lower limbs and cores. Besides, because there is no sensor attached to arm rests, the amount of force subject would have applied on arm rests to assist the STS motion is impossible to be recorded. Apart from this hands-on-armrests posture that needed to be avoided, both subjects did not give a conscious effort on sitting postures. Consequently, three sitting postures, arms-free, arms-crossed, and hands-on-knees were observed throughout all the movements performed by both subjects, which coincided with the mainstream of posture analysis in STS study (Schlicht et al, 2001; Etnyre and Thomas, 2007; Yamada and Demura, 2009).

Therefore, to enable smart chair to become well suitable for supporting different users, two main error-related factors below were extracted and investigated.

- i). Width of shoes
- ii). Width of seated stance

The below advantages are realised when considering the concept of shoe width

- It can be easily extracted through different numbers of FSRs activated by subject's feet while stepping on the footmat. In comparison, a larger shoes size will create a larger contact region with the footmat hence result in more FSRs being activated. The width of shoes can be normalised in a fashion using the average No. of FSRs activated per row as only this value affects the obtained LAT.
- The width of shoes also reflects the size of shoes which has a correlation with subjects' biomechanical features suggested by several anthropometric researches (Robbins 1986; Siminoski 1993; Ozden, 2005).
- The analysis on shoe geometry is essentially an affecting factor for the lateral balancing during STS process (Tencer et al, 2004; Lord et al, 2007). This offers an expansion opportunity for the robot chair to be able to investigate the relationship between rate of Successful STS and shoe geometry. However this is beyond the scope of this study as it is impossible to recruit the elderly subject with falling risks. This could provide suggestions for the shoes that chair user should wear to reduce the risks of fall.

Although it is preferably to use a wide stance for more stabilisation while standing up, it is common that different people show difference in stance width owing to causal sitting habits. For example, as Table 5.2 suggests, given the percentage of arms-free posture (78.3%) used by Subject A, he would also favourite a wider stance along with this type of posture . The average captured distance between feet is 6.12 units (cell-to-cell distance). In addition, the seated stance measured from Subject B's was noticeably narrower. Both subjects reported that they were naïve to the focus of this sitting posture test and sat spontaneously because they were only informed to perform the three types of movements for the required sets. The seated stance may also be a Gender Preference (Gunter et al, 2000) but needs to be further investigated/ confirmed.

Therefore, the investigation on stance width has four main advantages,

- It is readily extractable via processing blocks through the information gathered from the footmat. Width of seated stance of each subject is derived by his/her COP of each foot when stepping on footmat. For example, subject A has an average stance width of 5.4, derived from 30 test results. Same principle applied, subject B has an average stance width

of 4.76 units.

- When being analysed in conjunction with width of shoes, it helps verify the biomechanical features of Subject. Although the height of subject is not directly measurable from the chair setups, it can still be perceived/ extracted through the combination of stance width and shoe width, given the fact that a subject with longer limbs, would be more likely to result in a broader stance during STS process (Fujiwara et al, 2009)
- It can help verify the type of sitting postures because it was realised when subjects conduct STS movements under arms-free or arms-crossed movements, the respecting width of seated stance is significantly higher than that of hands-on-knees (Table 5.2)
- More importantly, it can rectify the cases that variations in seated stance result in different measured LAT while subject proceeding movements with same buttocks travelling distance.

From Table 5.3 it can be seen the variations in stance width under different postures adopted by Subject A and B when performing STS movements.

Table 5.3 The extracted stance width of each subject under different sitting postures

	Stance Width As per Sitting Posture/ Subject					
	Subject A			Subject B		
Posture	arms-free	arms-crossed	hands-on-knees	arms-free	arms-crossed	hands-on-knees
Average Stance Width	6.12	5.93	4.55	5.39	5.55	3.89
(Unit: cell-to-cell distance)	Overall Stance Width		5.83	Overall Stance Width		4.76

Conventional FIS requires “predetermined” variables either determined based on trial-and-error or via experimental results, as elaborated in point-wise, ACLS and MDLS fuzzy logic based classifiers from the previous chapter. These variables, including boundaries of all fuzzy sets, cannot be directly transferred to other chair users, apparently.

To further expand the Fuzzy based classifier to a more robust multi-user oriented classifier considering inter-subject biomechanical variations, a self-adaptive system is developed.

## 5.2 Self-adaptive fuzzy classification for handling 1st biomechanical feature

### 5.2.1 Manual adaptation and discussion

The influence of the variations in shoe width, the 1st biomechanical features, on the fuzzy sets and corresponding rules of ACLS and MDLS classification was investigated separately.

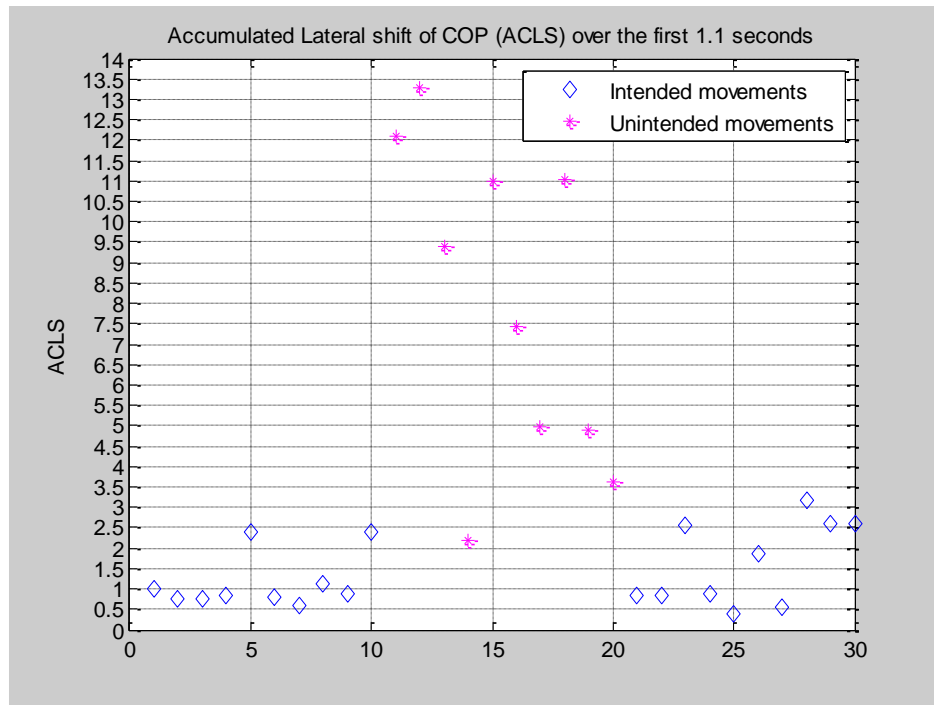


Figure 5.3 Distribution of ACLS of the respecting Unintended and Intended movements performed by Subject B

Because the ACLS classification uses accumulated change in LAT value extracted from Subject B's experimental data as input, the determination of fuzzy sets for ACLS classifier followed the same procedure illustrated in Chapter 4. As the accumulated change in LAT values show positive values only and the classifier aims to yield two classis, Unintended and Intended, two fuzzy sets A and B were defined based on the distribution plot shown in Figure 5.3.

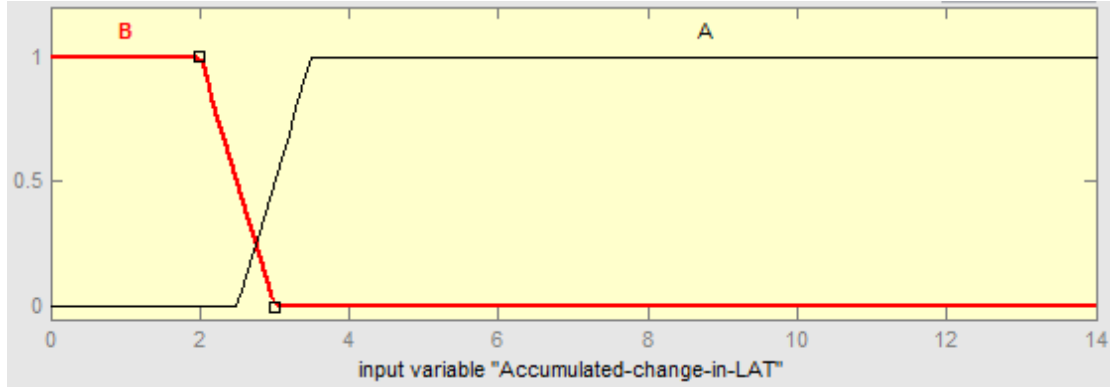


Figure 5.4 Input fuzzy sets of A and B of ACLS classifier for Subject B

Figure 5.4 shows the fuzzy sets of ACLS classifier, re-defined for Subject B. Fuzzy set A represents Unintended movements, with boundaries set as [2.5, 3.5, 14]. Fuzzy set B represents Intended movements, with boundaries set as [0, 2, 3]. The shape of membership functions was again set as trapezoid for its simplicity. Fuzzy rules and the corresponding truth degrees were established as:

**Rule 1:** If ACLS = “A”, then intention = “Unintended”, with a truth degree of 0.9 (9/10).

**Rule 2:** If ACLS = “B”, then intention = “Intended”, with a truth degree of 0.95 (19/20).

**Rule 3:** If ACLS = “A”, then intention = “Intended”, with a truth degree of 0.1 (1/10).

**Rule 4:** If ACLS = “B”, then intention = “Unintended”, with a truth degree of 0.05 (1/20).

The same procedure was then applied on MDLS classifier to re-define the fuzzy sets for Subject B. The determination of fuzzy sets for MDLS classifier was based on distribution of MDLS values yielded by Subject B, shown as Figure 5.5.



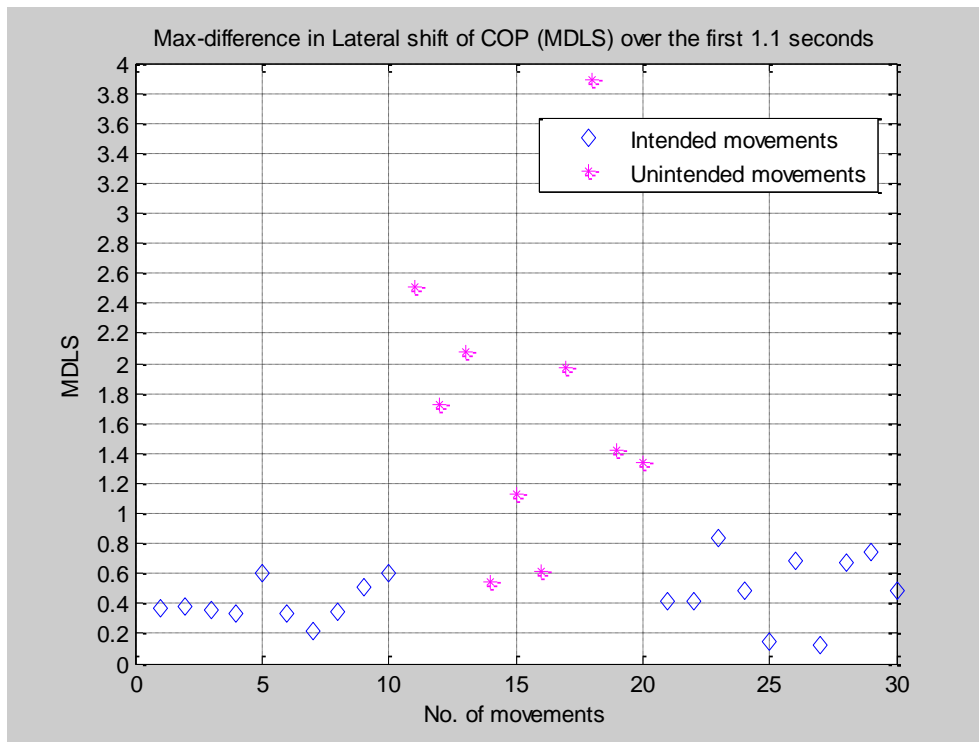


Figure 5.5 Distribution of MDLS of the respecting Unintended and Intended movements performed by Subject B

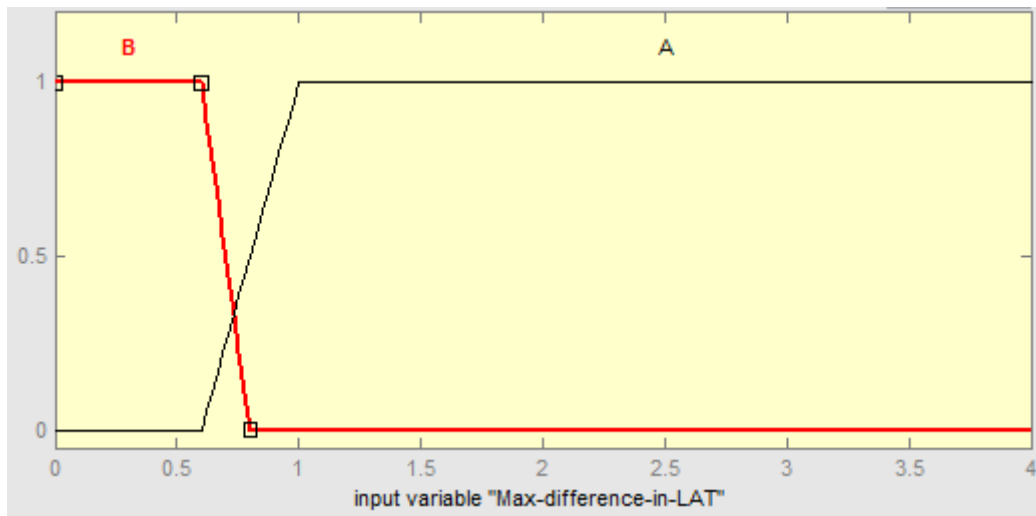


Figure 5.6 Fuzzy sets of A and B respecting to the MDLS classifier for Subject B

Fuzzy set A represents Unintended movements, with boundaries set as  $[0.6, 1, 4]$ . Fuzzy set B represents Intended movements, with boundaries set as  $[0, 0.6, 0.8]$  (Figure 5.6). The shape of membership functions remained the same as trapezoid. Fuzzy rules and the corresponding truth degrees were established as:

**Rule 1:** If MDLS = “A” then “Unintended”, with a truth degree of 0.9 (9/10).

**Rule 2:** If MDLS = “B” then “Intended”, with a truth degree of 0.95 (19/20).

**Rule 3:** If MDLS = “A” then “Intended”, with a truth degree of 0.1 (1/10).

**Rule 4:** If MDLS = “B” then “Unintended”, with a truth degree of 0.05 (1/20).

		Classification	Results
		<i>Unintended</i>	<i>Intended</i>
Actual Datasets	Unintended	90% True Positive	10% False Negative
	Intended	0% False Positive	100% True Negative

Figure 5.7 Confusion Matrix of ACLS applied on Subject B after manual adjustment

		Classification	Results
		<i>Unintended</i>	<i>Intended</i>
Actual Datasets	Unintended	90% True Positive	10% False Negative
	Intended	0% False Positive	100% True Negative

Figure 5.8 Confusion matrix of MDLS applied on Subject B after manual adjustment

Comparing the confusion matrices shown in Figure 5.7 and 5.8 against those shown in Figure 5.1 and 5.2, it can be seen the necessity for the shoe-width adaptation on fuzzy sets and rules to satisfy different users.

### 5.2.2 Self-adaptive neural fuzzy classification

Because of the ununiformed geometry of shoe soles and the limited number of FSRs adopted on footmat, it would be unrealistic to acquire the exact widths of shoes.



(a)

(b)

Figure 5.9 The distance between (a) the widest points of subject A's trainer: 116.95mm, (b) the narrowest points of Subject A's trainer: 79.85mm

Figure 5.9 shows the measurements on the trainer Subject A wears of the widest and narrowest points, respectively.



(a)

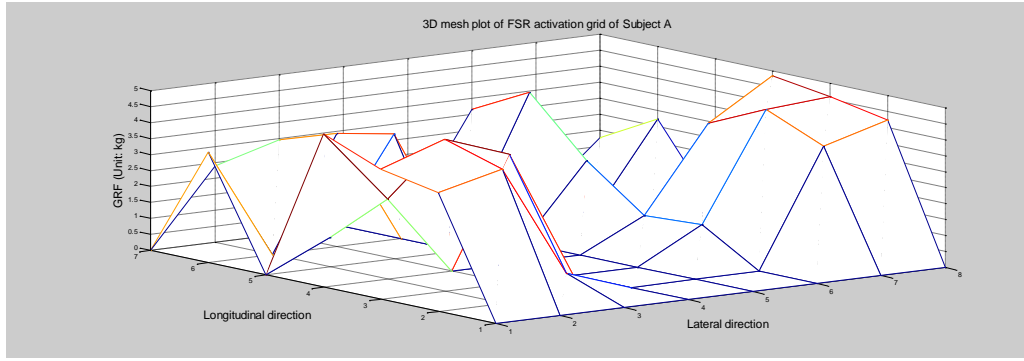
(b)

Figure 5.10 The distance between (a) the widest points of subject B's flat: 83.05mm, (b) the narrowest points of subject B's flat: 81.45mm

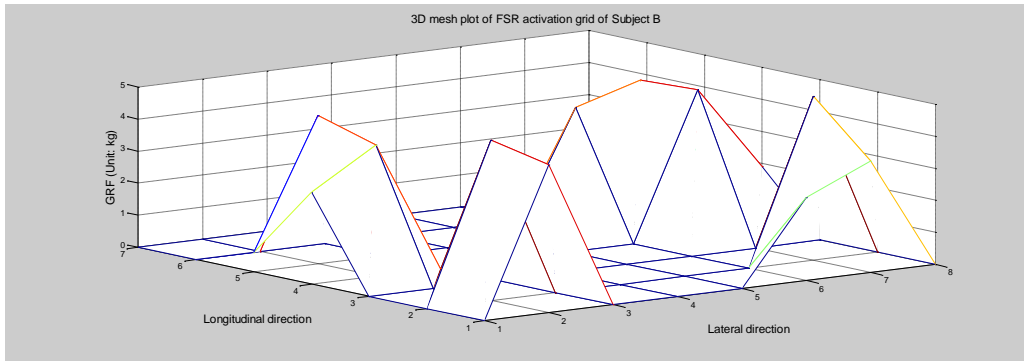
Figure 5.10 shows the measurements on Subject B's flat shoe at different points, such a substantial difference in geometries of shoe soles will certainly cause different areas of footmat being activated while subjects sitting on the robot chair.

The 3D mesh plot, Figure 5.11, demonstrates the difference in number of activated cells as well as GRF patterns (cell-wise) generated by the two subjects. In Figure 5.5, the horizontal rectangular grid reflects the actual positioning of FSRs being activated while the vertical direction represents the single-valued GRF output of each cell with no smoothing effects added to the plot. This shows the different manifestations on footmat caused by different geometric

shapes of shoe.



(a)



(b)

Figure 5.11 3D mesh plot of activated FSRs with height being cell-wise GRF values generated by Subject A (a) and Subject B (b), respectively

From Figure 5.11 it can be seen that Subject A occupies 7 rows and 26 cells while Subject B occupies 6 rows and 15 cells. However, the number of rows and the total number of cells activated by the same subject are rather fixed. This offers a possibility that the shoe widths of individuals can be normalised and converted to a computational feature. In order to realise this normalisation, the average number of cells occupied in each row was investigated in a way that only the number of cells activated per row was considered, regardless of the number of rows (of FSR cells) occupied by both feet.

Hence the normalised shoe width,  $w_s$ , was derived as,

$$w_s = \frac{\text{Number of FSRs}}{\text{Number of Rows}} \quad (5.1)$$

As to the 60 sets of movements performed by Subject A, each foot can active in average of 13.12 FSRs when stepping on the footmat, comparing to merely 7.54 FSRs activated by Subject B. They were both normalised to an average of 3.75 and 2.51 FSRs across each row, activated by both feet of the two subjects, which were denoted as normalised shoe width. And the span of this normalised shoe width, [2.51 3.75], resembles a range of all possible shoe widths of all eligible chair uses because of the characteristics of Subject A and B.

A hybrid method incorporating neural network (ANN) and fuzzy logic system is implemented to achieve self-adaptation of the classifier. As it can reflect the biomechanical feature of different users,  $w_s$  is used as a signal to tune the fuzzy sets of this hybrid neural fuzzy system, which will be further demonstrated using the structure of ACLS and MDLS models. In general, this self-adaptation equips the conventional fuzzy logic based classifier the abilities of adapting to complex individual characteristics and condition variables despite the compact architecture. All MFs of input fuzzy sets are able to adapt themselves to new subject once figured out his/her biomechanical feature, namely the normalised shoe width.

To better understand the model, a reference setting was introduced prior to the training process: a full set of MFs with predefined parameters was generated as a starting point where the hybrid system initialises. This follows the identical procedure as previous FIS models, using the empirical data. In the training process, which employed LSE-BP combined method, the contribution of ANN is to tune the reference setting, through automatically expanding, shrinking or shifting the reference MFs. All the computational efforts will be undertaken by ANN part of the model through training process.

The structure of the hybrid neural fuzzy classification is shown in Figure 5.12.

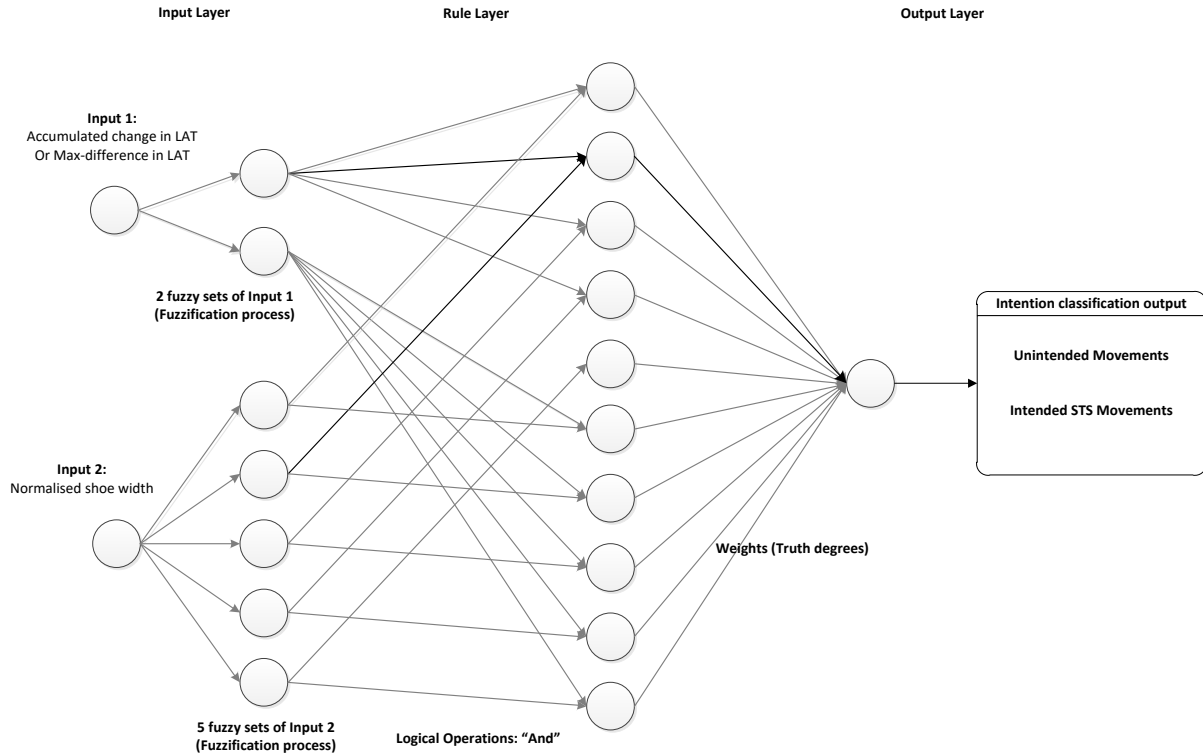


Figure 5.12 Architecture of hybrid neural fuzzy system for ACLS and MDLS classification handling the variations in shoe width

Such architecture was determined with the followings:

- Number of inputs: 2.

Input 1 is the Accumulated change in LAT or Max-difference in LAT. Input 2 is the normalised shoe width  $w_s$ .

- Number of Fuzzy sets for each input

Input 1 (MDLS/ ACLS): 2,

Input 2 (Normalised shoe width  $w_s$ ): 5,

The number of fuzzy sets for  $w_s$  was set as 5 to achieve a refined partition. The boundaries of all fuzzy sets of both inputs, in addition to the parameters of the corresponding MFs, would be optimised through the training of the ANN of such a hybrid system.

- Shape (type) of MFs “Bell, Trapezoid, Triangle, ...”

The shape of MFs of each input fuzzy set has been determined through the comparison of training results (Table 5.4) to figure out the most suitable one for the MDLS and ACLS model.

- Output: constant “2” and “1”

“2” and “1” represent Unintended and Intended STS movements, respectively.

The connections between input layer and output layer are described as fuzzy rules, where all possible combinations of fuzzy sets of the two inputs are bonded together using “and” logical operations. Afterwards, the output node computes the weighted sum of the outputs generated by the fired rules, which is also known as defuzzification process in fuzzy logic system. The crisp result of this output node is the classified intention, apparently.

### 5.2.3 Training and testing results

Training process of this inter-subject self-adaptive classifier has incorporated 60 sets of data, comprising of 30 sets of movements, namely 10 Intended Successful STS, 10 Unintended and 10 Unsuccessful STS movements, generated by Subjects A and B, respectively. A training method of LSE-BP was adopted.

It is also worth to mention that the shape of input MFs has been determined through comparison among Bell, Gaussian and trapezoid, which was previously adopted in fuzzy logic based classification for Subject A as well as manual adjustments on Subject B. The training performances yielded by the different shapes of MF were listed in Table 5.4. The metrics discussed in Chapter 4, TMR and FMR in relation to accuracy and safety were used to find out the ideal shape of MFs. Through the separate training carried out on each type of MF, the Gaussian-type was found to be superior to others for both ACLS and MDLS classifications.

Table 5.4 Training results investigating the shape of MFs for both classifiers

Self-adaptive classification for handling normalised Shoe Width									
Shape of MF	ACLS classification					MDLS classification			
	Trapezoid	Triangle	Gaussian	Bell		Trapezoid	Triangle	Gaussian	Bell
TMR (%)	85.00	90.00	90.00	85.00		85.00	85.00	90.00	85.00
FMR (%)	2.50	5.00	2.50	2.50		2.50	2.50	0.00	0.00
Average convergence time (Seconds)	2.40	2.30	3.80	4.70		1.90	2.00	2.80	3.90
No. of epochs	44	39	73	62		49	45	57	69

As to the above hybrid structure with the optimised shape of MFs, the convergence of training error is shown in Figure 5.13. The convergence of training error was evaluated using mean

squared error (MSE) for its simplicity, which will be further explained in Chapter 6. The training reached its best performance at epoch 73, which signifies the end of convergence process as the performance was no longer improving.

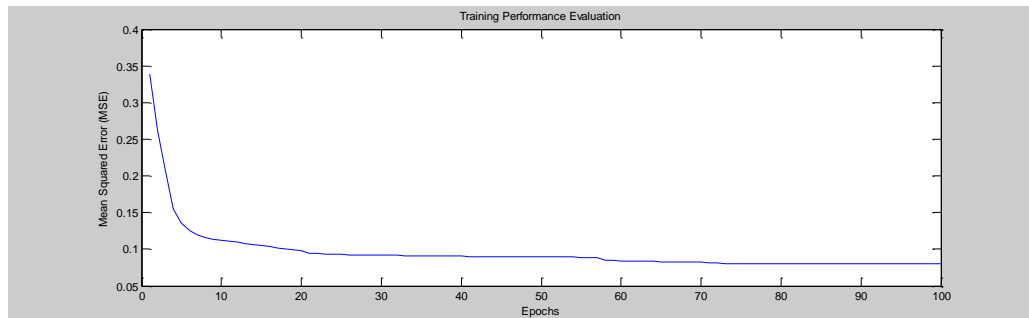


Figure 5.13 The convergence of training error of ACLS self-adaptive classifier

To test the trained ACLS and MDLS self-adaptive classifiers, another 60 sets of movements were allocated, including 10 Intended Successful STS, 10 Unintended and 10 Unsuccessful STS movements, generated by Subjects A and B, respectively. The test results of the trained ACLS classifier can be seen in Figure 5.14, where 3 sets of Unintended movements were classified as Intended while 1 set of Intended STS movement was classified as Unintended. This caused a TMR of 85% and FMR of 2.5%, which forms the confusion in Figure 5.15.

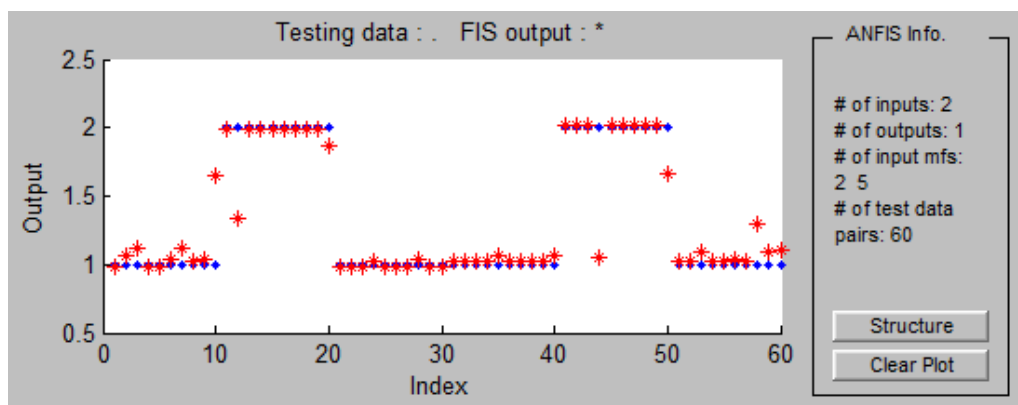


Figure 5.14 Test results with the raw defuzzification outputs generated by ACLS self-adaptive classifier



		Classification		Results	
		<i>Unintended</i>		<i>Intended</i>	
Actual Datasets	Unintended	90%	True Positive	10%	False Negative
	Intended	2.5%	False Positive	97.5%	True Negative

Figure 5.15 Confusion Matrix of the self-adaptive ACLS classifier tested by two subjects along with their 1<sup>st</sup> biomechanical feature (60 sets of pure test data)

		Classification		Results	
		<i>Unintended</i>		<i>Intended</i>	
Actual Datasets	Unintended	90%	True Positive	10%	False Negative
	Intended	0	False Positive	100%	True Negative

Figure 5.16 Confusion matrix of self-adaptive MDLS classifier tested by two subjects along with their 1<sup>st</sup> biomechanical feature (60 sets of pure test data)

The test with same data was also conducted on the self-adaptive MDLS classifier, with confusion matrix shown in Figure 5.16. Apparently, both results outperformed the test results shown in Figure 5.1 and 5.2 where the ACLS and MDLS classifiers defined for Subject A were applied to Subject B. However, when comparing them against those manually adjusted classifiers (for Subject B), the combination of Subject A and B's test results has to be taken into consideration. In order to achieve a like-to-like comparison, the test data fed in self-adaptive classifier needs to be identical to that used for the previously defined classifiers.

The results shown in Figure 5.7, along with the test results in Figure 4.24, has yielded an overall TMR of 95% and FMR of 15%. The manual adaptation test results of Subject B (Figure 5.8), together with the results of Subject A (Figure 4.26), has reached an overall TMR of 95% and FMR of 17.5%. Therefore it can be addressed that the self-adaptive ACLS classifier generates less TMR (90% against 95%) but less FMR (2.5% against 15%), when applied on the same test data. The latter was reduced in a good manner because it relates to the safety concerns of the robot chair and was discussed as the primary measure of criteria in Chapter 4. The self-adaptive MDLS classifier generates less TMR (90% against 95%) but less FMR (0 against 17.5%) when applied on the same test data. Therefore, such self-adaptation on the 1<sup>st</sup> biomechanical feature has its merit in terms of reducing the FMR of the classification.

The following shows how rules are triggered in the self-adaptive ACLS classifier based on the input variables. Given the value of accumulated change in LAT as 3.31, which is the sampled value of input 1 from an Intended movement, generated by Subject A at a measured shoe width of 3.69, fuzzy rule No. 4, 5, 9 and 10 were triggered, as shown in Figure 5.17.

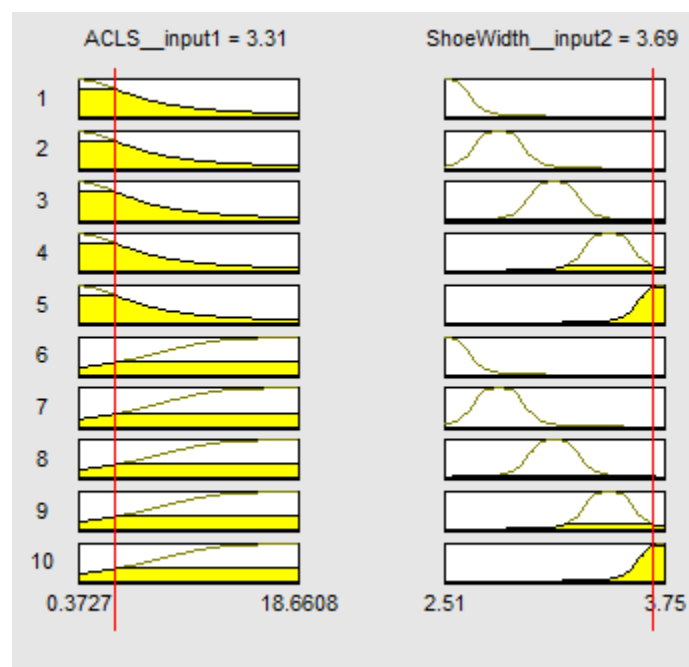


Figure 5.17 Rules fired by Example 5.1 in the self-adaptive ACLS classifier

### 5.3 Self-adaptive fuzzy classification for handling 2nd biomechanical feature

Previously, the manual adaptation on both ACLS and MDLS was elaborated prior to the implementation of the neural fuzzy based classifier for a better understanding of the self-adaptation process. However, the manual adaptation process was omitted because it is difficult to generalise in multi-subject scenarios, albeit decent results were generated for Subject B. When implemented and trained properly, the neural fuzzy based classifier would be able to tackle the variations in width of stance in a time-efficient manner.

The remedy to deal with the seated stance was called the 2<sup>nd</sup> biomechanical adaptation, where the classifier has to actively adapt to the changes yielded by the different stances generated from the same subject between movements. The seated stance width cannot be ascribed as an attribute to different subjects because each movement performed by the same subject will show variations in stance width appearing on the footmat.

As the experimental data suggests, for the same amount of buttock movement achieved, the subject with a naturally wider stance while seated will produce a greater difference between COPs on both feet. However, such a relationship is not linear and would be difficult to describe mathematically for the following reasons:

- Due to different thigh lengths of subjects for the same stance width, the resultant LAT will vary.
- The positioning of the upper trunk will result in different captured LAT for the same subject at the same stance width, through observations. As the activities of the head-arm-torso (HAT) system will vary its position and velocity when the subject performs each experimental movement.
- Because the muscle activation patterns in STS transfers with the same sitting posture and stance may alter (O'Sullivan et al, 2002), the resultant LAT will be different.

Although it is unrealistic to model mathematically the influence of stance width on LAT, the necessary capture of this 2<sup>nd</sup> biomechanical feature has been performed at the instance of

initialising every single movement. This was achieved by computing the magnitude difference between the COP generated by both feet in lateral directions, at a unit of cell-to-cell distance. Note the COP of each foot's pressure pattern (Figure 5.11) is different to the geometric centre of each foot. As an outcome, the normalised stance width of subject A varied from 4.1 to 6.2, whereas the normalised value of Subject B ranged from 3.2 to 5.9, with cell-to-cell distance as per unit. The narrowest possible stance was only achieved by placing both feet extremely close to each other (with the edges of both shoes touching side by side).

### 5.3.1 Architecture of self-adaptive ANFIS classification

The structure of the self-adaptive classifier handling 2<sup>nd</sup> biomechanical feature was formed as follows.

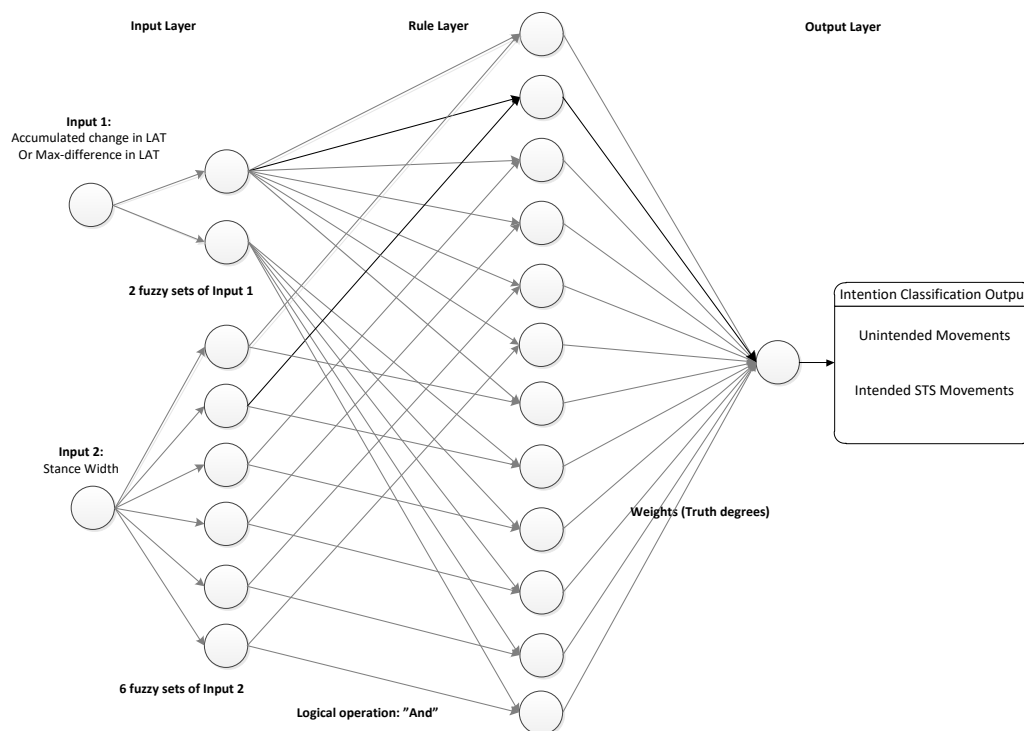


Figure 5.18 Architecture of hybrid neural fuzzy system for ACLS and MDLS classification handling the variations in stance width

- Number of inputs: 2 (MDLS/ ACLS and Stance width)  
Input 1 is the Accumulated change in LAT or Max-difference in LAT.  
Input 2 is the normalised stance width.

- Number of Fuzzy sets for each input

Input 1 (MDLS/ ACLS): 2,

Input 2 (Stance width): 6 Compared against the previous self-adaptive classifier, more fuzzy sets were assigned to Input 2 as the training data on stance width incorporates available values in a range of 3.2 to 6.9, rather than merely two normalised shoe widths from two subjects.

- Shape (type) of MFs: “Bell, Trapezoid, Triangle, ...”

The shape of MFs of each input fuzzy set has been determined through the comparison of training results (Table 5.5) to figure out the most suitable conditions for the MDLS and ACLS model.

- Output: constant “2” and “1”

“2” and “1” represent Unintended and Intended STS movements, respectively.

### 5.3.2 Training and testing results

The training process of this self-adaptive classifier has incorporated 60 sets of data, which consist of 30 sets of movements generated by each of the two subjects, namely 10 Unintended and 20 Intended STS movements. The corresponding stance width of each movement has been computed using the data processing methods introduced before. A training method of LSE-BP was adopted.

Table 5.5 Training results investigating the shape of MFs for both classifiers

Training performance as per type of MF									
Self-adaptive classification for handling normalised Stance Width									
ACLS classification					MDLS classification				
Shape of MF	Trapezoid	Triangle	Gaussian	Bell	Trapezoid	Triangle	Gaussian	Bell	
TMR (%)	85.00	95.00	100.00	95.00	90.00	90.00	95.00	95.00	
FMR (%)	2.50	5.00	2.50	2.50	2.50	5.00	2.50	2.50	
Average convergence time (Seconds)	9.30	13.80	14.50	15.00	5.00	7.50	6.50	6.00	
No. of epochs	411	497	991	605	347	611	760	742	

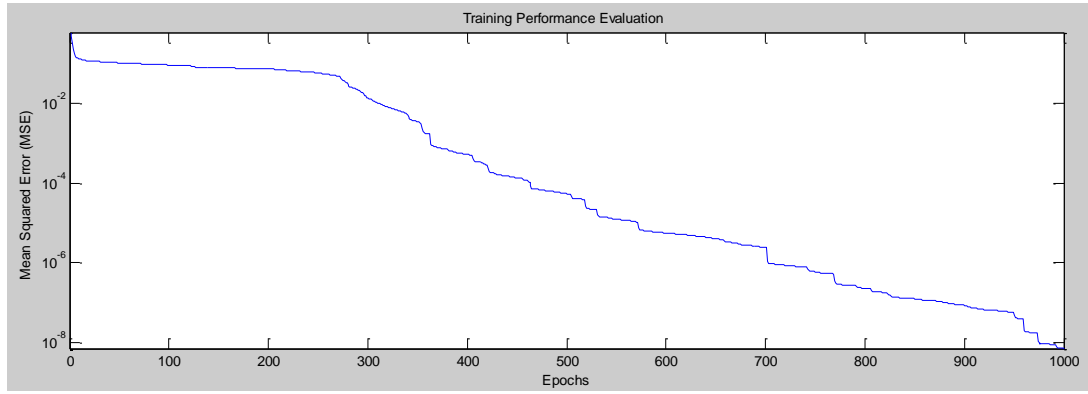


Figure 5.19 The convergence of training error (MSE) of the ACLS self-adaptive classifier on 2<sup>nd</sup> biomechanical adaptation

The training of the ANN model has its convergence of MSE shown in Figure 5.19. The training reached its best performance at epoch 991, which signifies the end of convergence process as the performance was no longer improving.

To test the trained ACLS and MDLS self-adaptive classifiers, another 60 sets of movements were allocated, including 10 Unintended and 20 Intended STS movements STS movements, generated by Subjects A and B, respectively. The test results of the trained ACLS classifier can be seen in Figure 5.20, where 2 out of 20 sets of all Unintended movements were classified as Intended while 1 out of 40 sets of all Intended STS movements was classified as Unintended. This caused a TMR of 90% and FMR of 2.5%, which forms the confusion matrix in Figure 5.20. The confusion matrix of the 2<sup>nd</sup> biomechanical adaptation tested on MDLS classifier is presented in Figure 5.21.

		Classification		Results	
		<i>Unintended</i>		<i>Intended</i>	
Actual Datasets	Unintended	90%	True Positive	10%	False Negative
	Intended	2.5%	False Positive	97.5%	True Negative

Figure 5.20 Confusion Matrix of self-adaptive ACLS classifier tested by two subjects along with their 2nd biomechanical feature (60 sets of pure test data)

		Classification		Results	
		<i>Unintended</i>		<i>Intended</i>	
Actual Datasets	Unintended	95%	True Positive	5%	False Negative
	Intended	0%	False Positive	100%	True Negative

Figure 5.21 Confusion matrix of self-adaptive MDLS classifier tested by two subjects along with their 2nd biomechanical feature (60 sets of pure test data)

Comparing to those test results generated by the manually constructed fuzzy based classifiers, both 2<sup>nd</sup> feature ACLS and MDLS self-adaptive classifiers yielded better performance in terms of the respective TMR and FMR, referring to Table 5.6. For both ACLS and MDLS classifiers, it is interesting to see results generated by this self-adaptive classification with the 2<sup>nd</sup> biomechanical feature outperformed those with the 1<sup>st</sup> biomechanical feature.

Table 5.6 Test results generated by ACLS and MDLS classifiers

		ACLS Classifier				MDLS Classifier			
		Manul Fuzzy Classification	Self-adaptive classification			Manul Fuzzy Classification	Self-adaptive Classification		
Biomechanical Feature		Not applicable	Shoe Width	Stance Width		Not applicable	Shoe Width	Stance Width	
Overall Accuracy (%)		88.33	93.33	95.00		86.67	96.67	98.33	
	TMR (%)	95.00	85.00	90.00		95.00	90.00	95.00	
	FMR (%)	15.00	2.50	2.50		17.50	0.00	0.00	

## 5.4 Discussion

As the self-adaptive classifier is as an enhancement of the manually defined fuzzy based classifier introduced in Chapter 4, those previously proposed criteria should be reviewed first.

- FMR is the primary measure related to safety issues, which should be minimised as false matching will cause a potential hazard when an assist motion is provided to the user who has no intention to stand up and is not expecting to be pushed upwards.
- TMR is the essential measure for the accuracy. This should be maximised as the aim of the self-adaptive classification is accurately recognise the intentions of the user, regardless of the variations in biomechanical features.
- Variety in sample data (VD) is used to measure the robustness. In addition to the VD in captured LAT discussed in Chapter 4, VD also concerns the biomechanical features newly introduced: normalised shoe width and stance width. The high uncertainty level in the sample data implies the capabilities of handling the uncertainty in intention recognition.
- Responding time of the classification (RT) reflects the time criterion set for intention recognition; STS movement classification must be completed at the end of the first 1.1 seconds period.

The first two measures, the FMR and the TMR, were considered together according to the four confusion matrices listed in Figures 5.15, 5.16, 5.20 and 5.21. As the test results indicated, the 2<sup>nd</sup> adaptive classification has outperformed the 1<sup>st</sup> adaptive classification) in terms of both TMR and FMR, when applied to either ACLS or MDLS classifier. However, whether the 2<sup>nd</sup> adaptive classification is always superior to the 1<sup>st</sup> one is an open question. It is worth investigating whether there are circumstances where the 2<sup>nd</sup> adaptive classification generates incorrect results while the 1<sup>st</sup> biomechanical classification generates correct ones. From the results of the 1<sup>st</sup> adaptive classification applied on the ACLS classifiers, the erroneous



classification outputs appeared at movements Nos. 12 and 44 (meant to be Unintended) and No. 10 (meant to be Intended), which contribute to a TMR of 90% and a FMR of 2.5%. When applying the 2<sup>nd</sup> adaptive classification on the ACLS classifiers, the test results show errors at movements Nos. 12 and 44 (meant to be Unintended), resulting in a TMR of 90%. This signifies that the misclassified movements generated by the 2<sup>nd</sup> adaptive classification would also be misclassified by the 1<sup>st</sup> adaptive classification. The same pattern was also observed when implementing both adaptations on the MDLS classifiers.

Consequently, the possible explanation would be, that the 2<sup>nd</sup> biomechanical feature, rooted in the sitting postures when subjects perform STS movements, has greater influence on the extracted ACLS and MDLS values, albeit the degree of impact is difficult to prove mathematically, as previously stated. Therefore, the self-adaptive classification incorporating normalised stance width deserves higher priority than the one incorporating normalised shoe width.

As explained before, when comparing the two self-adaptive classifications, it is crucial to have the test data with 1<sup>st</sup> inputs, the ACLS or MDLS values as well as the classification targets fixed. This primarily ensures the VD, which refers to the different ways in which COP shifts. As discussed in previous chapters, the VD in LS of COP is provided by subjects' STS strategies, muscle activation patterns, and postures, and how they position their arms, upper torso, buttocks, ankles and feet. These factors are also interrelated because, for instance, different sitting postures will result in different STS strategies, which all contribute to a rich VD from one aspect.

As to another of the VD, the biomechanical features incorporated by both classifications, shoe width and stance width, should be thoroughly analysed. As demonstrated in Section 5.2.2, the shoe widths of both subjects after normalisation have only two mean values simply because of the number of subjects, although the actual shoe width extracted from the footmat can be slightly different between movements performed by the same subject. Because of the limitation that confines this study, it has been difficult to employ more subjects willing to conduct the test. Although two subjects fulfilled the home-use scenarios, further subjects will certainly enrich

the variations in shoe widths, hence increasing the VD. In contrast, the stance width generated by both subjects has a much wider range [3.2, 6.9] and greater variations owing to the different postures adopted (Table 5.3) for the movements. The second facet of VD confirms the ability to adapt to a wide range of the targeted feature, in which the 2<sup>nd</sup> adaptive classification is superior to the 1<sup>st</sup> adaptive classification.

When it comes to the RT, both self-adaptive classifications were characterised as time efficient and capable of handling different kinds of uncertainties. The processing times of the 1<sup>st</sup> adaptive classification applied to the ACLS and MDLS classifiers were recorded as 0.006 seconds and 0.004 seconds, respectively. The processing times of the 2<sup>nd</sup> adaptive classification applied on the ACLS and MDLS classifiers were recorded as 0.01 seconds and 0.007 seconds, respectively. These are considered negligible compared to the 1.1 seconds of input data extraction.

Therefore, all four performance measures ensure that under the current experimental setups and conditions, with the test data used so far, the 2<sup>nd</sup> adaptive classification applied to the MDLS classifier deserves more credibility over the other combinations, and hence was finalised as the most competent intention classifier. And in the sense of the first three performance measures and RT concerns, there is no need for integrating both self-adaptive classifications.

## **5.5 Summary**

In this chapter, a new subject with completely different biomechanical features was introduced to fulfil the demand of the home-use scenario where one or two users can receive personalised STS aided by the robot chair. The previously defined fuzzy logic based intention recognition should be expanded to a multi-user scenario where subjects of completely different heights and sitting habits can be recognised during STS transfer. The self-adaptive classifications handling 1<sup>st</sup> and 2<sup>nd</sup> biomechanical features were developed separately, incorporating both knowledge-based fuzzy logic part and ANN part. The testing process using pure fresh data generated by Subjects A and B was then carried out. This ensured the self-adaptive classification trained with

existing (training) data will generalise so that it will be well-suitable for new test data involving different biomechanical features. The results generated by both adaptive classifications were also evaluated through the proposed measures of criteria.

Applying this self-adaptive fuzzy system will encourage a multi-user scenario. Moreover, having adaptive fuzzy sets and corresponding MFs can advance the fuzzy logic based classifier to its maximum potential, especially when the same subject changes sitting postures to adapt to different environmental and physical conditions.

## **CHAPTER 6 NEURAL NETWORK BASED ASSISTANCE PREDICTION**

After the recognition of the user's intention of standing up, a prediction on the GRF a couple of steps ahead will enable the robot chair to foresee the user's needs for assistance. This prediction is also regarded as intent recognition. The predicted GRF can then be used to compare against the personalised ideal GRF indicating Successful STS as described in Section 4.1. The difference between the two is proportional to the amount of assistance required to stand up.

GRF contains both spatial information and temporal information, which are related to the trajectory (posture changes along with time) of the chair user during the later stages of the STS process. Therefore, the recorded GRF data are of the form of time series. This research developed artificial neural network (ANN) based predictor that undertake predictions based on the time series data.

### **6.1 Background Knowledge on time series prediction**

Time series is widely known as a sequence of continuous data that includes information of historical values over a period of time. Time series forecasting refers to predicting the future value of a time series based upon previous historical records. This prediction can be challenging as time series data largely comprises of random noise in spite of the identifiable and predictable mainstream trends.

Difficulties confronted in time series prediction due to its non-linear modelling because data is only formed through given observation. It is hard to presume any statistical distributions through this observation of the timely phenomenon. Therefore to tackle this prediction problem, possible predictor has to be self-adaptive without the exact mathematical model of the data instincts. Primarily, a briefing analysis on the observed series has to be conducted to explore

the underlying of how series are generated and evolved (Chatfield, 1996). Besides, understanding how time series are affected by other factors, if any, is of the same importance as the model itself.

Traditional methods handling time series data are commonly recognised such as moving average (MA) as well as regression models (RG), like linear trend and exponential smoothing. These methods share similarities in terms of attempting to assume a constant model for the series solely based on statistical analysis. Variance of the error is separated into two parts, error when estimating the mean of series and error brought in by noise. The new estimate is the old estimate plus a proportion of the observed error.

The selection of a forecasting method is a difficult but pre-requisite task that must be achieved on the basis of instincts of time series itself. This is commonly a trial-and-error process due to the intangible characteristics of data. Without a concrete understanding of model, it is hard to adequately fit the system because whether trend is driven by fundamental change or purely random noise is far from interpretable.

Also, based on statistical principles, the most recent fitting errors have more impact on the predicted value. This explains the reason that for all these moving average and regression methods, accuracy will decrease dramatically with predictions into the future, which is also known as prediction horizons due to the accumulation of random noise.

## **6.2 Feed forward neural network and its regimes**

As the overwhelming advantage, ANN does not require time series model to be thoroughly interpreted. This offers ANN the capability of modelling highly non-linear systems with complexities beyond human expectations and mathematic estimations that exist in human behaviour, natural phenomena and financial time series. Using ANN to handle these temporal-spatial data in order to predict future values is called neural network time series (NNTS).

ANNs, including feed forward neural networks (FFNNs) and recurrent neural networks (RNNs), have been widely used in time series prediction over decades. Figure 6.1 illustrates the basic scheme of FFNN used in NNTS.

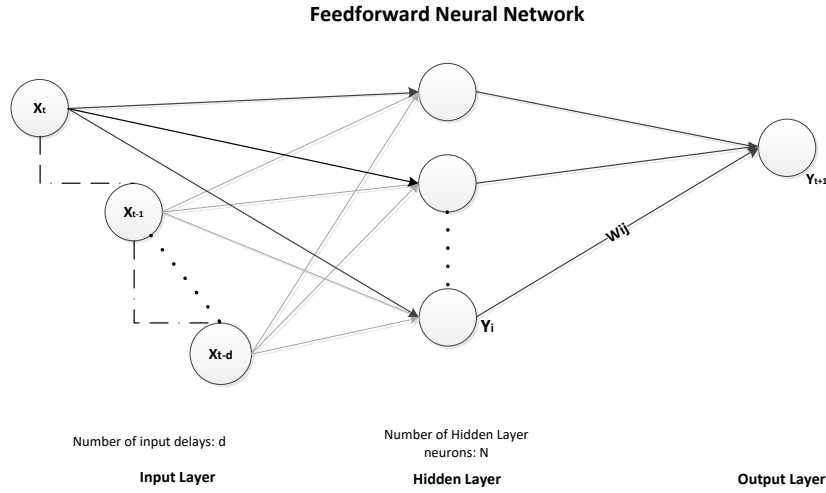


Figure 6.1 Schematic structure of FFNN for time series prediction

Figure 6.1 illustrates a simplified structure of FFNN used in time series prediction. Firstly, time series data feed in the input layer in a manner of tapped delay. Data is then forward propagated into hidden layer. Hidden layer generates output  $y_i$ , with  $i$  representing one of hidden layer neurons. Subsequently, data flow reaches output neuron  $j$  which accordingly delivers output  $y_j$ , regarded as next time step predicted value  $y_j$  from the viewpoint of time series prediction.

Each neuron  $j$  contains a summation function and an activation function. The summation is a weighted sum of all the outputs generated by the previous layer and received by neuron  $j$ . Activation function is used for the sake of handling non-linear data, the greater magnitude of input (weighted sum) is, the closer activation is to 1. The output of a neuron can therefore be represented as,

$$y_j = \varphi\left(\sum_{i=0}^N w_{ij} \cdot y_i\right) \quad (6.1)$$

where  $\varphi$  is the activation function of the neuron and  $\sum_{i=0}^N w_{ij} \cdot y_i$  is the summation of weighted inputs that are the outputs of the neurons from the previous layer.

## 6.3 FFNN based GRF Prediction

### 6.3.1 FFNN Structure

As can be readily seen in Figure 4.2, the Successful GRF curves follow a similar pattern, with intuitive observations. The study on temporal GRF features a human autoregressive (AR) time series without exogenous input, focusing on trend rather than seasonal or cyclic as mainstream of components. This instinct nature offers the potential of reconstructing a particular STS pattern for the featured GRF curve using ANN, namely. All input data are sequences of consecutive discrete GRF points of measurement:

This FFNN based predictor aims at foreseeing the oncoming GRF values and compare them with standard personalised curve obtained via continuous training.

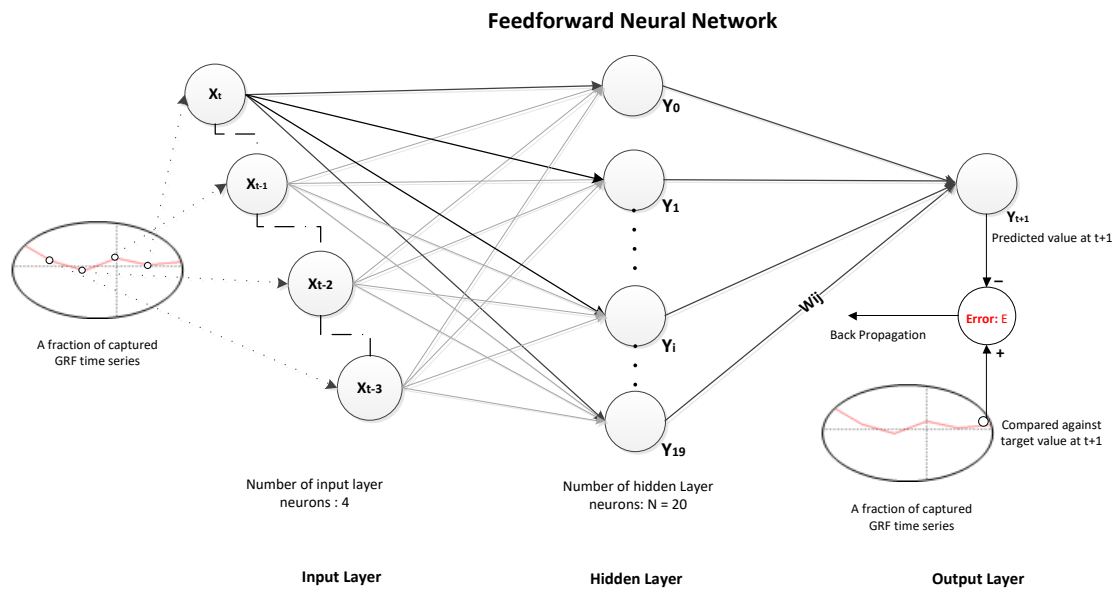


Figure 6.2 Structure outline of FFNN used to handle time series GRF data

Based on the simplified scheme design, the FFNN model to predict the future values of GRF was structured in Figure 6.2. It can be seen the predicted output solely depends on the past values of the captured GRF within the duration of time delay. The BP training was conducted based on the error occurred in output layer, and back propagated to update the weights at hidden layer.

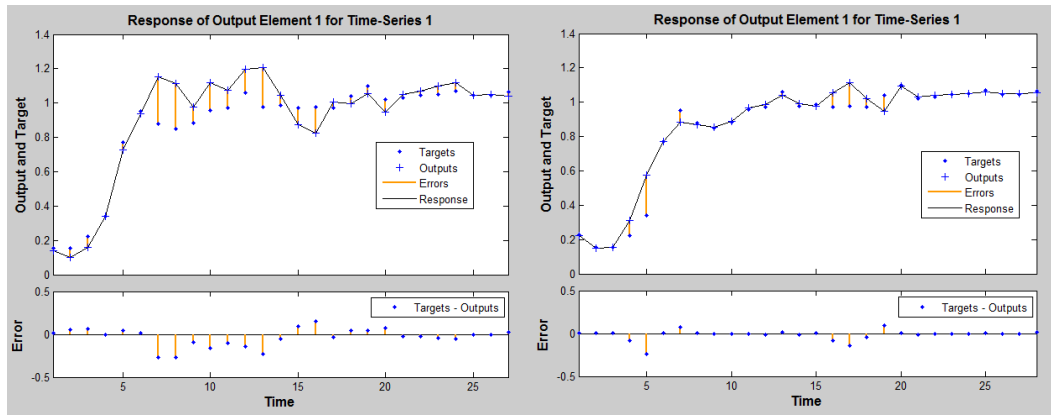
This FFNN has a 3-layer design, namely input layer, output layer and one hidden layer in between. Given the GRF being the only input and output feature of the FFNN, only one hidden layer was employed for its computational simplicity and fast response. FFNN with 1 hidden layer has been long employed as effective predictor by study on time series prediction, which can be seen from related work on FFNN incorporating one hidden layer for clinical prediction (Fogel et al, 1995; Colin, 2004; Mohktar, 2013) and foreign exchange rate prediction (Oancea and Clucu, 2014). Specifically, the input layer incorporates 4 neurons, the hidden layer employs 20, and the output layer has 1 neuron, generating 1 predicted value for each time step after delays. The entire process that configured the structure is demonstrated below.

Such structure of the FFNN was determined by manipulating the initial parameters, namely, the number of input neurons, representing time delays in NNTS, and the number of hidden neurons. GRF with time delays are the input of the network and the number of delays in addition to the GRF value at time  $t$  refers to the number of input neurons. When determining the steps of time delay, 1, 2, and 3 time delay steps were considered, respectively. The time delay,  $d$ , is not suitable to be set too long for the prediction of GRF. This is because the GRF captured at the beginning of STS movement, typically 0.4 seconds, implies the initiation event of STS for the elderly, suggested by (Kerr et al, 1997; Etnyre and Thomas, 2007). This implies that the robot chair should be able to figure out whether assistance is needed within the initial period of 0.4 seconds. If the chair failed to do so, the elderly users may have already stated to sit back.

The number of hidden neurons greatly affects the performance of network, because the prediction result is the function of weighted sum of hidden layer outputs.

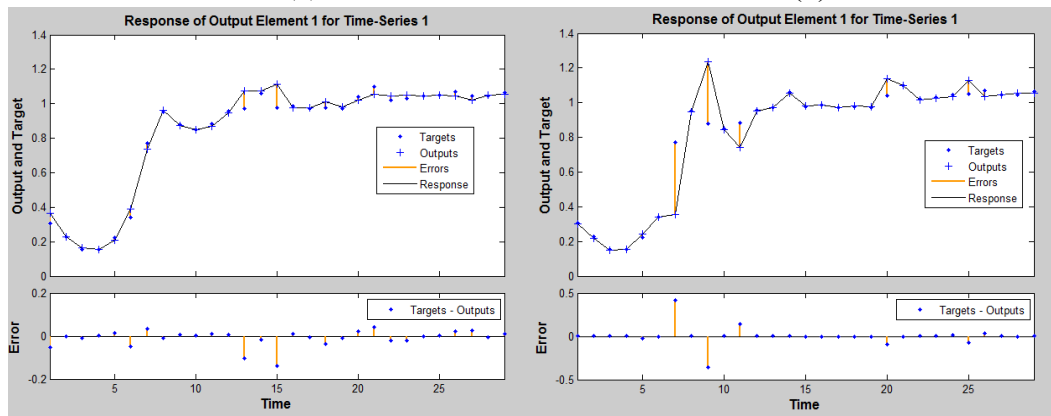
The delay,  $d$ , reflected by the time intervals taken as the predictor's inputs, and the number of hidden neurons,  $N$ , were purposefully varied to figure out the effect of both on prediction results. All responses of GRF time series generated by the FFNNs with different  $d$  and  $N$  are plotted below. This network response test is performed to select appropriate FFNN structure.





(a)

(b)

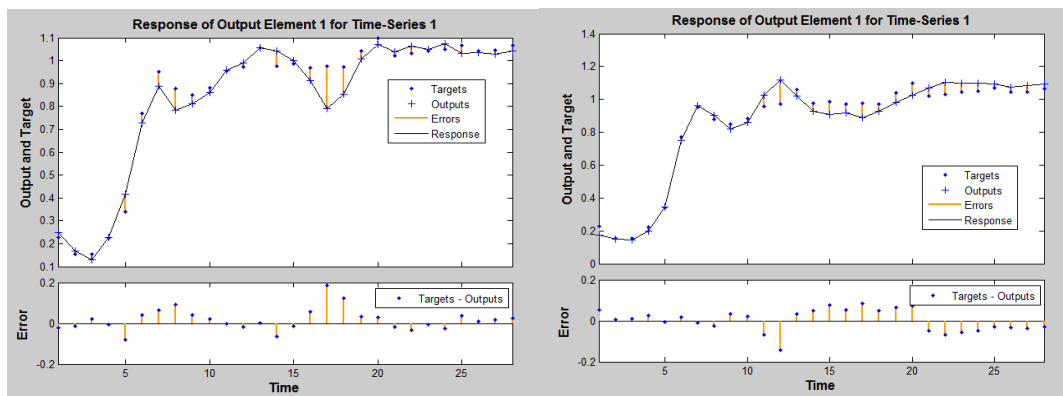


(c)

(d)

Figure 6.3 Prediction and deviations against the captured actual GRF curve

(a)  $d = 1$ ,  $N = 5$ , (b)  $d = 1$ ,  $N = 10$ , (c)  $d = 1$ ,  $N = 20$ , (d)  $d = 1$ ,  $N = 50$



(a)

(b)

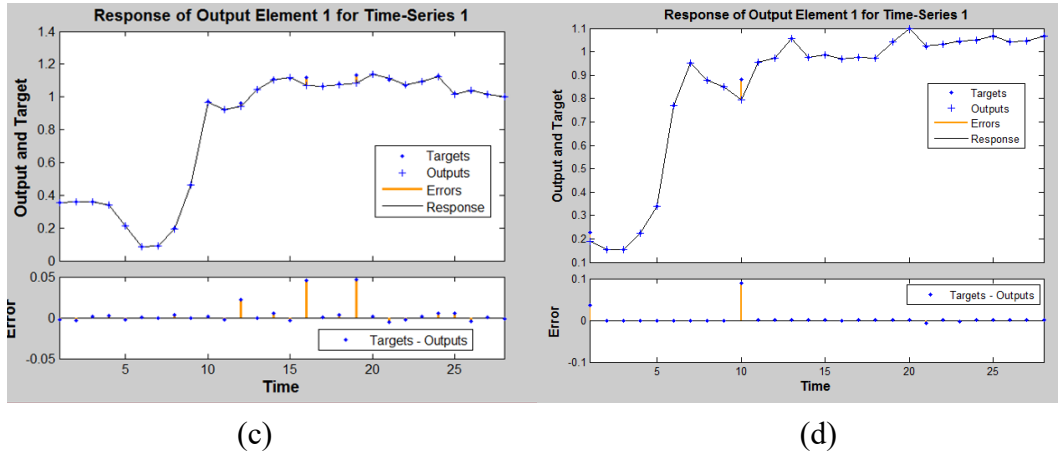


Figure 6.4 Prediction and deviations against the captured actual GRF curve

(a)  $d = 2$ ,  $N = 5$ , (b)  $d = 2$ ,  $N = 10$ , (c)  $d = 2$ ,  $N = 20$ , (d)  $d = 2$ ,  $N = 50$

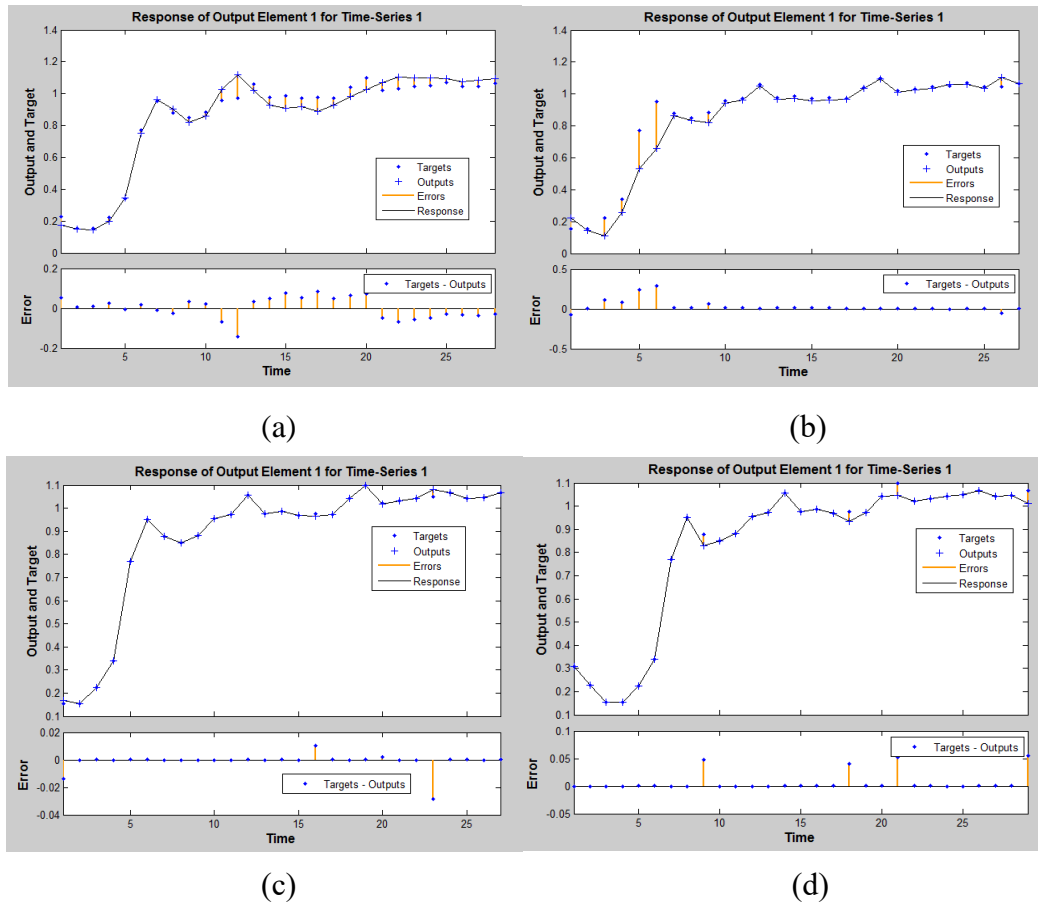


Figure 6.5 Prediction and deviations against the captured actual GRF curve

(a)  $d = 3$ ,  $N = 5$ , (b)  $d = 3$ ,  $N = 10$ , (c)  $d = 3$ ,  $N = 20$ , (d)  $d = 3$ ,  $N = 50$

From these comparative predictions, it can be clearly drawn that the FFNN predictor reached a good result when  $d = 3$  and  $N = 20$ . The definition of delay  $d$  suggests the number of past

values (in the captured GRF time series) feeding into the developed FFNN. The network deploys 4 inputs, including the 3 input delays and the input point at time  $t$ , suggested by Figure 6.2. The network with delay  $d=3$  outperforms that with  $d=1$  because the former plotted test results (network response) is closer to the actual curve of GRF data, yielding less deviations. The FFNNs with  $N = 10$  or less provided poor results as the network structure might not be able to reflect the complexity of the GRF time series. Whilst the FFNN with 50 hidden layer neurons seem to over fit the system, despite the number of input delay time steps. In this case although some training and validation results are seemingly satisfying, the network with overfitting issues are difficult to generalise to new input data, resulting in poor predictions. However, network with delay  $d=3$  outperforms that with  $d=1$  because the former plotted test results (network response) is closer to the actual curve of GRF data, yielding less deviations.

### 6.3.2 FFNN training

The general procedure of the FFNN training can be summarised as:

1. Randomise weights
2. Predict value of oncoming time steps
3. Compare the prediction results against targets
4. Update the weights of hidden layer neurons (guided by the selected regularisation techniques)
5. Iterations until the local minimum update of weights triggers the set criteria.

However, overtraining could be incurred as network may be trained to be so well adequate for certain batch of training data but may not be able to generate satisfying prediction results for new test data.

Therefore two regularisation techniques are investigated to mitigate overtraining and facilitate generalisation of the network, namely, early stopping (ES) and Bayesian regularisation (BR). Both training techniques belong to epoch-wise training, which resets the network state at the beginning of each epoch.

The algorithm with ES is Levenberg-Marquardt optimization. Often used in non-linear optimisation problems, the Levenberg-Marquardt (LM) algorithm can be viewed as a robust algorithm mixing the steepest descent method and the Gauss–Newton method. It incorporates the speed advantage of the Gauss–Newton algorithm and the stability of the steepest descent method (Levenberg, 1944; Marquardt; 1963 and Roweis, 1996).

The basic concept of the LM algorithm is that it performs a combined training process (Roweis, 1996): Around the area with complex curvature (on the error surface), the LM algorithm switches to the steepest descent algorithm, until the local curvature is proper to make a quadratic approximation; then it approximately becomes the Gauss–Newton algorithm, which can speed up the convergence significantly. The briefings on these algorithms are explained below.

#### **i).The gradient decent method**

The gradient decent method uses the first-order derivative of the overall error function to find the minima in error space. The gradient  $\mathbf{g}$  is defined as the first-order derivative of the overall error (Yu and Wilamowski, 2011):

$$\mathbf{g} = \left[ \frac{\partial E}{\partial w_1} \quad \frac{\partial E}{\partial w_2} \quad \dots \quad \frac{\partial E}{\partial w_N} \right]^T \quad (6.2)$$

When updating the weight with each iteration, the method function is presented as:

$$\mathbf{w}_k = \mathbf{w}_{k-1} - \alpha \mathbf{g}_k \quad (6.3)$$

where  $\mathbf{w}_k$  is the weight vector at iteration k,  $\alpha$  is the learning constant (step size).

#### **ii).The Gauss-Newton method**

The Gauss-Newton method assumes that all the gradient components  $g_1, g_2, \dots, g_N$  are functions of weights and all weights are linearly independent. This method uses second-order derivations (with the help of Hessian matrix) to evaluate error surface (Hagen & Menhaj, 1994). It features fast convergence speed compared against the gradient decent method.

Hessian is a square matrix of second-order partial derivatives of the overall error function, representing how error changes related to weight updates. With the second-order derivatives of

the overall error:

$$\mathbf{H} = \begin{bmatrix} \frac{\partial^2 E}{\partial w_1^2} & \cdots & \frac{\partial^2 E}{\partial w_1 w_N} \\ \vdots & \ddots & \vdots \\ \frac{\partial^2 E}{\partial w_N w_1} & \cdots & \frac{\partial^2 E}{\partial w_N^2} \end{bmatrix} \quad (6.4)$$

where  $w_1, \dots, w_N$  represent the weights at nodes  $1 \dots N$ .

Hessian matrix  $\mathbf{H}$  gives an evaluation of how weight changes (gradient) will affect gradient:

$$\mathbf{w}_k = \mathbf{w}_{k-1} - \mathbf{H}_k \mathbf{g}_k \quad (6.5)$$

Under the assumptions given by Newton's method (Hagen & Menhaj, 1994), Hessian matrix can be simplified as:

$$\mathbf{H} \approx \mathbf{J}^T \mathbf{J} \quad (6.6)$$

where  $\mathbf{J}$  is defined as Jacobian matrix.

The relationship between gradient  $\mathbf{g}$  and Jacobian matrix  $\mathbf{J}$  is represented as:

$$\mathbf{g} = \mathbf{J}^T \mathbf{e} \quad (6.7)$$

where  $\mathbf{e}$  is the overall (training) error vector, namely the difference between predicted value and target value.

When combining the above three equations (6.3-5), the Gauss-Newton method can be represented as:

$$\mathbf{w}_k = \mathbf{w}_{k-1} - [\mathbf{J}^T \mathbf{J}]^{-1} \mathbf{J}^T \mathbf{e} \quad (6.8)$$

### iii).The Levenberg-Marquardt algorithm

LM algorithm presents an approximation of the Hessian matrix as following:

$$\mathbf{H} \approx \mathbf{J}^T \mathbf{J} + \mu \mathbf{I} \quad (6.9)$$

where  $\mu$  is always positive, called combination coefficient,  $\mathbf{I}$  is the identity matrix.

When applying such approximation to Equation (6.3) and (6.5),

$$\mathbf{w}_k = \mathbf{w}_{k+1} + [\mathbf{J}^T \mathbf{J} + \mu \mathbf{I}]^{-1} \mathbf{J}^T \mathbf{e} \quad (6.10)$$

where  $\mathbf{w}_k$  is the weight vector at iteration k,  $\mathbf{e}$  is the overall errors (in vector form) of the network,  $\mu$  is known as LM's damping (adjustment) factor and  $\mathbf{I}$  is the identity matrix.

The damping factor  $\mu$  is adjusted in every iteration step, guiding the trend of generalisation. When the damping factor  $\mu$  is very small (closing to zero), the above equation is approaching to the Gauss–Newton algorithm (6.8). When  $\mu$  is taken as a large value, the LM equation approximates the gradient descent method Equation (6.3).

In the ES, the performance of neural network training is primarily examined via a validation process in each epoch of training against Mean Squared Error (MSE), denoted as  $E_{va}$ . Benefiting from its simplicity, MSE is qualified as an easy-to-use method to give an overall look of the system, without the need to account the scale of predicted values. Hence it was firstly checked to optimise the structure of FFNNs. The stopping criterion is

$$E_{va}(k) > E_{va}(k - 1) \quad (6.11)$$

$$E_{va}(k - 1) > E_{va}(k - 2) \quad (6.12)$$

Equation (6.11) along with (6.12) stand for a criterion where two consecutive epochs have both generated the validation MSE ( $E_{va}$ ) that is greater than the  $E_{va}$  of previous epoch. This means the network will not see the improvement on performance.

If this criterion is not satisfying after a long training process, 3 other criteria were considered so that training will automatically complete with any of the followings fulfilled:

- The set maximum number of epochs is reached
- The maximum computation time is reached
- The set minimum gradient is reached

The training process was executed using batch mode, where weights and biases were updated only after all the training data was presented in each epoch. In each epoch, input data comprised 20 Successful STS movements, to ensure sample quantity being 10 times greater than the Degree of Freedom (DOF) of feature to be statistically convincing. All of these 20 sets of GRF data were assigned with a separation rate of 2-to-1 for training and validation. This separation was randomised so that there did not exist a fixed training group with same GRF data feeding to the network. Each training epoch contains training and validation. The training was executed with batch mode, where weights and biases were updated only after all the training data was

presented in each epoch. Taking into account of limited data used for training (only 20 Successful STS movements), “random sampling” was adopted when choosing training data from the pool of the 20 data sets. This mitigated potential problems caused by the particular same samples repeatedly used in training, as suggested by Witten & Frank (2005). Two-third of the 20 data sets were used as training data and for validation in each epoch.

The validation in each epoch serves for two purposes. One is to check the network performance outside of training data and the other to avoid overtraining. Although the validation set of one epoch can contain data that were used in training in the previous epochs, implying not “purely independent” data used in the validation, it can argue that the random sampling adopted in this research served well for the second purpose. Figures 6.6 and 6.7 show the clear difference between  $E_{tr}$  and  $E_{va}$ .  $E_{va}$  did not decrease alongside  $E_{tr}$ , indicating the identification of overtraining.

The construction and training of network, including the ES and BR generalisations, were implemented via Neural Network Toolbox provided by MATLAB 2014a. The training and validation errors,  $E_{tr}$  and  $E_{va}$ , of the network with  $d = 3$  and  $N = 20$  are shown in Figure 6.6 in blue and in green, respectively. The training stopped at Epoch 8 because of  $E_{va}(8) > E_{va}(7) > E_{va}(6)$ . The performance of the FFNN at Epoch 6 was then considered as the best before it started to be over trained. The weights obtained at this epoch were adopted.

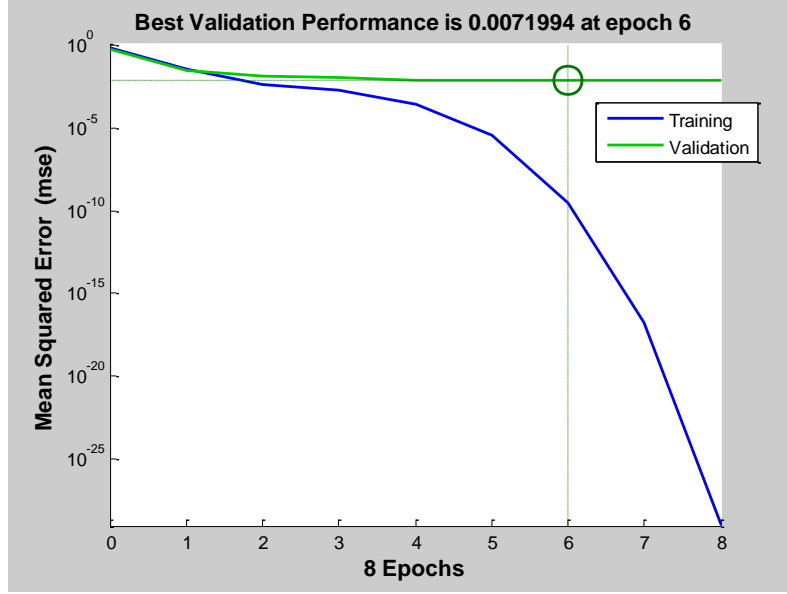


Figure 6.6 FFNN ( $d = 3$ ,  $N = 20$ ) training performance validation with early stopping

On the other hand, BR is also known as a suitable ANN generalisation technique for time series data within range of  $[-1, 1]$  (Foresee and Hagan, 1997). It brings the concept of mean squared weights (MSW) in BP and offers smaller and smoother weight updates (Narendra and Mukhopadhyay, 1997). In BR, the regularisation process is mathematically represented as:

$$REG = \alpha \cdot MSE + \beta \cdot MSW \quad (6.13)$$

REG is denoted as regularisation function, where  $\alpha$  and  $\beta$  are arbitrary numbers, taking the values  $[0, 1]$  and the sum of both is 1. The two parameters are used to adjust the influence of mean squared error (MSE) and MSW. MSW is defined as:

$$MSW = \frac{1}{N} \sum_{i=1}^N (w_{ij})^2 \quad (6.14)$$

The combination of both regularisation parameters determines the trade-off between minimising MSE by penalising large weight updates, or vice versa (Mackay, 1992). Also note that the above equations contain acronyms adapted to this model. For the basic BP learning process, choosing a high learning rate can help speed up the training process, however, if the learning rate is set too high, the weights are not likely to converge. The training process of BR successfully solved this trade-off with Bayes' rules applied in which the posterior distribution optimises both parameters, in which the appropriate priors are used to enable minimisation of weight updates.



Different from the basic gradient descent function (6.3) which only focuses on minimising MSE regardless whether the weight update is a local minima or a global one, the regularisation process takes the combination of MSE and MSW updates into account. It automatically optimises the minimisation process and reduces the overhead computational difficulties. This is superior to the conventional gradient descent method which can be trapped at local minima, hence resulting better generalisation. Consequently, this technique attempts to modestly update the weights, in the sense that the real underlying function is assumed to have a certain level of smoothness. This is regarded as the criterion of when BR needs to stop. Related work (Mackay, 1996; Wang, 2007; Kelemen and Liang, 2008) suggests, BR commonly produces a well generalised ANN, resulting considerably higher training performance than ES.

When training with BR regularisation, weight updates of the network follow LM algorithm, as shown in Equation (6.10). The stopping criteria are considered as signals to cease the training process:

- The set maximum number of epochs is reached
- The maximum computation time is reached
- The desired performance has achieved
- The set minimum gradient is reached
- The set  $\mu$  (LM's damping factor) exceeds the predefined maximum value

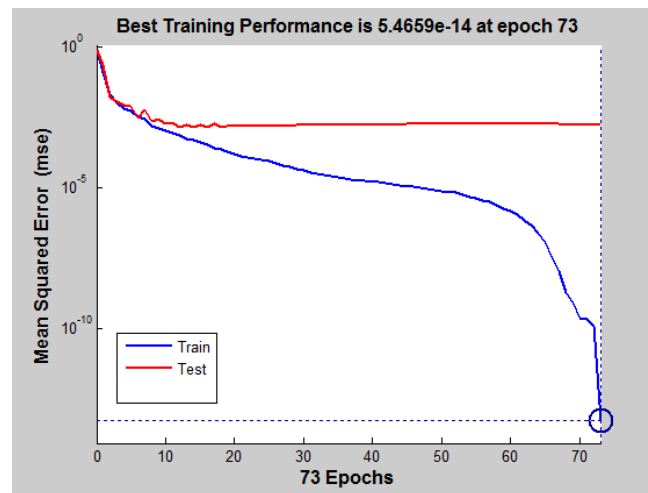


Figure 6.7 FFNN ( $d = 3$ ,  $N = 20$ ) training performance with Bayesian regularisation

Figure 6.7 depicts the training process which has ceased at Epoch 73 where the combination of MSE and MSW has reached its minimum value (refer to Equation (6.13)), signifying the convergence of the network.

The FFNN of various initiations were thus compared in conjunction with both generalisation techniques, results of which can be seen in Table 6.1. In addition, Table 6.1 records the average convergence time as well as number of training iterations, computed with the same computer and operation system. When training the network with 2 generalisation techniques respectively, it was also noticed that the number of iterations required before reaching its expected standards reveals the computation time of training. And the training iterations are in accordance of the complexity of network, which can be manipulated with hidden neuron size and input delays.

Table 6.1 Training results of ES and BR (compared in conjunction with) respect to various initialisations of FFNN

		Training Performance (MSE)							
Number of Delays		Early Stopping				Bayesian Regularisation			
(d)	Size (N)	5	10	20	50	5	10	20	50
1		1.5E-02	9.2E-03	7.5E-04	8.7E-03	2.6E-04	9.0E-13	1.3E-14	5.2E-13
2		5.2E-03	2.6E-04	6.5E-05	5.0E-04	7.6E-05	5.0E-13	2.7E-15	1.7E-14
3		7.9E-03	5.8E-05	3.7E-06	3.3E-04	7.6E-15	7.1E-15	2.9E-17	7.7E-15
Average convergence time (Seconds)		0.8	1.1	1.5	3.9	12	19	70	480
No. of epochs		9	11	12	11	180	273	322	331

Table 6.1 suggests under all network initialisations, BR has outperformed ES and it was adopted as the training method for the FFNN.

### 6.3.3 Prediction results and discussion

Three metrics (measures) were used to examine the performance of the FFNN with the optimised structure and trained by the generalisation technique in the sense of GRF prediction as follows:

1. MSE is still recognised as the most popular performance metric to examine ANN structures and training results, regardless of the scale of units.
2. Error autocorrelations depict the dependence of significant prediction errors

respecting to previous errors. It reflects the robustness of prediction because a credible prediction results should have errors fairly independent to the previous prediction errors. By significant, it is meant the error is above a pre-defined threshold, which is recognised as confidence limit.

3. Regressions of prediction results are equally important as MSE in terms of judging the prediction outputs against the actual target GRF measurements.

From Figure 6.8 it can be seen that the optimised FFNN generalised by BR has achieved satisfying prediction results respecting 3-fold test data, i.e. among the 30 sets of Successful STS data, 20 sets were used for training while the rest are used for testing.

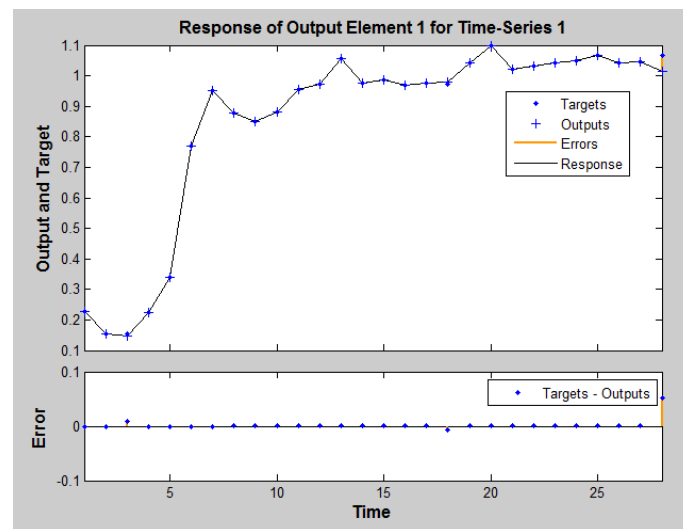


Figure 6.8 GRF prediction result to 3-fold test data achieved by the optimised FFNN after BR generalisation (a random test sample is presented)

From Figure 6.8 it can be seen that the optimised FFNN generalised by BR has achieved satisfying prediction results respecting to pure test data. The greatest error along with time was captured as 6.1% body weight from the GRF prediction shown in Figure 6.8. An MSE of  $6.7 \times 10^{-6}$  was recorded from the prediction results respecting to 3-fold data in the following diagram, which is noticeably higher than MSE generated by training results for the same FFNN. However such test result is acceptable when compared against the actual GRF curve in STS movements, hence considered as credible prediction results. The metric of MSE has been fulfilled regarding to 3-fold data.

The autocorrelation of significant error at time  $t$  and errors that occurred at the adjacent time

steps with lag  $L$  in between signifies the robustness of the prediction. If the predictor is robust, a significant error should not be the consequent of the previous prediction errors at different lags.

For the same GRF prediction value (variable), the autocorrelations between error at time  $t$  and the previous error with lag  $L$ , is given by Equation (6.15), where  $L$  is the lag between two variables in one time series, namely  $L = \pm 1, \pm 2, \pm 3 \dots$  time steps of the GRF.

$$\phi(L) = \frac{1}{T-2L} \sum_{L}^{T-L} X_t \cdot X_{t-L} \quad (6.15)$$

This is derived from autocorrelation function (ACF) (Hartmann, 2014, p.133), with acronyms adapted to this model.  $T$  is the length of GRF time series, consists of 27 ( $30 - d, d = 3$ ) time steps. Note that with lag  $L=0$  substituted in (6.15),  $\phi(0) = X_t^2$ , which is MSE of the predicted GRF because it indicates the errors occurred without lag, regardless of the scale of variables.

With  $X$  replaced by  $y_t - t_t$ , the prediction error at time  $t$ , such equation is modified as,

$$\phi(L) = \frac{1}{T-2L} \sum_{L}^{T-L} (y_t - t_t) \cdot (y_{t-L} - t_{t-L}) \quad (6.16)$$

Based on Equation (6.16), the following error autocorrelation of the optimized FFNN's 3 prediction results is shown in Figure 6.9. The blue bars represent the autocorrelations and the red bands depict 95% confidence limit that is used to test whether the autocorrelation at lag  $L$  is significant.

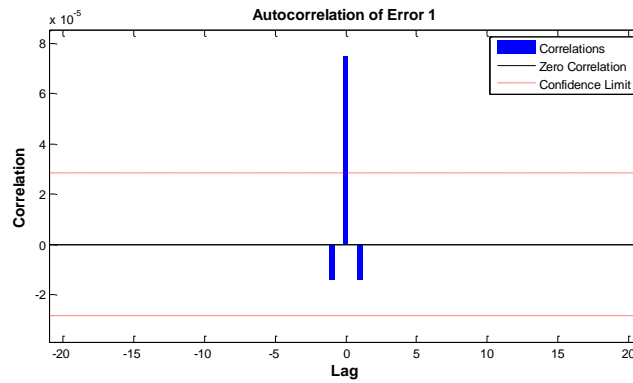


Figure 6.9 Autocorrelation of prediction errors when  $d = 3, N = 20$

Such plot of error autocorrelation is compared against those generated by FFNNs with varying delays, shown in Figure 6.10 and 6.11. This is investigated because error autocorrelation is

significantly affected by inappropriately assigned delay  $d$ .

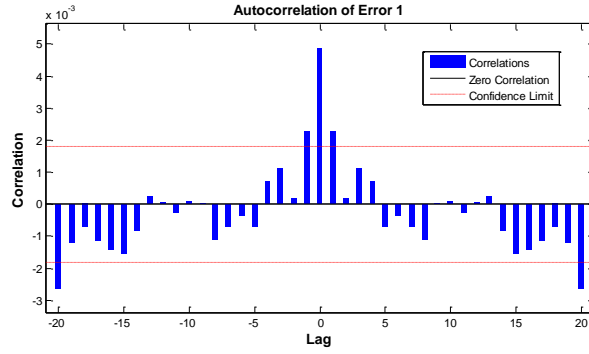


Figure 6.10 Autocorrelation of prediction errors when  $d = 1$ ,  $N = 20$

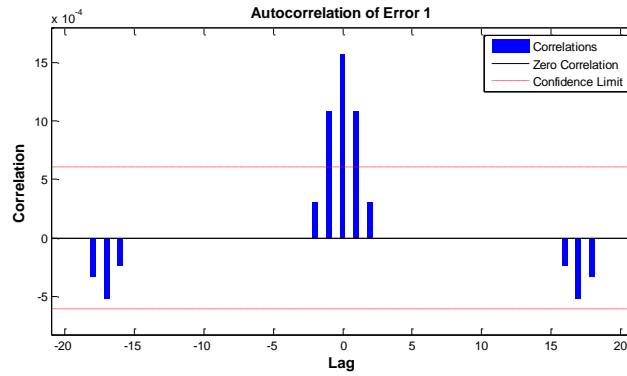


Figure 6.11 Autocorrelation of prediction errors when  $d = 2$ ,  $N = 20$

From this comparison, it can be readily seen that FFNN with input delay of 3 time steps is superior to others in the interest of resulting lower significant error autocorrelations with non-zero lags. Also, the autocorrelations at non-zero lags shown in Figure 6.10 are not considered as significant because they both fell within the confidence bands. Hence the FFNN with 3 input time delays is proven to be robust.

The regression test was also conducted to examine the relationships between the actual GRF of 3-fold data and its predicted values generated by trained networks. With this principle applied, ideally, a well converged network should generate prediction values with  $R$  approaching to 1. This regression correlation value  $R$ , is defined as

$$R^2 \equiv 1 - \frac{SS_{res}}{SS_{tot}} \quad (6.17)$$

of which  $SS_{tot}$  represents the sum of squared target values while  $SS_{res}$ , the sum of squared residual value, is computed as,

$$SS_{res} = \sum_{t=1}^{T+1-d} (y_t - t_t)^2 \quad (6.18)$$

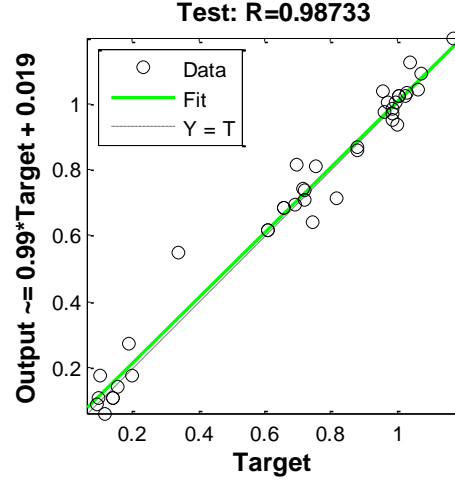


Figure 6.12 The regression correlation between 3-fold test data and prediction results with FFNN generalised by BR

The regression correlation of results regarding to 3-fold test data is plotted in Figure 6.12, with vertical axis and horizontal axis representing the prediction output and actual GRF value, respectively. The regression line, also known as best-fitting line, is shown as green solid line. The regression line is imposed based on the estimation that the predicted values and respecting targets values are linearly correlated. Because the prediction is only meaningful if this linear correlation exists: network responses are high when the actual GRF measurements are high, vice versa. And the coefficient R describes how credible is such an estimation. As when  $SS_{res}$  is huge, the linear fit is expected to be poor.

Ideally, a linear slop of 1 will be obtained when the predicted values show no error comparing against the actual values, indicating  $y_t = t_t$  throughout the entire period of prediction. This is depicted as dotted line in Figure 6.12. The green solid line stays reasonably close to dotted line, hence it suggests strong correlation between the tested prediction results and the actual GRF values of 3-fold data (R=0.99).

## 6.4 MSAP network

### 6.4.1 Structure and training

The significant amount of assistance is provided via seatpan lifting height of 50mm, proposed by (Moon, 2010) in a similar study. For the lifting mechanism to generate this required motion, a minimal extension of 70mm at the linear actuator has to be provided. Considering a chair user with BW of 85kg, the average time required to reach this minimal extension was recorded as  $T_{act}$  at the nominal voltage.

From Table 6.2, the minimum assistance could only be reached after 0.77 seconds since the initiation of actuating motion. This suggests the need for multiple steps ahead prediction (MSAP) and determines the minimum time steps required to be predicted ahead.

Table 6.2 Actuator characteristics (experimentally obtained)

Actuator characteristics									
Nominal voltage: 24V 0.68-0.81A									
Full stroke (15cm)		130mm extension		100mm extension		70mm extension		40mm extension	
	Time (s)		Time (s)		Time (s)		Time (s)		Time (s)
Upwards	1.46	Upwards	1.29	Upwards	1.05	Upwards	0.78	Upwards	0.48
	1.44		1.32		1.07		0.76		0.50
	1.47		1.28		1.06		0.77		0.50
	1.48		1.28		1.04		0.76		0.48
	1.47		1.29		1.09		0.78		0.49
Average	1.46	Average	1.29	Average	1.06	Average	0.77	Average	0.49
with positive load* of 85kg		with positive load* of 85kg		with positive load* of 85kg		with positive load* of 85kg		with positive load* of 85kg	

This inspired the necessity to further enhance and evolve the FFNN to MSAP. The previous FFNN can be considered as an open loop network in the sense that data is only allowed to flow forward to generate the prediction value. However, the MSAP would need the prediction to feedback to the network for carrying on future prediction.

There are three items need to concern when determining the number of steps ahead for prediction, that is, the prediction horizon of network (PH). First, PH should be greater than the minimum time required by the actuator to provide the desired assistive motion. This inequality can be represented such as

$$PH \times T_{step} > T_{act} \quad (6.20)$$

where  $T_{act}$  is the minimum time interval required for the actuator to be able to complete the desired raising movement and  $T_{step}$  stands for the time span of each time step, 0.1 seconds.

Second, the prediction must be done before the critical point. The critical point, denoted as  $T_{cr}$ , is the time point at which the subject fell back to seatpan if the required assistance is not provided. This time point was figured out through examining Unsuccessful movements of the subject. From 30 Unsuccessful STS movements, the mean value of  $T_{cr}$  was obtained at 2.4 seconds, from the initiation of movement, with standard deviation of 0.3 seconds. Figure 6.13 shows the GRF curves of a selection of Unsuccessful STS movements from which the critical points are pointed out.

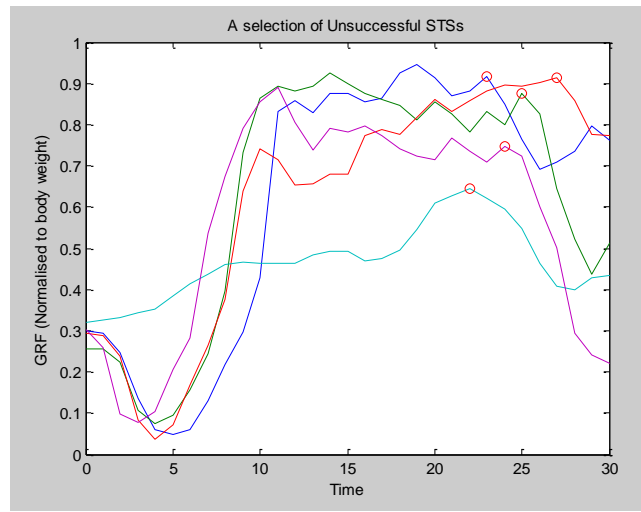


Figure 6.13 Plot of selected Unsuccessful GRF curves to examine the critical point which indicates the instance of falling back to seatpan

Therefore, this inequity is expressed as,

$$(PH + d_{MSAP}) \times T_{step} < T_{cr} = 2.4 \quad (6.21)$$

where  $d_{MSAP}$  is the number of input delays taken by MSAP network, which is chosen as 4 through experimental optimisation, similar to the process with FFNN in Section 6.3 where the network responses with different delays were compared.

Third, PH should be set as short as possible as to reduce the error. As Table 6.2 suggests,  $T_{act}(70mm) = 0.77s$ . Therefore the inequity for determining PH can be represented such as,

$$\frac{T_{cr}}{T_{step}} - d_{MSAP} > PH > \frac{T_{act}}{T_{step}} \quad (6.22)$$

where  $d_{MSAP}$  is the number of input delays taken by MSAP network, which is later configured



through experimental optimisation as 4, through experimental optimisation, similar to the process with FFNN in Section 6.3. The verdict was proven by the fact the MASP network responses with different delays were compared. With the parameters substituted by the actual values, (6.22) can be rewritten as  $20 > PH > 7.7$ . Thus the ideal value is chosen as 8.

It can also be observed from Table 6.2 that the extension of linear actuator has shown non-linear characteristics against the measured time. The non-linear factors are characterised by A) load at seatpan, in terms of subject's BW subtracted by GRF, being highly non-linear; B) the geometric transfer from actuator extension to displacement of raising motion and C) lesser terms like back lashing of the actuator gearbox, the variations at power supply, etc.

However, the relation between actuator extension and measured time can be approximated to a linear relation, which can be expressed as 1<sup>st</sup> order linearisation.

$$y_n = \beta_0 + \beta_1 x_n \quad (6.23)$$

where  $y$  represents the extension of actuator (in mm),  $x$  stands for the measured time (seconds) for the actuator to reach the desired position with subject seated on chair (as positive load).  $\hat{y}_n$  is the estimated value of  $y$  with linear model.  $\beta_1$  is the slope and  $\beta_0$  is known as  $y$ -intercept. Producing such linear estimation requires minimising the sum of the squares of errors (SSE), which is known as least squared error (LSE) method.

$$SSE = \sum_n (y_n - \beta_0 + \beta_1 x)^2 \quad (6.24)$$

$$\beta_1 = \frac{\sum_n (y_n - \bar{y}_n)(x_n - \bar{x}_n)}{\sum_n (x_n - \bar{x}_n)^2} \quad (6.25)$$

The coefficient  $R$  evaluates how well the linear estimation will fit the model (Im, 1996), which is calculated with Equation (6.17) applied, the  $SS_{res}$  and  $SS_{tot}$  are

$$SS_{res} = \sum_n (y_n - \hat{y}_n)^2 \quad (6.26)$$

$$SS_{tot} = \sum_n (y_n - \bar{y}_n)^2 \quad (6.27)$$

Based on the regression with LSE method applied, the closest liner regression obtained to estimate the actuator characteristics has a  $\beta_0 = -6$  and  $\beta_1 = 1.02$ . However, in reality the extension of actuator should be 0 at time step 0. As shown in Figure 6.14, such actuation time regarding to the displacement of raising motion can be simplified as a linear correlation ( $R=$

0.998).

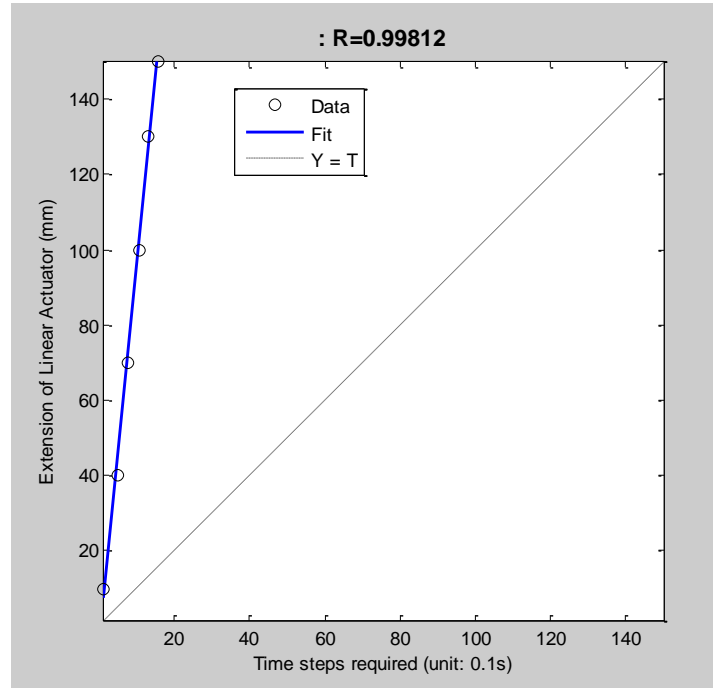


Figure 6.14 Regression of Extension of actuator respecting to time steps required

This linearised relation confirms the 8-step-ahead prediction valid at any time during the raising motion of seatpan, also considered as a proof of robustness of this MSAP model.

The MSA prediction, in fact, is the process of repeating (chaining) one-step-ahead predictor with the previously predicted outputs  $\hat{y}_{t-PH+1}, \dots, \hat{y}_{t-1}, \hat{y}_t$  as inputs to predict the GRF value at  $(t + 1)$ .

There are 2 options of conducting MSAP. One is to use the prediction output at time  $(t - PH + 1), \dots, (t - 1), t$  yielded by 8,  $(PH = 8)$  previously trained FFNN. This network can be recognised in a closed-loop form with 8 identical FFNN chained together. However, as shown in Figure 6.18, the transformation between open loop network and closed loop network was undertaken directly as the prediction outputs were treated as inputs to predict the MSA values onwards. Hence the characteristics of FFNN would be inherited to MSAP, which means the error would be accumulated with the prediction into the future.

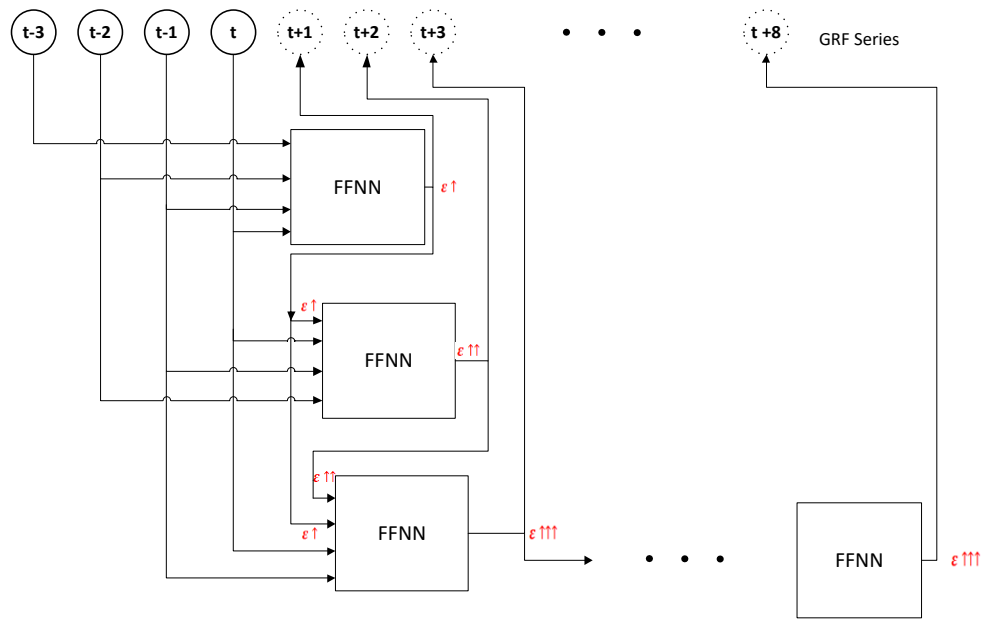


Figure 6.15 The schematic structure of MSAP using multi previously trained FFNNs (Option 1 is conducted without regulation process)

In comparison, option 2 provides a regulation process that facilitates the generalisation of this MSAP network. It accounts the available GRF series within the period of PH as training data to mitigate the accumulation of prediction errors as prediction carried on to future steps, as presented in Figure 6.16.

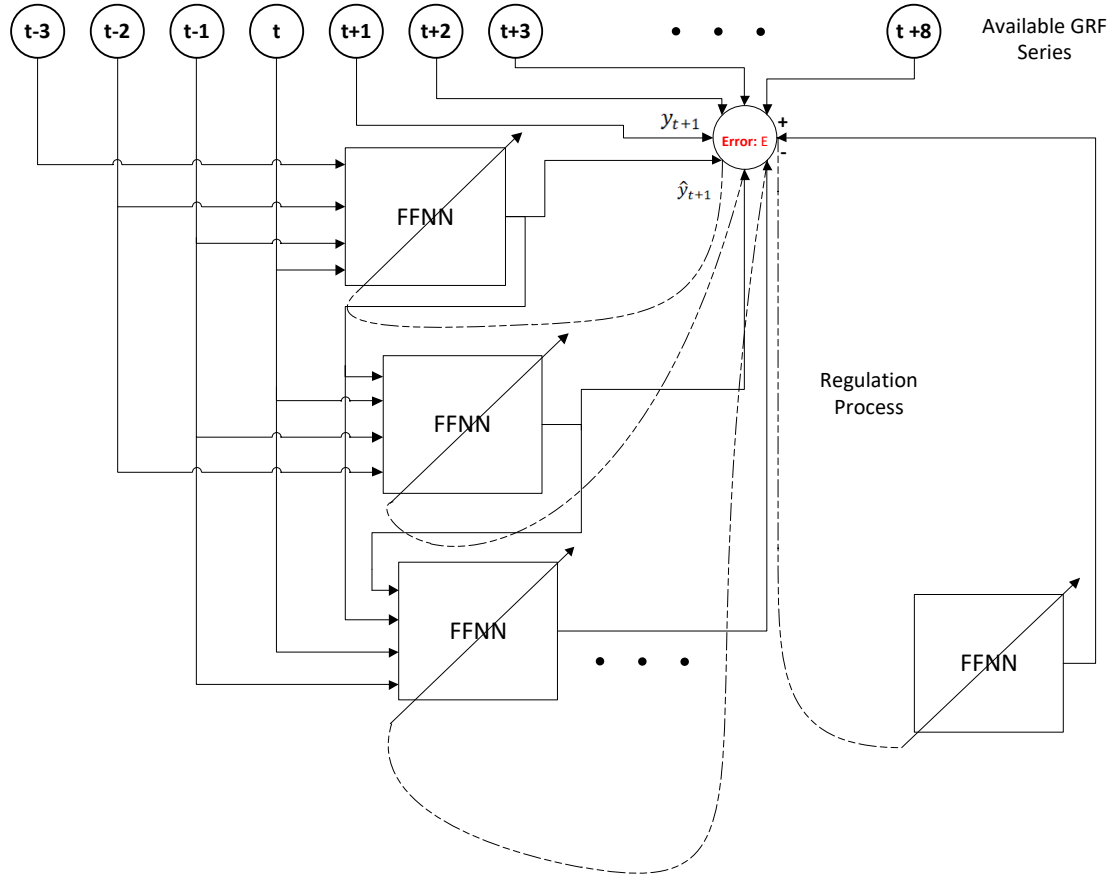


Figure 6.16 The schematic structure of MSAP with available GRF sequence within the period of PH taken for the regulation process (Option 2)

#### 6.4.2 Discussion

To examine the training and testing results of this MSAP network with the structure shown in Figure 6.15, six metrics (measures) were proposed.

- Prediction accuracy is reviewed by MSE to validate the network performance. The error is calculated as each prediction point (that is 8 time steps ahead of the current time step) compared against its actual GRF value. This is primarily examined by MSEs of both training and testing results to give an overall assessment regardless of the scale of GRF values. In addition to MSE, the responses of MSAP on training and testing data were also investigated.
- Error autocorrelation is a measure of criterion to confirm the robustness of MSAP on test data. As previously explained, this investigates whether the prediction errors generated by MSAP show great autocorrelations with errors yielded at different lags in between.

- Regression is also examined as it determines whether the prediction outputs generated strong correlations with the actual target GRF measurements.
- Specifically for the MSA prediction, capability of prediction into the future is equally important as it enables the chair robot to proactively predicting the GRF value at multi step ahead, which was denoted as capable PH in this study.
- Generalisation is considered to be another critical measure to investigate how this regularised MSAP model can adapt to unfamiliar data. This brings extra challenges to the MSAP by feeding completely unfamiliar test data - GRF series of Unsuccessful STS movements into the network.
- Having a variety of data (VD) in the captured GRFs between each STS set gives credit to the generalisation of MSAP network from stochastic viewpoints.

For the robot chair prototype, the prediction accuracy determines the deficit between chair user's predicted GRF value and his/her personalised GRF value at instances where assistance is needed. Hence this guarantees the correct amount of assistance is provided to chair user in order to help him overcome STS difficulties.

The 20 available Successful GRF data sets were split into 5-fold data with 16 and 4 sets being training and testing data, respectively. The training process of MSAP network was conducted using BR on 16 Successful GRF data sets, with best training MSE obtained as  $2.32 \times 10^{-4}$ . Accordingly, a set of representative response on training data is plotted in Figure 6.17. The red dashed line represents the predicted output whereas the blue solid line is the actual target GRF curve. Because the first 10 time steps (from 0 to 1 second of the movement) merely contains the information of the early stages of STS process, namely, initiation as shown in Figure 4.1. It would be meaningless to use this portion of GRF series as the only input of the 8-step-ahead predictor. Therefore the response is only investigated on the GRF values predicted from 1.9 to 3 seconds. As discussed in Section 6.3.1, this portion of series covers the region where subject would fell back without proper assistance provided.

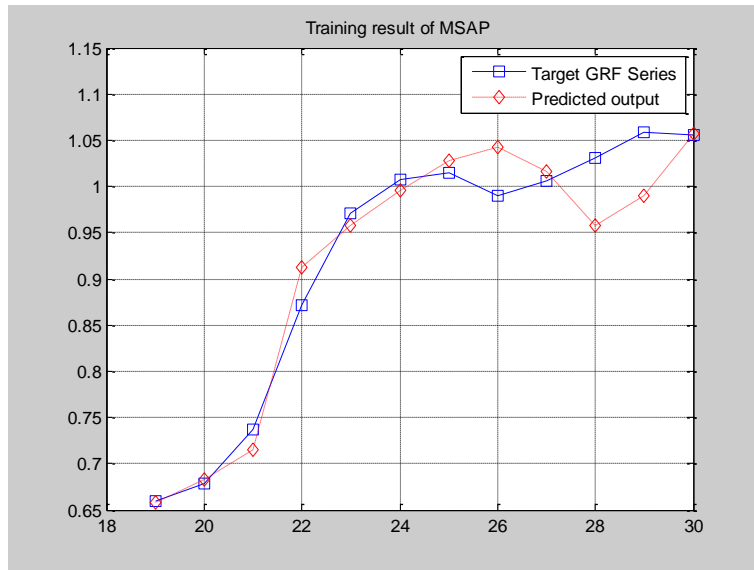


Figure 6.17 The MSAP response on 5-fold training data

Of the rest 4 Successful STS movements used for testing, one is randomly selected and plotted as Figure 6.18. It can be readily observed that the generated errors have enlarged comparing against the errors yielded in the training set. The corresponding MSE recorded from 5-fold testing data sees a drop to  $1.9 \times 10^{-3}$ , compared against the training MSE of  $2.3 \times 10^{-4}$ .

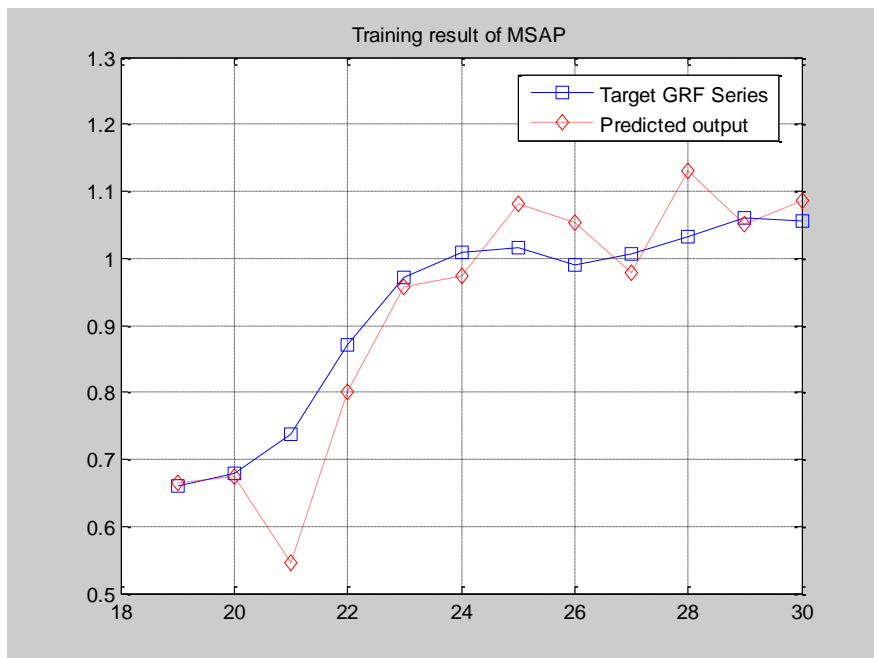


Figure 6.18 The MSAP response on 5-fold test data (MSE = 0.0019)

The error autocorrelation of 5-fold test data is plotted as Figure 6.19. From the chart of error correlations it can be seen all non-zero errors are observed between the pre-defined thresholds

indicating significant errors, which is also recognised as confidence limit. This confirms all errors yielded by MSA prediction are independent to each other, hence contributes to the robustness of such prediction.

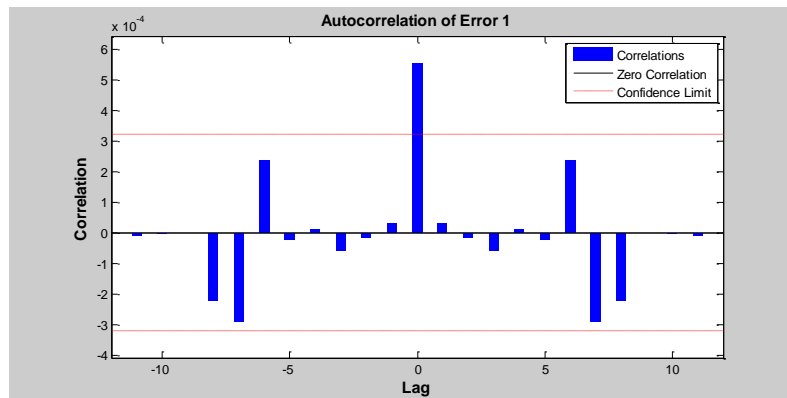


Figure 6.19 Autocorrelation of prediction errors of 5-fold test data

The corresponding regression of prediction test result is shown in Figure 6.20, with vertical and horizontal axis representing the MSA prediction outputs and actual GRF values, respectively. As discussed in Section 6.2.2, a slop of 1 indicates the ideal correlation between predicted values and actual GRF values. And the regression coefficient is obtained as 0.91, which proves high correlation between GRF values predicted 8 steps ahead and actual GRF values measured at the same instances.

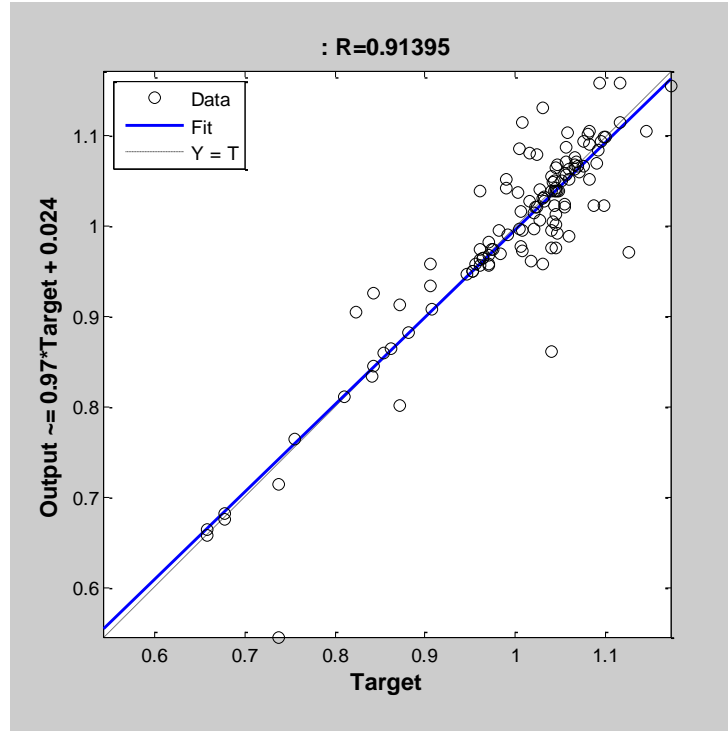


Figure 6.20 Regression of MSA prediction on 5-fold test data

As to the capable PH, the MSA prediction features an 8-step-ahead forecasting on future GRF values. This is greater than  $T_{act}$  (time required by the actuator to generate the minimum level of assistance) so that the limitation on actuator side is mitigated. Otherwise chair user will still fell back to seated position at critical points without proper assistance applied.

In addition to the above metrics that were used to assess the performance of network on 5-fold test data, the test on how MSAP performs on Unsuccessful data has also been carried out. This is essential because in reality the MSA predictor has to be able to deal with the scenarios where chair user struggles to generate enough GRF that close to his/her personalised one.

Because of the numerous reasons discussed in Chapter 2 that lead to Unsuccessful STS, most of the Unsuccessful STS data sets feature inconsistent GRF pattern between each other. Therefor it would be unrealistic for the chair robot to learn from the Unsuccessful GRF curves. However, the MSAP of chair robot has to be eligible to determine the difference between the GRF values of 8-step-ahead and the personalised value at that instance.



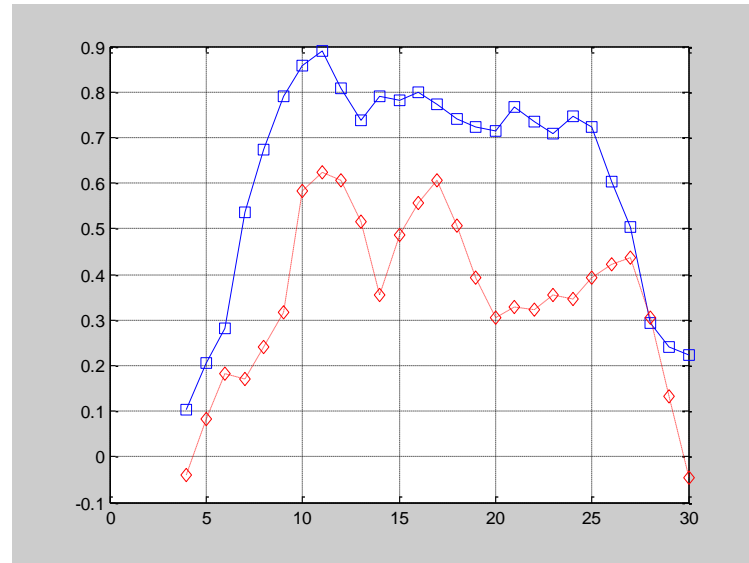


Figure 6.21 The MSAP response on one set of Unsuccessful STS movement

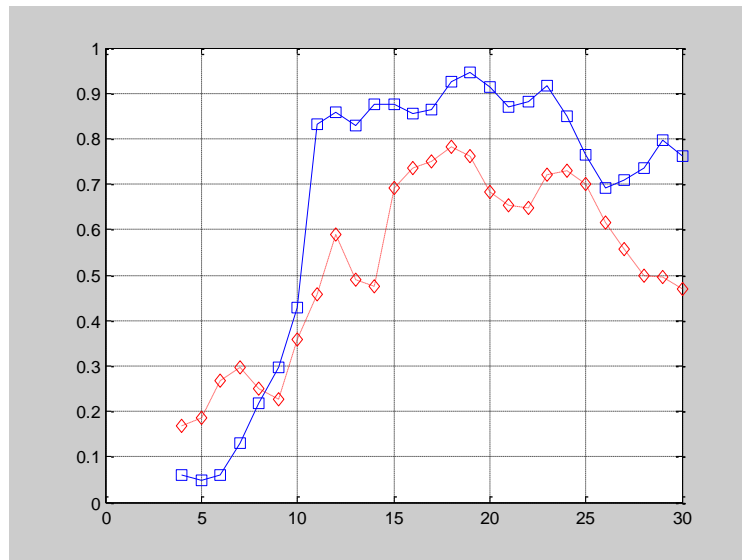


Figure 6.22 The MSAP response on another set of Unsuccessful STS movement

Given the massive difference in GRF patterns of Unsuccessful and Successful STS movements, which MSAP network has been trained for, the errors of such unfamiliar test data appear more prominent than prediction errors of test Successful data. However, as Figure 6.21 and 6.22 suggest, from 1.9 to 3 seconds, the predicted GRF values stay underneath the actual ones, which means the predictor is still able to observe and react to such deficit on GRF values (compared against the subject's personalised GRF).

Meanwhile, it is important to always have randomness in both kinds of testing data because

training process of ANN can be biased in a way that weight updates follow the GRF trends existing in training data only. The following VD factors will affect the actual measurement of GRF data: variations in BW of same subject, changes of physical conditions, randomness in seated positions like feet placement, arm positioning and deferent types of imbalance occurred in Unsuccessful STS movements.

## 6.5 Summary

This chapter presented the second stage GRF predictor by reviewing the advantage of NNTS handling time series over other conventional techniques in the beginning. Based on this background, a FFNN with optimised structure was firstly developed for its simplicity. Such FFNN was generalised through comparative study on ES and BR, with the latter proved to be involving less overtraining issues. Three metrics were then established to examine the performance of this FFNN on test data.

However, owing to the limitations on the actuator side, the appropriate amount of assistance can only be delivered after a period of  $T_{act}$ . In order to mitigate this, the ANN based predictor has advanced to a MSA predictor. Afterwards, both training and test results have been evaluated by the above stated performance metrics. In addition to this, the MSAP was also assessed from PH and VD viewpoints. More importantly, the network has undertaken challenges brought by Unsuccessful STS data sets, which is configured as completely unfamiliar test data for the MSAP. This means the MSAP is eligible to deal with all types of STS movements in reality, with Unintended movements being ruled out by the FIS based first stage classifier. Effectively implementing this MSA predictor paves the road for the smart chair to be able to assist the subject proactively and appropriately whenever he/she struggles during STS process.

## **CHAPTER 7 CONCLUSIONS AND FUTHER WORK**

This chapter presents a summary of how methodologies were implemented to achieve the main objectives proposed in the beginning of the thesis, followed by discussions on the limitations of the study, and then the further work is outlined for strengthening the way the robot chair provides “assistance as needed”.

### **7.1 Research summary**

The main research achievements of this study to human robot interaction in the context of STS are in three folds, namely, intention recognition, self-adaptation and assistance prediction.

#### **i). Intention recognition**

The first stage classification described in Chapter 4 identifies human users’ intention of standing up through filtering out Unintended movements using the feasible features. In order to handle vagueness between intended movements and the Unintended ones, different fuzzy logic based approaches were developed and investigated. Fuzzy sets and their membership functions, and fuzzy rules and their truth degrees were determined based on experiments. The performance of the fuzzy logic based classifiers were compared using two types of test data fed in, 2-fold test data and pure test data generated from experimental results. This ensures the fuzzy based classifiers will work not only on the data used to determine the fuzzy membership functions, but also on the pure data generated for testing. Four crucial evaluation metrics were proposed to test the accuracy and robustness required by the STS intention recognition and, more important, safety to prevent false actuation of the lifting mechanism when the chair user does not hold a STS intention.

#### **ii). Self-adaptation**

The classifiers were then further advanced to suit a multi-user based scenario, where multiple subjects of significantly different physics are expected to receive personalised STS assistances. However, in STS movements, the most significant features reflecting the difference in

biomechanical features were configured as shoe width and (seated) stance width. Accordingly, two self-adaptive fuzzy classifications were developed with emphases on the above features. Compared against the fuzzy based classifier demonstrated in Chapter 5, the self-adaptive classification has its superiority in determining the fuzzy membership functions. This process is conducted by effective training instead of merely depending on experimental results and understanding towards the system. To validate the effectiveness of self-adaptive fuzzy classifications, both 1st and 2nd feature adaptation in either ACLS or MDLS classifier were examined, respectively. This generated four combinations, which were laterally compared using the proposed performance metrics. Eventually, the 2nd biomechanical feature adaptation applied to the MDLS classifier was proved to be more credible over the others. Moreover, having this adaptive feature helps advance the 1<sup>st</sup> stage classifier to its maximum potentials, especially when the same subject changes sitting postures to adapt to different environmental and physical conditions.

### **iii). Assistance prediction**

To the provision of delivery the “assistance-as-needed”, the ANN based prediction on GRF time series data was developed. The determinants of the network structure were experimentally obtained. The corresponding training techniques were also optimised according to various performance metrics. BR was found to be more suitable for the network. It avoids overtraining and encourages network generalisation. Afterwards, to validate the prediction results, MSE, error autocorrelations and regressions were examined. The aim of obtaining the personalised capable STS curve was realised through effective training. The assistance predictor was then extended to perform MSA prediction, considering the imperfection of the actuator. The improved predictor is competent of forecasting a couple of steps ahead, according to the time required by the actuator to complete the assistive motion. Apart from the three performance metrics, generalisation of the MSAP network was examined by feeding completely unfamiliar test data - GRF series captured in Unsuccessful STS movements.

It can be concluded that the above three folds, in conjunction with the development of chair structure as well as the sensing footmat, have encapsulated the main contributions, in regard to

the aim and objectives of this study.

## **7.2 Thesis contributions and publications**

### **7.2.1 Research contributions**

The transferability of the above contributions towards other HRI researches is promising. The self-adaptive fuzzy based classifier can be adopted in human motion or posture recognitions with uncertainties introduced by 1). multiple users, 2). same subject at different physiological or environmental conditions. Through effective training, the self-adaptive classifier developed in this study successfully coped with the uncertainties that caused by different body types as well as sitting postures.

The MSA assistance prediction developed in this research promotes an actuation compensatory mechanism that may be adopted by other studies on rehabilitation and exoskeleton applications. It takes the imperfection of the actuators into account where the amount of time required by the actuator to complete the desired motion is not negligible. However, this was ignored by some previous researches (e.g. Kiguchi & Hayashi 2012; Reza, 2014). The subject users' features measured by sensory systems, such as force, orientation and posture, may have had changed by the time actuator completes its motion. Therefore, the prediction into the future needs to be carried out with how the subject responses to the actuation incorporated in the training process.

The innovative parts of the study are summarised as below:

- A comprehensive literature review has been conducted to understand the background of STS problems and the health implications confronted by the elderly. Related work on biomechanics of STS problems further explains the weakness in physiologic and psychologic that causing the problem. A summary on commercial assistive devices has verified the potential problems may incur that will be detrimental to the elderly. Meanwhile, in-depth review on chair-based experimental prototypes has proofed the possibility of developing a robot chair that is able to provide “assistive-as-needed”. Based on the above findings, two survey papers have been published (Conference: Lu et al, 2013 August) and

(Journal: Lu et al, 2013). Apart from the background acknowledgement, the former focuses on the experiment layouts and how did the related work tackle the STS problems in general. The published journal paper has an emphasis on chair-based sensing techniques with analysis on whether they are feasible in the robot chair scenario. A taxonomy of sensors has been presented and compared, which also sets bench markings for the robot chair when it comes to extracting important STS features.

- In terms of hardware development, an innovative quad-pivot mechanism in Chapter 3 provides tilting and lifting motions simultaneously through the seatpan. This not only reduces the number of actuators but also reduces the complexity of the control of the assistive motion. The developed sensing footmat combines the functionality of a force plate (Munro et al, 1998; Yamada & Demura, 2009; Jamwal et al, 2014) and complex sensing matrix (Tan et al, 2001; Yokota, 2009), referring to the related work demonstrated in Chapter 2. It is capable of measuring GRF as well as the pressure patterns, albeit a rather cost-effective solution compared against the one used by (Tan et al, 2001). The complexity of pressure patterns can be exploited to capture the **lateral shift (LS) of COP** in Chapter 4 and derive **shoe width** (Section 5.2) as well as **stance width** (Section 5.3). The development of chair mechanics as well as sensing footmat is highlighted in the published paper (Lu and Li, 2014).
- When developing the 1<sup>st</sup> stage STS classifier, efforts have been made to figure out essential features that bring possibility to intention recognition. Preliminary tests showed solely relying on GRF data would not distinguish the Unintended movements from Intended STS movements. Therefore LS was extracted to capture the change in COP over time that contributes to recognise the chair users' STS intentions. The LS was applied to three fuzzy logic based classifiers in three configurations, **point-wise LS**, **ACLS** and **MDLS**, correspondingly. The fuzzy sets and membership functions were manually defined with regard to the experimental results, with the target features located in distinguishable regions for different STS intentions.
- To achieve the multi-user self-adaptive classification, the system needs to react differently according to the chair users' biomechanical features. However, due to the limited sensory configurations it was difficult to distinguish the users with different body types through

height or length of thighs, which are often captured by inferred camera or motion sensory in related work (e.g. Kamnik & Bajd, 2004; Randeniya et al, 2008; Taslim Reza, 2014). This research configured two feasible features that can be acquired by the sensing footmat, width of shoes and width of stance, as input data for the self-adaptive classifier. This facilitates the adaptations in the sense of handling the uncertainties introduced by different users. Afterwards, it was confirmed the width of stance has more significance of uncertainties over the other feature in the context of intention recognition for STS transfer.

### 7.2.2 A list of publications

Lu, H., Li, D., Oyekan, J., & Maple, C. (2013, August). A survey on assistive chair and related integrated sensing techniques. In *Manipulation, Manufacturing and Measurement on the Nanoscale (3M-NANO)*, 2013 International Conference on (pp. 129-134). IEEE.

Lu, H., Li, D., Oyekan, J., & Maple, C. (2013). Integrated Sensing Techniques for Assistive Chairs: A Survey towards Sit-to-Stand Problems. In *International Journal of Intelligent Mechatronics and Robotics (IJIMR)*, 3(4), 58-70.

Lu, H., & Li, D. (2014, July). The development of a smart chair to assist sit-to-stand transferring process. In *Control (CONTROL)*, 2014 UKACC International Conference on (pp. 714-719). IEEE.

## 7.3 Limitations

### 7.3.1 The limited capacity of the sensory data

As demonstrated in Chapter 4, the random movements (changing postures, grasping objects) suggesting Unintended STS movements were only captured through the sensing footmat. Having a sensor fusion system will enhance the intention recognition (robustness) and provide more system redundancy. Because the shifting position of the upper HAT would be better perceived from the pressure sensor placed underneath the buttock. Besides, instead of solely

depending on the GRF readouts from the footmat, the force captured at the seatpan may add additional channels to the ANN predictor. The pressure sensor under the buttock can either be in flexible form or a forceplate. A sensing seatpan similar to the study conducted by (Tan et al, 2001) can be developed when budget is not an issue. However, when using the forceplate, it is preferably to have at least two components, left and right, to capture the shift of COG of the subject.

### 7.3.2 The quickness of actuation

Although the linear actuator installed in the robot chair fulfils the requirements on system cost, feed force and stroke length, the feed velocity is rather slow. To attenuate this problem, efforts have been made when developing MSAP predictor in Chapter 6, where the predictor is capable of predicting several steps ahead. This can be seen as a compensatory mechanism because the less feed velocity the linear actuator is able to deliver, the more time steps are required to be predicted to the future.

However, to the provision of “assistance-as-needed”, the actuation needs to keep up the quickness of STS motion. This is particularly important to the encouragement of functional regain as when the elderly user attempts to speed up STS motion, he/she could still expect to receive the assistance if it is required.

## 7.4 Future extension

### 7.4.1 3D Biomechanical model based chair design

A 3D biomechanical model regarding actual STS movements is in demand, especially for those performed by elderly who struggle in STS transfers. Because of the lack of such 3D biomechanical models, the event times used in this study were statistical data. The actual STS model of elderly might be mitigating the need of point of assistance introduced in Chapter 6, where the point of failure was considered with related work and assumptions. Also, having a dynamic model of the elderly subject performing Unsuccessful STS movements will help better discover the actual need to fulfil the achievement of “assistance-as-needed”. As the elderly



often face lower limbs strength issues accompanied with postural control difficulties, with the relationship between the both very hard to simulate.

A complete 3D biomechanical model for STS, the future work shall be more focusing on the range of assistive motion, which was determined merely from the related work and preliminary experiments (on actuation durations in different cases). Based on the robot chair configurations, a specific 3D biomechanical STS model targeting on physiologically weaker elderly will be established. This could be achieved by additional sensory channels, such as pressure sensors placed at seatpan and armrests. Meanwhile, vision system can be introduced at this stage to capture the entire body motion during the STS transfer. Compared to the STS data used in this study, a more realistic 3D could help better understand when the elderly users experience STS difficulties and how they response to the assistive motion.

#### 7.4.2 Enhancing classifications with multiple sensing channels

The robot chair may be able to collect richer data about the users' movement from other force/pressure sensing channels to support the classification. The analysis of the data may lead to the discovery of new and more reliable patterns apart from the lateral shift of COP. The sensors include those placed on seatpan (cushion), seatback and armrests. The approaches with sensors imbedded in seatpan for a different purpose was presented by Tanimoto (1998), Tan, et al, (2001) and Yokota (2009), sensors on both seatpan and cushion can be seen in Forlizzi et al. (2005), Xu et al (2012) and Schrempf, et al (2011) for the modification of office chairs.

#### 7.4.3 Adaptive control with gain scheduling control scheme

Since this research essentially focuses on the intention recognition and personalised GRF prediction, the development of effective autonomous control of the lifting mechanism needs to be carried out. Adaptive control with gain scheduling control scheme is considered as competent solution to the problem given the lack of access to both biomechanical and mathematic model towards the dynamics of STS transfers performed by different users. As an extension of the neural fuzzy hybrid system implemented in self-adaptive classifier developed

in Chapter 5, the biomechanical uncertainties brought by different users need to be handled. Moreover, the parameters of the dynamic model of the plant will change unpredictably in time. Because the assistive motion delivered by the actuator is not a transient process, which means how the chair user responses to the assistive motion will also affect the “assistance-as-needed”. As previously explained in Chapter 2, the related work conducted by Hussein et al (2014), ANFIS-PID applied FES control, offered possibilities of realising this problem. The work has successfully controlled the FES parameters using knee trajectories as input measurements, which incorporates high level of uncertainties and environmental complexity.

A possible hybrid control scheme could be: once the STS intention is confirmed, the gain scheduling serves the function as a coarse controller, which assigns the lifting motion when the deficits between the measured STS features and the desired ones are significant. This is performed in open-loop form as the effective of the coarse control is not measured and feedback. Afterwards, adaptive ANFIS control takes over the fine-tuning control dealing with the dynamic variations introduced by i). actuator characteristics under various circumstances, ii). different postures, physiological conditions of the same user, and iii). differences in biomechanical features given by multiple users. Thus further research will be needed to establish the desired relationship between environment measurements (extractable STS performance features) and controller parameters. In addition to the studied GRF values, the longitudinal shift of COP could also be used as inputs for this adaptive control with gain scheduling control scheme.

#### 7.4.4 More accurate GRF prediction with deep learning

Further research will be needed to incorporate deep learning in the GRF prediction. Deep learning is multi-layers ANN based. Each layer extracts features from the output of the previous layer. But features produced at one layer are more generic than the ones of the previous layer. In the developed ANN-based predictor, one hidden layer was employed to deal with the time series of GRF data. The prediction is not perfect when the subject uses a significantly different pace at the seat-off event. This is also known as time temporal distortions, where the segments of time series are shifted in time scale. It might be worth to try multi-layer ANNs to train each

layer separately with unsupervised learning and then the entire network with supervised learning, which is also called fine-tuning in deep learning. With deep learning, the ANNs can also create training data on their own. This might be a solution to the confined capability of sensory device and the limitation of insufficient data from subjects in regard to STS movements.

#### 7.4.5 Embedded system implementation

An embedded system will also be proposed with the help of Printed circuit board. Instead of having a PC aside that computes intention recognition and assistance prediction, the work will be generated within the robot chair assembly. The complete HRI is going to be executed by a PCB that integrated in the robot chair for a compact design. However, the computational speed, especially for the training process in the self-adaptive classifier, needs to improve.

One step further, the logged data that implies the usage of lower limbs motor functions shall be collected as clinical data. This may be achieved in either offline or online manners to keep the health advisor updated. For instance, if a degeneration in STS performance (reduced GRF or STS speed) was perceived, it needs to be verified to what significant level it could be concluded as a functional decline or influence to the upcoming STS transfers.

## REFERENCES

- Abraham A. (2001). Neuro fuzzy systems: State-of-the-art modeling techniques [J]. *Connectionist models of neurons, learning processes, and artificial intelligence*, 269-276.
- Abu Bakar, N. and Abdullah, A. (2011). Dynamic Simulation of Sit to Stand Exercise for Paraplegia. *IEEE International Conference on Control System, Computing and Engineering, Malaysia*, 114-118.
- Aggarwal, J. K., and Ryoo, M. S. (2011). Human activity analysis: A review, *ACM Computing Surveys (CSUR)*, 43(3), 16.
- Akram, S. B., and McIlroy, W. E. (2011). Challenging horizontal movement of the body during sit-to-stand: impact on stability in the young and elderly. *Journal of motor behavior*, 43(2), pp.147-153.
- Alexander, N. B, Koester, D.J and Grunawalt, J.A. (1996). Chair design affects how older adults rise from a chair. *J Am Geriatr Soc.* 44:356–362.
- Aubert, B.A. (1987). Body lift and walker for paralytics. *U.S. Patent* 4,704,749.
- Arborelius, U.P., Wretenberg, P. and Lindberg, F. (1992). The effects of armrests and high seat heights on lower-limb joint load and muscular activity during sitting and rising, *Ergonomics*, 35 (11), pp.1377-1391.
- Bae, J. H., and Moon, I. (2010, October). Design of electric assist-standing chair for persons with disability design of electric chair to assist person with disability in stand up and sitting down. *2010 International Conference on Control Automation and Systems (ICCAS)*, (pp. 574-575). IEEE.

Bae, J. H., and Moon, I. (2011, June). Biomechanical assessment of electric lifting chair for persons with disability. *2011 IEEE International Conference on Rehabilitation Robotics (ICORR)*, (pp. 1-5). IEEE.

Barton, J.G. and Lees, A. (1997). An application of neural networks for distinguishing gait patterns on the basis of hip-knee joint angle diagrams. *Gait & Posture*, 5(1), pp:28-33.

Barrett, C. L., Mann, G. E., Taylor, P. N., and Strike, P. (March 2009). A randomized trial to investigate the effects of functional electrical stimulation and therapeutic exercise on walking performance for people with multiple sclerosis. *Multiple Sclerosis*.

Berger, R. A., Riley, P. O., Mann, R. W., and Hodge, W. A. (1988). Total body dynamics in ascending stairs and rising from a chair following total knee arthroplasty. *Proceedings of Trans 34th A Mtg Orthop Res Soc*, 542.

Biswas, A., Oh, P. I., Faulkner, G. E., Bajaj, R. R., Silver, M. A., Mitchell, M. S., and Alter, D. A. (2015). Sedentary time and its association with risk for disease incidence, mortality, and hospitalization in adults: a systematic review and meta-analysis. *Annals of Internal Medicine*, 162(2), 123-132.

Bohannon, R. W., Bubela, D. J., Magasi, S. R., Wang, Y. C., and Gershon, R. C. (2010). Sit-to-stand test: performance and determinants across the age-span. *Isokinetics and exercise science*, 18(4), 235-240.

Borg, G. (1970). Perceived exertion as an indicator of somatic stress. *Scandinavian Journal of Rehabilitation Medicine*, 2-3, 92-98.

Boyd, C. M., Landefeld, C. S., Counsell, S. R., Palmer, R. M., Fortinsky, R. H., Kresevic, D., and Covinsky, K. E. (2008). Recovery of activities of daily living in older adults after hospitalization for acute medical illness. *Journal of the American Geriatrics Society*, 56(12),

2171-2179.

Breazeal, C. L. (2004). *Designing sociable robots*. MIT press.

Brezak, D., Bacek, T., Majetic, D., Kasac, J. and Novakovic, B. (2012, March). A comparison of feed-forward and recurrent neural networks in time series forecasting. In *Computational Intelligence for Financial Engineering & Economics (CIFEr)*, 2012 IEEE Conference on (pp. 1-6). IEEE.

Bromley, I. (2006). *Tetraplegia and Paraplegia: A Guide for Physiotherapists*. Elsevier, Philadelphia

Cacciatore, T. (2011, September). General studies of the sit to stand movement. *STATNews*.

Chatfield, C. (1996). Model uncertainty and forecast accuracy. *Journal of Forecasting*, 15(7), 495-508.

Chau, J. Y., Grunseit, A., Midthjell, K., Holmen, J., Holmen, T. L., Bauman, A. E., and Van der Ploeg, H. P. (2015). Sedentary behaviour and risk of mortality from all-causes and cardiometabolic diseases in adults: evidence from the HUNT3 population cohort. *British journal of sports medicine*, 49(11), 737-742.

Chen, S. C., Nguyen, V. S., Le, D. K., and Hsu, M. M. (2013, July). ANFIS controller for an active magnetic bearing system. *Fuzzy Systems (FUZZ)*, 2013 IEEE International Conference on (pp. 1-8).

Cheng, P., Liaw, M., Wong, M., Tang, F., Lee, M. and Lin, P. (1998) 'The sit-to-stand movement in stroke patients and its correlation with falling', *Archives of Physical Medicine and Rehabilitation*, 79 (9), pp.1043-1046.

Chugo, D., Fujita, K., Sakaida, Y., Yokota, S., and Takase, K. (2011, April). Development of depressurization system for a seated patient on a wheelchair. In *Mechatronics (ICM), IEEE International Conference*, pp. 615-620.

Coggrave, M.J. and Rose, L.S. (2003) A specialist seating assessment clinic: changing pressure relief practice. *Spinal Cord*, 41, pp.692-695.

Claus, A.P., Hides, J.A., Moseley, G.L. and Hodges, P.W. (2016). Thoracic and lumbar posture behaviour in sitting tasks and standing: Progressing the biomechanics from observations to measurements. *Applied ergonomics*, 53, pp.161-168.

Cuesta-Vargas, A. I., and González-Sánchez, M. (2013). Differences in Muscle Activation Patterns during Sit to Stand Task among Subjects with and without Intellectual Disability. *BioMed research international*, 2013.

Dautenhahn, K. (2007). Socially intelligent robots: dimensions of human–robot interaction. *Philosophical Transactions of the Royal Society of London B: Biological Sciences*, 362(1480), 679-704.

Davis, M. G., Fox, K. R., Hillsdon, M., Sharp, D. J., Coulson, J. C., and Thompson, J. L. (2011). Objectively measured physical activity in a diverse sample of older urban UK adults. *Med Sci Sports Exerc*, 43(4), 647-654.

Demura, S., and Yamada, T. (2007). Height of chair seat and movement characteristics in sit-to-stand by young and elderly adults. *Perceptual and motor skills*, 104(1), 21-31.

Dias, F.M., Antunes, A. and Mota, A.M. (2003). Regularization versus early stopping: A case study with a real system. In *2nd IFAC Conference Control Systems Design, Bratislava, República Eslovaca*.

Cuesta-Vargas, A. I., and González-Sánchez, M. (2013). Differences in muscle activation patterns during sit to stand task among subjects with and without intellectual disability. *BioMed research international*, 2013.

Disabled World. (2011). Lift Chairs and Seating Products for Seniors and Disabled. *Disabled world towards tomorrow*.

Retrieved November 20, 2015, from <http://www.disabled-world.com/assistivedevices/seating/>.

Drewniak, E. I., Crisco, J. J., Spenciner, D. B., and Fleming, B. C. (2007). Accuracy of circular contact area measurements with thin-film pressure sensors. *Journal of biomechanics*, 40(11), 2569-2572.

Engardt, M., Knutsson, E., Jonsson, M., and Sternhag, M. (1995). Dynamic muscle strength training in stroke patients: effects on knee extension torque, electromyographic activity, and motor function. *Archives of physical medicine and rehabilitation*, 76(5), 419-425.

Etnyre, B. and Thomas, DQ. (2007). Event standardization of sit-to-stand movements, *Physical Therapy*, 87 (12), pp.1651-1666.

Fausett, L. (1994). Fundamentals of neural networks: architectures, algorithms, and applications. Prentice-Hall, Inc.

Fontecchio, B.E. and Spiegelhalter, A., Invercan, Inc. (1990). Lift for wheelchairs. *U.S. Patent* 4, 909, 700.

Foresee, F.D. and Hagan, M.T. (1997). Gauss-Newton approximation to Bayesian regularization, *Proceedings of the 1997 International Joint Conference on Neural Networks*, pp. 1930–1935

Forlizzi, J., DiSalvo, C., Zimmerman, J., Mutlu, B., and Hurst, A. (2005, November). The



SenseChair: The lounge chair as an intelligent assistive device for elders. In Proceedings of the 2005 conference on Designing for User eXperience (p. 31). AIGA: American Institute of Graphic Arts.

Fujiwara, K., Tomita, H., Kurokawa, N., Asai, H. and Maeda, K., (2009). Effects of stance width on postural movement pattern and anticipatory postural control associated with unilateral arm abduction. *Journal of Electromyography and Kinesiology*, 19(3), pp.187-196.

Franklyn, M., Oakes, B., Field, B., Wells, P., and Morgan, D. (2008). Section modulus is the optimum geometric predictor for stress fractures and medial tibial stress syndrome in both male and female athletes. *The American journal of sports medicine*, 36(6), 1179-1189.

Galumbeck, M. H., Buschbacher, R. M., Wilder, R. P., Winters, K. L., Hudson, M. A., and Edlich, R. (2004). The Sit & Stand™ chair. A revolutionary advance in adaptive seating systems. *Journal of long-term effects of medical implants*, 14(6).

Gioftsos, G., and Grieve, D. W. (1996). The use of artificial neural networks to identify patients with chronic low-back pain conditions from patterns of sit-to-stand manoeuvres. *Clinical Biomechanics*, 11(5), 275-280.

Golden Technologies. (n.d.). Power Lift & Recline Chair OWNER'S MANUAL.

Goulart, F. R. D. P., and Valls-Solé, J. (1999). Patterned electromyographic activity in the sit-to-stand movement. *Clinical neurophysiology*, 110(9), 1634-1640.

Gunter, K. B., White, K. N., Hayes, W. C., and Snow, C. M. (2000). Functional mobility discriminates nonfallers from one-time and frequent fallers. *The Journals of Gerontology Series A: Biological Sciences and Medical Sciences*, 55(11), M672-M676.

Gross, M. M., Stevenson, P. J., Charette, S. L., Pyka, G., and Marcus, R. (1998). Effect of

muscle strength and movement speed on the biomechanics of rising from a chair in healthy elderly and young women. *Gait & posture*, 8(3), 175-185.

Gyi, D.E., Sims, R., Porter, J.M., Marshall, R. and Case, K. (2004). Representing older and disabled people in virtual user trials: Data collection methods, *Applied Ergonomics*, 35 (5), pp.443-451.

Hartmann, D. L. (2014). 'Time (or Space) Series Analysis - Section 6a', in *ATMS 552: Objective Analysis Notes*. University of Washington, 4 February 2014 (pp.128-150). Available at [http://www.atmos.washington.edu/~dennis/552\\_Notes\\_6a.pdf](http://www.atmos.washington.edu/~dennis/552_Notes_6a.pdf) (Accessed:17 January 2016).

Hedge, A., Yates, T., Copeland, R.J., Loosemore, M., Hamer, M., Bradley, G. and Dunstan, D.W. (2015) The sedentary office: a growing case for change towards better health and productivity.

Hodge, W. A., Fijan, R. S., Carlson, K. L., Burgess, R. G., Harris, W. H., and Mann, R. W. (1986). Contact pressures in the human hip joint measured in vivo. *Proceedings of the National Academy of Sciences*, 83(9), 2879-2883.

Horak, F. B., and Nashner, L. M. (1986). Central programming of postural movements: adaptation to altered support-surface configurations. *Journal of neurophysiology*, 55(6), 1369-1381.

Hu, F. B., Li, T. Y., Colditz, G. A., Willett, W. C., and Manson, J. E. (2003). Television watching and other sedentary behaviors in relation to risk of obesity and type 2 diabetes mellitus in women. *JAMA: the journal of the American Medical Association*, 289(14), 1785-1791.

Hughes, M. A., Myers, B. S., and Schenkman, M. L. (1996). The role of strength in rising from a chair in the functionally impaired elderly. *Journal of biomechanics*, 29(12), 1509-1513.

Hughes, M. A., and Schenkman, M. L. (1996). Chair rise strategy in the functionally impaired elderly. *Journal of rehabilitation research and development*, 33(4), 409.

Huskisson, E.C. (1974). Measurement of pain. *Lancet* 11, 1127—1131.

Hussain, R., Massoud, R., and Mawaldi, M. (2014). ANFIS-PID Control FES-Supported Sit-to-Stand in Paraplegics:(Simulation Study). *Journal of Biomedical Science and Engineering*, 7(4), 208.

Hvid, L. G., Ørtenblad, N., Aagaard, P., Kjaer, M., and Suetta, C. (2011). Effects of ageing on single muscle fibre contractile function following short-term immobilisation. *The Journal of Physiology*, 589(19), 4745-4757.

Im, E. I. (1996). A Note on Derivation of the Least Squares Estimator (No. 199611). Available at [http://www.economics.hawaii.edu/research/workingpapers/88-98/WP\\_96-11.pdf](http://www.economics.hawaii.edu/research/workingpapers/88-98/WP_96-11.pdf) (Accessed: 30 January 2016).

Janssen, W.G., Bussmann, H.B. and Stam, H.J. (2002) 'Determinants of the sit-to-stand movement: A review', *Physical Therapy*, 82 (9), pp.866-879.

Kaplan, G. A., Strawbridge, W. J., Camacho, T., and Cohen, R. D. (1993). Factors Associated with Change in Physical Functioning in the Elderly A Six-Year Prospective Study. *Journal of Aging and Health*, 5(1), 140-153.

Kamnik, R., and Bajd, T. (2004). Standing-up robot: an assistive rehabilitative device for training and assessment. *Journal of Medical Engineering & Technology*, 28(2), 74-80.

Kaya, B. K., Krebs, D. E., and Riley, P. O. (1998). Dynamic stability in elders: momentum control in locomotor ADL. *The Journals of Gerontology Series A: Biological Sciences and Medical Sciences*, 53(2), M126-M134.

Kerr, K. M., White, J. A., Barr, D. A., and Mollan, R. A. B. (1997). Analysis of the sit-stand-sit movement cycle in normal subjects. *Clinical Biomechanics*, 12(4), 236-245.

Kiguchi, K., and Hayashi, Y. (2012). An EMG-based control for an upper-limb power-assist exoskeleton robot. *Systems, Man, and Cybernetics, Part B: Cybernetics, IEEE Transactions on*, 42(4), 1064-1071.

Kirvesoja, H., Väyrynen, S. and Häikiö, A. (2000) 'Three evaluations of task-surface heights in elderly people's homes', *Applied Ergonomics*, 31 (2), pp.109-119.

Kleinpell, R. M., Fletcher, K., and Jennings, B. M. (2008). Reducing Functional Decline in Hospitalized Elderly. *Patient safety and quality: An evidence-based handbook for nurses*.

Klous, M., Mikulic, P., and Latash, M. L. (2011). Two aspects of feedforward postural control: anticipatory postural adjustments and anticipatory synergy adjustments. *Journal of neurophysiology*, 105(5), 2275-2288.

Kuo, A. D., and Zajac, F. E. (1992). Human standing posture: multi-joint movement strategies based on biomechanical constraints. *Progress in brain research*, 97, 349-358.

Lawton, M.P., and Brody, E.M. (1969). Assessment of older people: Self-maintaining and instrumental activities of daily living. *The Gerontologist*, 9(3), 179-186.

La-Z-Boy. (n.d). AVENGER luxury lift chair. [Online]. Available at: <http://www.la-z-boy.co.uk/product/78/Lift--n--Rise-chair>. Accessed on 28th March 2016.

Lee, J. K., and Nam, Y. (2008, October). Knee joint moment estimation using neural network system identification in sit-to-stand movement. In *Control, Automation and Systems, 2008. ICCAS 2008. International Conference on* (pp. 544-547). IEEE.

Levenberg, K. (1944). A method for the solution of certain problems in least squares, *Quarterly of Applied Mathematics*, 5, 164–168.

Li, H., Yu, J., Hilton, C. and Liu, H. (2013). Adaptive sliding-mode control for nonlinear active suspension vehicle systems using T–S fuzzy approach. *Industrial Electronics, IEEE Transactions on*, 60(8), pp.3328-3338.

Liang, Y. and Kelemen, A. (2008). Statistical advances and challenges for analyzing correlated high dimensional SNP data in genomic study for complex diseases. *Statistics Surveys*, 2, 43-60.

Lin, Z., Zecca, M., Sessa, S., Bartolomeo, L., Ishii, H., Itoh, K., and Takanishi, A. (2010, December). Development of an ultra-miniaturized inertial measurement unit WB-3 for human body motion tracking. In *System Integration (SII), 2010 IEEE/SICE International Symposium on* (pp. 414-419). IEEE.

Lord, S. R., Murray, S. M., Chapman, K., Munro, B., and Tiedemann, A. (2002). Sit-to-stand performance depends on sensation, speed, balance, and psychological status in addition to strength in older people. *The Journals of Gerontology Series A: Biological Sciences and Medical Sciences*, 57(8), M539-M543.

Lord, S.R., Sherrington, C., Menz, H.B. and Close, J.C., (2007). *Falls in older people: risk factors and strategies for prevention*. Cambridge University Press.

Lynch, C. and Popovic, M. (2008) Functional Electrical Stimulation: Closed-Loop Control of Induced Muscle Contractions. *IEEE Control System Magazine*, 28, 40-49.

MacKay, D. J. (1999). Comparison of approximate methods for handling hyperparameters. *Neural computation*, 11(5), 1035-1068.

MacKay, D. J. (2003). *Information theory, inference and learning algorithms*. Cambridge university press.

Magnan, A., McFadyen, B. J., and St-Vincent, G. (1996). Modification of the sit-to-stand task with the addition of gait initiation. *Gait & Posture*, 4(3), 232-241.

Mak, M. K., Pang, M. Y., and Mok, V. (2011). Gait difficulty, postural instability, and muscle weakness are associated with fear of falling in people with Parkinson's disease. *Parkinson's Disease*, 2012.

Mamdani, E. H. and Assilian, S. (1975). An experiment in linguistic synthesis with a fuzzy logic controller. *International journal of man-machine studies*, 7(1), 1-13.

Massion, J. (1992). Movement, posture and equilibrium: interaction and coordination. *Progress in neurobiology*, 38(1), 35-56.

Markowitz, N. (2012). Nick's Fire - Electrical- Safety and Security Blog Electrically Operated Lift Chair Dangers, Retrieved November 20, 2013, from <http://nickmarkowitz.blogspot.co.uk/2012/03/electrically-operated-lift-chair.html>

Matthews, C. E., Chen, K. Y., Freedson, P. S., Buchowski, M. S., Beech, B. M., Pate, R. R., and Troiano, R. P. (2008). Amount of time spent in sedentary behaviors in the United States, 2003–2004. *American journal of epidemiology*, 167(7), 875-881.

Médéric, P., Pasqui, V., Plumet, F., Bidaud, P. and Guinot, J.C. (2004). Design of a walking-aid and sit to stand transfer assisting device for elderly people. In 7th Int. Conference on *Climbing on Walking Robots (CLAWAR'04)*, Madrid, Spain.

Moeslund, T. B., Hilton, A., and Krüger, V. (2006). A survey of advances in vision-based human motion capture and analysis. *Computer vision and image understanding*, 104(2), 90-126.

Munton, J. S., Ellis, M. I., CHAMBERLAIN, M. A., and Wright, V. (1981). An investigation into the problems of easy chairs used by the arthritic and the elderly. *Rheumatology*, 20(3), 164-173.

Murray, A. M., Levkoff, S. E., Wetle, T. T., Beckett, L., Cleary, P. D., Schor, J. D. and Evans, D. A. (1993). Acute delirium and functional decline in the hospitalized elderly patient. *Journals of Gerontology*, 48, M181-M181.

Narendra, K. S., and Mukhopadhyay, S. (1997). Adaptive control using neural networks and approximate models. *Neural Networks, IEEE Transactions on*, 8(3), 475-485.

Nguyen, T. V., Center, J. R., and Eisman, J. A. (2000). Osteoporosis in elderly men and women: effects of dietary calcium, physical activity, and body mass index. *Journal of bone and mineral research*, 15(2), 322-331.

Nitz, J. C., and Choy, M. N. L. (2004). The relationship between ankle dorsiflexion range, falls and activity level in women aged 40 to 80 years. *NZ Journal of Physiotherapy*, 32(3), 122.

Ng, S. S., Cheung, S. Y., Lai, L. S., Liu, A. S., Ieong, S. H. and Fong, S. S. (2015). Five Times Sit-To-Stand Test Completion Times Among Older Women: Influence of Seat Height and Arm Position. *Journal of rehabilitation medicine*, 47(3), 262-266.

Oancea, B. and Ciucu, Ș.C. (2014). Time series forecasting using neural networks. *arXiv preprint arXiv:1401.1333*.

Ozden, H., Balci, Y., Demirüstü, C., Turgut, A. and Ertugrul, M. (2005). Stature and sex estimate using foot and shoe dimensions. *Forensic Science International*, 147(2), pp.181-184.

O'Sullivan, P. B., Grahamslaw, K. M., Kendell, M., Lapenskie, S. C., Möller, N. E., and

Richards, K. V. (2002). The effect of different standing and sitting postures on trunk muscle activity in a pain-free population. *Spine*, 27(11), 1238-1244.

Papa, E., and Cappozzo, A. (2000). Sit-to-stand motor strategies investigated in able-bodied young and elderly subjects. *Journal of biomechanics*, 33(9), 1113-1122.

Petković, D., Čojbašić, Ž., and Nikolić, V. (2013). Adaptive neuro-fuzzy approach for wind turbine power coefficient estimation. *Renewable and Sustainable Energy Reviews*, 28, 191-195.

Pearson, V. I. (2000). Assessment of function in older adults. *Assessing older persons: Measures, meaning, and practical applications*, 17-48.

Perry, B. C. (1982). Falls among the elderly. *Journal of the American Geriatrics Society*, 30(6), 367-371.

Pheasant, S.T. and Haslegrave, C.M. (2006) Bodyspace: Anthropometry, ergonomics, and the design of work. *CRC Press*.

Praschberger. (n.d.). Standing frame. [Online].

Available at: <http://www.praschberger.com/en/stehtisch/stehtisch/>. Accessed on 28th March 2016.

Prince, F., Winter, D. A., Stergiou, P., & Walt, S. E. (1994). Anticipatory control of upper body balance during human locomotion. *Gait & Posture*, 2(1), 19-25.

Qiu, R., Ji, Z., Noyvirt, A., Soroka, A., Setchi, R., Pham, D. T., ... & Smrz, P. (2012, October). Towards robust personal assistant robots: Experience gained in the SRS project. In *Intelligent Robots and Systems (IROS), 2012 IEEE/RSJ International Conference on* (pp. 1651-1657). IEEE.



Ramsey, V. K., Miszko, T. A. and Horvat, M. (2004). Muscle activation and force production in Parkinson's patients during sit to stand transfers. *Clinical Biomechanics*, 19(4), 377-384.

Ramsey, V. K., Miszko, T. A., and Horvat, M. (2004). Muscle activation and force production in Parkinson's patients during sit to stand transfers. *Clinical Biomechanics*, 19(4), 377-384.

Randeniya, D. I. B., Gunaratne, M., Sarkar, S. and Nazef, A. (2008). Calibration of inertial and vision systems as a prelude to multi-sensor fusion. *Transportation Research Part C: Emerging Technologies*, 16(2), 255-274.

Restwell. (n.d.). Seattle intalift rise recliner. [Online]. Available at:  
<http://www.motionhaus.co.uk/product/sea0/restwell-seattle-intalift-rise-recliner-armchair-choose-colour>. Accessed on 28th March 2016.

Rica. (n.d.). Wheeled walking frames. [Online]. Available at:  
<http://www.rica.org.uk/content/features-wheeled-walking-frames>. Accessed on 28th March 2016.

Riedmiller, M. and Braun, H. (1993). A direct adaptive method for faster backpropagation learning: The RPROP algorithm. In *Neural Networks*, IEEE International Conference, pp. 586-591.

Riley, P. O., Krebs, D. E. and Popat, R. A. (1997). Biomechanical analysis of failed sit-to-stand. *Rehabilitation Engineering*, IEEE Transactions on, 5(4), 353-359.

Rubenstein, L. Z., Josephson, K. R. and Robbins, A. S. (1994). Falls in the nursing home. *Annals of internal medicine*, 121(6), 442-451.

Robbins, L.M. (1986). Estimating height and weight from size of footprints. *Journal of Forensic Science*, 31(1), pp.143-152.

Rocha, J. G., Carvalho, H., Duarte, F. M., Carvalho, M., and Moreira, V. M. (2008, June). System providing discomfort monitoring for people in wheelchairs. *In Industrial Electronics*, 2008. ISIE 2008. IEEE International Symposium on (pp. 961-966). IEEE.

Roche, N., Bonnyaud, C., Geiger, M., Bussel, B. and Bensmail, D. (2015). Relationship between hip flexion and ankle dorsiflexion during swing phase in chronic stroke patients. *Clinical Biomechanics*, 30(3), 219-225.

Roweis, S. (1996). Levenberg-marquardt optimization. *Notes*, University of Toronto.

Runge, C. F., Shupert, C. L., Horak, F. B., and Zajac, F. E. (1999). Ankle and hip postural strategies defined by joint torques. *Gait & posture*, 10(2), 161-170.

Salah, O., Ramadan, A.A., Sessa, S., Ismail, A.A., Fujie, M. and Takanishi, A. (2013). Anfis-based sensor fusion system of sit-to-stand for elderly people assistive device protocols. *International Journal of Automation and Computing*, 10(5), pp.405-413.

Sager, M.A., Franke, T., Inouye, S.K., Landefeld, C.S., Morgan, T.M., Rudberg, M.A., Siebens, H. and Winograd, C.H. (1996). Functional outcomes of acute medical illness and hospitalization in older persons. *Archives of Internal Medicine*, 156(6), pp.645-652.

Saroha, S., & Aggarwal, S. K. (2014). Multi step ahead forecasting of wind power by different class of neural networks. *Engineering and Computational Sciences (RAECS), 2014 Recent Advances*, pp. 1-6.

Schenkman, M., Riley, P. O., and Pieper, C. (1996). Sit to stand from progressively lower seat heights—alterations in angular velocity. *Clinical Biomechanics*, 11(3), 153-158.

Schlicht, J., Camaione, D. N., and Owen, S. V. (2001). Effect of intense strength training on

standing balance, walking speed, and sit-to-stand performance in older adults. *The Journals of Gerontology Series A: Biological Sciences and Medical Sciences*, 56(5), 281-286.

Schrempf, A., Schossleitner, G., Minarik, T., Haller, M., Gross, S. and Kurschl, W. (2011, August). PostureCare-Towards a novel system for posture monitoring and guidance. In *Proc. IFAC* (Vol. 11).

Sfetsos, A. (2000). A comparison of various forecasting techniques applied to mean hourly wind speed time series. *Renewable energy*, 21(1), 23-35.

Siminoski, K. and Bain, J. (1993). The relationships among height, penile length, and foot size. *Annals of Sex Research*, 6(3), pp.231-235.

Stuffseniorned. (n.d.). lifting cushion seat assist chair seat lift. [Online]. Available at: <http://stuffseniorned.com/lifting-cushion-seat-assist-chair-seat-lift/>. Accessed on 28th March 2016.

Su, H., Li, Z., Li, G., and Yang, C. (2013). EMG-Based neural network control of an upper-limb power-assist exoskeleton robot. In *Advances in Neural Networks–ISNN 2013* (pp. 204-211). Springer Berlin Heidelberg.

SystemRoMedic. (2012). ReTurn7600: Safe and active sit-to-stand and transfer. [Online]. Available at: <http://www.handicare.com/en/products/transfer-and-lifting/sittostand-aids/systemromedic-return7600/c-39/c-204/p-295>. Accessed on 28th March 2016.

Takagi, T. and Sugeno, M. (1985). Fuzzy identification of systems and its application to modeling and control. *IEEE Transactions on Systems, Man and Cybernetics*, 15 (1), 116–132.

Tan, H. Z., Slivovsky, L. A. and Pentland, A. (2001). A sensing chair using pressure distribution

sensors. *Mechatronics, IEEE/ASME Transactions on*, 6(3), 261-268.

Tao, Y., Hu, H. and Zhou, H. (2007). Integration of vision and inertial sensors for 3D arm motion tracking in home-based rehabilitation. *The International Journal of Robotics Research*, 26(6), 607-624.

Tanimoto, Y., Takechi, H., Nagahata, H. and Yamamoto, H. (1998, May). The study of pressure distribution in sitting position on cushions for patient with SCI. In *Instrumentation and Measurement Technology Conference, 1998. IMTC/98. Conference Proceedings. IEEE* (Vol. 1, pp. 219-224). IEEE.

Takagi, T. and Sugeno, M. (1985). Fuzzy identification of systems and its application to modeling and control. *IEEE Transactions on Systems, Man and Cybernetics*. 15 (1), 116–132.

Tencer, A.F., Koepsell, T.D., Wolf, M.E., Frankenfeld, C.L., Buchner, D.M., Kukull, W.A., LaCroix, A.Z., Larson, E.B. and Tautvydas, M., (2004). Biomechanical properties of shoes and risk of falls in older adults. *Journal of the American geriatrics society*, 52(11), pp.1840-1846.

Texas Instruments (2000, March). CMOS Analog Multiplexers/Demultiplexers with Logic Level Conversion. [Online].

Available at: [http://pdf.datasheetcatalog.com/datasheets/120/109150\\_DS.pdf](http://pdf.datasheetcatalog.com/datasheets/120/109150_DS.pdf) Accessed 30 May 2016.

Tian, Z. and Zuo, M. J. (2010). Health condition prediction of gears using a recurrent neural network approach. *Reliability, IEEE Transactions on*, 59(4), 700-705.

Townsend, N., Bhatnagar, P., Wickramasinghe, K., Scarborough, P., Foster, C. and Rayner, M. (2012). Physical activity statistics 2012. *London: British Heart Foundation*.

Tremblay, M. S., Colley, R. C., Saunders, T. J., Healy, G. N. and Owen, N. (2010).

Physiological and health implications of a sedentary lifestyle. *Applied Physiology, Nutrition, and Metabolism*, 35(6), 725-740.

Tsukahara, A., Kawanishi, R., Hasegawa, Y. and Sankai, Y. (2010). Sit-to-stand and stand-to-sit transfer support for complete paraplegic patients with robot suit HAL. *Advanced robotics*, 24(11), 1615-1638.

Trumble, H.C. (1930). The skin tolerances for pressure and pressure sores. *Medical Journal of Australia*, 2, 724-726.

U.S Medical Supplies. (2012). Pride Classic C-30 Casual Lift Chair. [Online]. Available at: <http://www.usmedicalsupplies.com/Pride-C-30-Casual-Lift-Chair.htm>. Accessed on 28th March 2016.

Various. (2016), Later Life Factsheet. [www.ageuk.org.uk](http://www.ageuk.org.uk), Available at: [http://www.ageuk.org.uk/Documents/EN-GB/Factsheets/Later\\_Life\\_UK\\_factsheet.pdf?dtrk=true](http://www.ageuk.org.uk/Documents/EN-GB/Factsheets/Later_Life_UK_factsheet.pdf?dtrk=true). Accessed on 27th March 2016.

Wang, W., Van gelder, P. H., and Vrijling, J. K. (2007). Comparing Bayesian regularization and cross-validated early-stopping for streamflow forecasting with ANN models. *IAHSAISH publication*, 216-221.

Warren, T. Y., Barry, V., Hooker, S. P., Sui, X., Church, T. S., and Blair, S. N. (2010). Sedentary behaviours increase risk of cardiovascular disease mortality in men. *Medicine and science in sports and exercise*, 42(5), 879.

Weiner, D. K., Long, R., Hughes, M. A., Chandler, J., and Studenski, S. (1993). When Older Adults Face the Chair-Rise Challenge: A Study of Chair Height Availability and Height - Modified Chair-Rise Performance in the Elderly. *Journal of the American Geriatrics Society*, 41(1), 6-10.

Witten, I. H., and Franklyn, E. (2005). Data mining, practical machine learning tools and techniques, 2nd edition, *Morgan Kaufmann*, pp149-150.

Xu, L., Chen, G., Wang, J., Shen, R., and Zhao, S. (2012, September). A sensing cushion using simple pressure distribution sensors. In *Multisensor Fusion and Integration for Intelligent Systems (MFI), 2012 IEEE Conference on* (pp. 451-456). IEEE.

Yao, J. and Tan, C.L. (2000). A case study on using neural networks to perform technical forecasting of forex. *Neurocomputing*, 34(1), pp.79-98.

Yamada, T., and Demura, S.I. (2009). Relationships between ground reaction force parameters during a sit-to-stand movement and physical activity and falling risk of the elderly and a comparison of the movement characteristics between the young and the elderly. *Archives of gerontology and geriatrics*, 48(1), 73-77.

Yokota, S., Hashimoto, H., Ohyama, Y., and She, J. H. (2009). Electric Wheelchair Controlled by Human Body Motion Interface. *IEEE Transactions on Electronics, Information and Systems*, 129, 1874-1880.

Yip, M., He, D. D., Winokur, E., Balderrama, A. G., Sheridan, R., and Ma, H. (2009, September). A flexible pressure monitoring system for pressure ulcer prevention. In *Engineering in Medicine and Biology Society, 2009. EMBC 2009. Annual International Conference of the IEEE* (pp. 1212-1215). IEEE.

Zalewski, W. (1991). *U.S. Patent No. 5,040,832. Washington, DC: U.S. Patent and Trademark Office.*

Zecchin, C., Facchinetti, A., Sparacino, G., De Nicolao, G., and Cobelli, C. (2012). Neural network incorporating meal information improves accuracy of short-time prediction of glucose concentration. *Biomedical Engineering, IEEE Transactions on*, 59(6), 1550-1560.

Zhang, K. and Zhu, D. (2004). Simulation Study of FES-Assisted Standing up with Neural Network Control. *26th Annual International Conference of the IEEE EMBS, San Francisco*.

Zhang, K., Sun, M., Lester, D. K., Pi-Sunyer, F. X., Boozer, C. N., and Longman, R. W. (2005). Assessment of human locomotion by using an insole measurement system and artificial neural networks. *Journal of Biomechanics*, 38(11), 2276-2287.

Zheng, Y., and Morrell, J. B. (2010). A vibrotactile feedback approach to posture guidance. In *Haptics Symposium, 2010 IEEE* (pp. 351-358). IEEE.

Zheng, S., Huang, K., and Tan, T. (2011, September). Evaluation framework on translation-invariant representation for cumulative foot pressure image. In *Image Processing (ICIP), 2011 18th IEEE International Conference on* (pp. 201-204). IEEE.

Zhou, H., Stone, T., Hu, H., and Harris, N. (2008). Use of multiple wearable inertial sensors in upper limb motion tracking. *Medical engineering & physics*, 30(1), 123-133.

Zimmermann, H. J. (2001). Fuzzy set theory and its applications. *Springer Science & Business Media*.